A STUDY OF MICROPYRETIC SYNTHESIS OF SLIP CAST COLLOIDAL SiO_2-Al-C EXOTHERMIC SYSTEM

A Disertation submitted to the

Division of Graduate Studies and Research
of the University of Cincinnati

in partial fulfillment of the
requirements for the degree of

DOCTOR OF PHILOSOPHY

in the Department of Materials Science and Engineering
of the College of Engineering

1994

By

Necip Suat Canarslan

B.S., Middle East Technical University, 1985
M.S., Anadolu University, 1988

Committee Chair: Prof. J.A. Sekhar

UNIVERSITY OF CINCINNATI

January 27 19 94

I hereby recommend that the thesis prepared under my supervision by Necip Suat Canarslan *entitled* "A Study of Micropyretic Synthesis of Slip Cast Colloidal SiO_2-Al-C Exothermic System"

be accepted as fulfilling this part of the requirements for the degree of Doctor of Philosophy

Approved by:

A STUDY OF MICROPYRETIC SYNTHESIS OF SLIP CAST COLLOIDAL SiO_2-Al-C EXOTHERMIC SYSTEM

A Disertation submitted to the

Division of Graduate Studies and Research
of the University of Cincinnati

in partial fulfillment of the
requirements for the degree of

DOCTOR OF PHILOSOPHY

in the Department of Materials Science and Engineering
of the College of Engineering

1994

By

Necip Suat Canarslan

B.S., Middle East Technical University, 1985
M.S., Anadolu University, 1988

Committee Chair: Prof. J.A. Sekhar

ABSTRACT

The feasibility of micropyretic synthesis in Al_2O_3-SiC composites through the slip casting route has been investigated. The slip rheology and combustion kinetics in a colloidal silica suspended SiO_2-Al-C system has been studied as an example of such processing. Colloidal silica functioned as a binder and also constituted part of the combustion source in the green compact. The degree of conversion and porosity level of the micropyretically synthesized product have been found to depend on the rheology of the suspensions including the solid concentration, particle size and pH value of the suspensions. The major phases, α-Al_2O_3 and β-SiC, in the composite produced with this new method were homogeneously distributed within each other. A modified analytical model for the slip cast micropyretic system has also been developed considering slip parameters and the thermophysical and chemical properties of the reactants. Results obtained from the model are noted to be in close agreement with the experimental values.

ACKNOWLEDGEMENTS

I would like to express my sincere appreciation to my thesis advisor, Prof. J. A. Sekhar for his continuous support, guidance and many invaluable discussions throughout this investigation.

I would also like to thank the members of the Graduate Committee, Prof. M.J. Pool and Prof. O.N.C. Uwakweh for taking the time necessary to review this work and their helpful comments, and thus, for contributing a broader perspective to the outcome.

I am grateful for all of the staff members and my colleagues in the Department of Materials Science and Engineering, University of Cincinnati for their cooperation and help.

I also wish to thank University of Anatolia, Turkiye, for the opportunity and support that have made this work possible.

Finally, I would like to express my appreciation to my parents, my wife, Nuket and daughter, Sevgi, who have always been very supportive and caring.

TABLE OF CONTENTS

LIST OF FIGURES

Page

LIST OF TABLES

1. INTRODUCTION

A significant amount of attention has recently been centered on the use of the chemical reactions, commonly referred to as the self-propagating high temperature synthesis (SHS) method, simply as combustion synthesis (CS) and/or micropyretic synthesis (MS), for materials processing purposes. MS is characterized by self propagation of preformed mixture of reactants which are usually in powder form.

Amongst the forming processing, compaction has received the bulk of attention while casting techniques have not been used in regard to MS. In this study, the processing of slip cast combustible slurries is studied for the first time in available knowledge.

In this thesis, the scientific principles that govern the art of processing the combustible slurries by slip casting are presented and discussed. Combustible mixtures of SiO_2-Al-C and Cr_2O_3-Al-C at stoichiometry as well as their combination at different percentages and SiC dilution as a slip constituent have been chosen to determine the feasibility of slip casting and micropyretically synthesizing of these systems to form the Al_2O_3-SiC composites. The Al_2O_3-SiC composite has numerous exceptional properties including high fracture toughness, high melting temperature and nonreactivity with various liquid metals which make the material an attractive candidate for high temperature structural applications, cutting tool material and material for erosive environments.

Details of the variables affecting the process are discussed and suggestions and ideas are presented for developing new techniques to fabricate refractory materials. Processing variables such as deflocculation level, particle size, amount and type of combustion source, suspending medium, binders and combustion type and the temperature were studied in relation to the processing of slip rheology, casting mechanism, and combustion synthesis and the final microstructure and the property. A number of relationships found in the literature were also examined and compared with experimental results. The modified analytical model of combustion velocity for slip cast micropyretic system has been developed considering slip parameters and both thermophysical and chemical properties for reactants and products. Application of this model to the micropyretic synthesis of the SiO_2-Al-C reaction has been carried out to study the variation of combustion front with the slip casting parameter, vol% solid loading. The comparison with the experimentally determined values are noted to be in close agreement. However, the validity of the model is found to be related to how precisely the thermophysical and chemical properties are known or determined.

Colloidal silica have been used as a major suspending medium, binder, and combustion source in the process. Distilled water to which binder, polyvinyl alcohol (PVA) and dispersant, Darvan-C™ were employed, were also used as a suspending medium.

Slips made with colloidal silica did not require any other binder and/or dispersant. Submicron particles from colloidal silica (30 wt% solid), 1430AT™, Nycol Co., had a multifunctional behavior in the slip and provided reasonable green strength level at cast bodies for handling. Also this phenomena lead to dense and fine microstructures at the final product.

All slips were deflocculated by 25 vol% distilled water diluted hydrochloric acid to determine the casting range at which minimum slip viscosity was obtained to make the rheological properties suitable for handling and to allow proper cast formation. The rheological properties have been studied by slip casting suspensions with pH values ranking from 2 to 11.

The slips suspended with colloidal silica exhibited lower viscosities as pH decreased . This pH range for the slips of SiO_2-Al-C system was closely related to solid concentration in the slurry. As solid concentration increased, the pH range for minimum viscosities narrowed and corresponding viscosities increased. The typical pH range for this micropyretic system was 3 to 5. Addition of Cr_2O_3-Al-C combustion source to SiO_2-Al-C system caused further widening at the pH range with viscosity decrease. SiC dilution in the same micropyretic system combination gave full deflocculation at entire pH range below 5. On the other hand, distilled water suspended slips, minimum viscosities were obtained at pH values higher than 7 where viscosities were almost same to the corresponding colloidal silica suspended slips.

Several solid and submicron colloidal silica powder concentrations of slips for both reaction systems were investigated. After pH adjustments, slips were cast into plaster mold using both casting modes, solid and drain casting. Castings were done at three different pH values where relatively lowest, highest viscosities noted and at the initial condition for the slip without pH adjustment.

The green bodies fabricated by slip casting were micropyretically synthesized using both modes of combustion, thermal explosion and wave propagation modes. At the thermal explosion mode, the samples were synthesized by placing the samples into the tube furnace. For wave propagation mode, the samples were synthesized by igniting one end with a propane torch after preheating the samples.

The final synthesized products quality were depended on the microstructure of the slip cast preform. The cast structure defined with the amount and size of porosity variation which was controlled in this study by solid concentration of the slurry, deflocculation level and submicron colloidal silica powder concentration.

The degree of packing density has been found to depend on the deflocculation level, the solid concentration of the slip and the submicron colloidal silica concentration. The agglomeration of powders in the suspensions increased the volume and size of pores in the green compacts, resulting in a decrease in the combustion

rate and reaction completeness. With initial porosity higher than ~50%, the exothermic reaction was not self-sustaining when synthesized at wave propagation mode without preheating. Higher packing densities have been obtained at higher solid concentration and colloidal silica concentration in the slip. It has been also observed that finer microstructures was possible and reaction completeness could be improved with higher colloidal silica concentration.

Micropyretic synthesis of both SiO_2-Al-C and Cr_2O_3-Al-C systems showed reaction incompleteness and highly porous structures. The conversion efficiency and porosity level were function of processing variables such as slip viscosity, solid loading and submicron powder concentration. The major phases, α-Al2O3 and β-SiC, in the composite produced with this new method were very homogeneously distributed within each other almost in the submicron scale.

The traditional micropyretic synthesis, powder pressing, was also performed for a few samples for comparison. 1430AT™ and polyethylene glycol were used as a binder and optimum pressure was 10,000 psi for the system studied. The results showed that lower porosity levels and more homogeneous structures were possible by using slip cast micropyretic synthesis.

2. LITERATURE REVIEW

Powder materials are formed into green shapes using different techniques which are dictated by several factors such as size, shape, microstructural requirements etc. In general, forming techniques can be classified as casting, plastic forming, and pressing and slip casting techniques have important place among them.

Forming process is usually followed by firing in which the loose mixture of discrete particulate phases into a dense homogeneous structure involves the application of numerous thermal treatments. The new emerging technology, micropyretic and/or combustion synthesis which has been mostly studied for compacted preforms, promises economic feasibility over the conventional procedures. The literature review will be given on micropyretic synthesis and slip casting in the following sections.

2.1. Micropyretic Synthesis

In chemical reactions that are sufficiently exothermic, the heat released is adequate to sustain the reaction of all reactants to completion. Such reacting systems have been extensively studied and utilized for various uses such as propellants, explosives and pyrotechnics since the discovery of black powder over 2000 years ago [1].

A significant amount of attention has recently been centered on the use of these types of reactions, commonly referred to as the self-propagating high temperature synthesis (SHS) method or simply as combustion (CS) and/or micropyretic synthesis (MS), for materials processing purposes. MS is characterized by self propagation of preformed mixture of reactants which are usually in powder form. Besides solid-solid reactions, solid-liquid [1,2] and solid-gas [2-5] reactions are also possible based on the variety of approaches that may give solid, liquid and gas products [1, 6-18].

After the initial published activities in Germany and USSR on adopting the MS method to produce materials, considerable interest has been stimulated elsewhere and programs have been initiated in Japan, the US and Poland [1]. Some of the claimed MS advantages over the conventional techniques include higher purity of the products, low energy requirement and the relative simplicity of the process [8-16].

In MS processing, preforms of the reactant mixtures can be prepared by conventional methods such as compacting. Then, the reaction is initiated by an external energy source. Once started at one end of the preform, the reaction can become self sustaining and a narrow zone of the reaction wave propagates throughout the sample at a certain rate by leaving behind the reaction product(s) as shown in Figure 2.1. This reaction mode, called wave propagation, is one of the most common mode in MS system in solid-solid highly exothermic reactions.

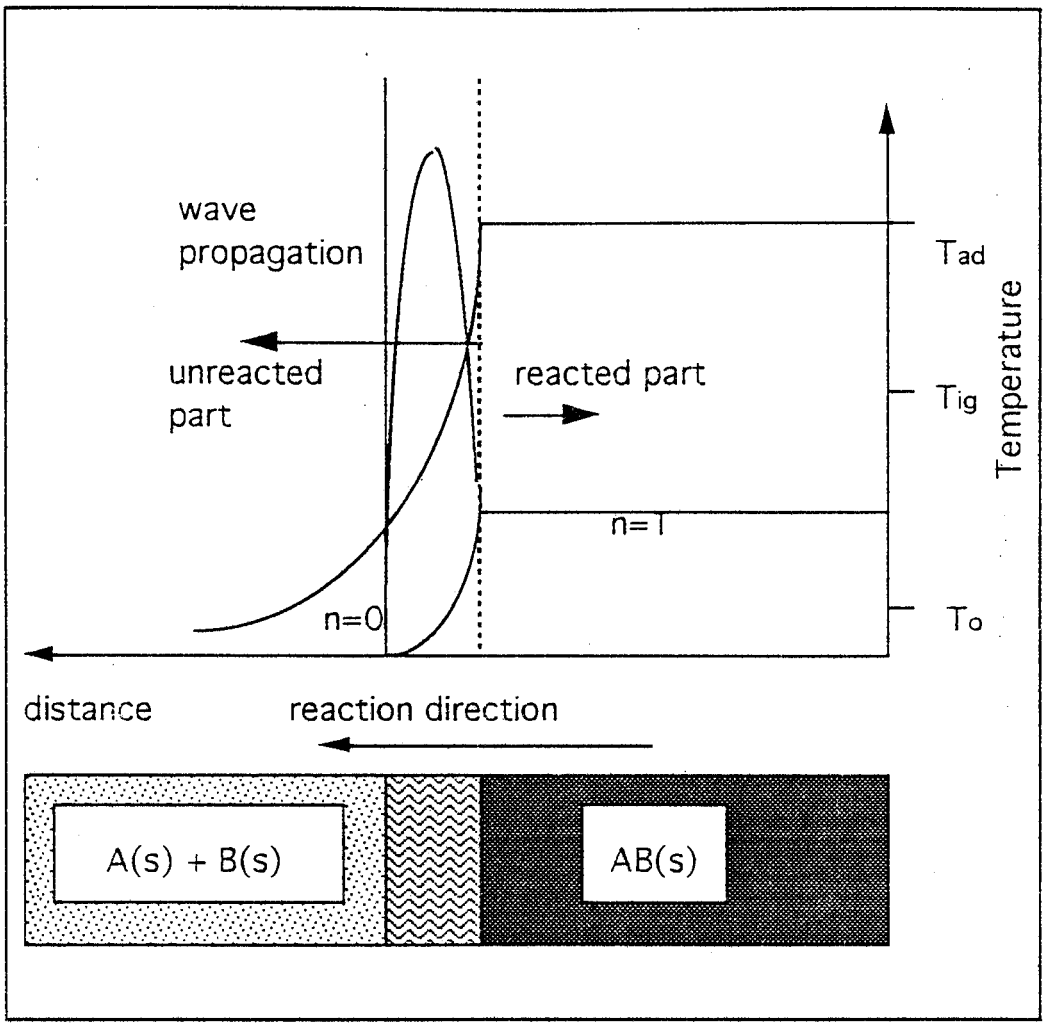

Figure 2.1. Schematic representation of the temperature, degree of conversion, and rate of heat generation in the combustion wave

Another approach, called thermal explosion mode of reaction, is used to synthesize relatively low exothermic reactions such as intermetallic synthesis [19-25]. It involves the heating of the entire sample up to the ignition temperature at which the reaction takes place simultaneously everywhere in the reactant mixture.

The reaction mechanism through heat generation and heat dissipation are a complex function of thermophysical properties of the reacting system and the processing variables such as reactant size, density and thermal environment.

Therefore an understanding of the parameters is critical involving the processing variables in order to obtain products with required properties and structures.

This review on MS will be concerned with the wave propagation mode and compacted systems in which the final product as well as the initial reactants are in the solid phase and the following pages will discuss both theoretical and experimental works in the literature.

2.1.1. The Micropyretic Process and Characteristics

MS is a process which utilizes the heat generated by an exothermic reaction. The heat released from the product formation, if exothermic enough, enables the reaction to propagate throughout the sample in the form of a combustion wave. The underlying thermodynamic principle for this process is basically dependent on the magnitude of the heat of formation.

As shown in Figure 2.2., the typical processing flow chart follows powder metallurgy procedures except for the sintering part.

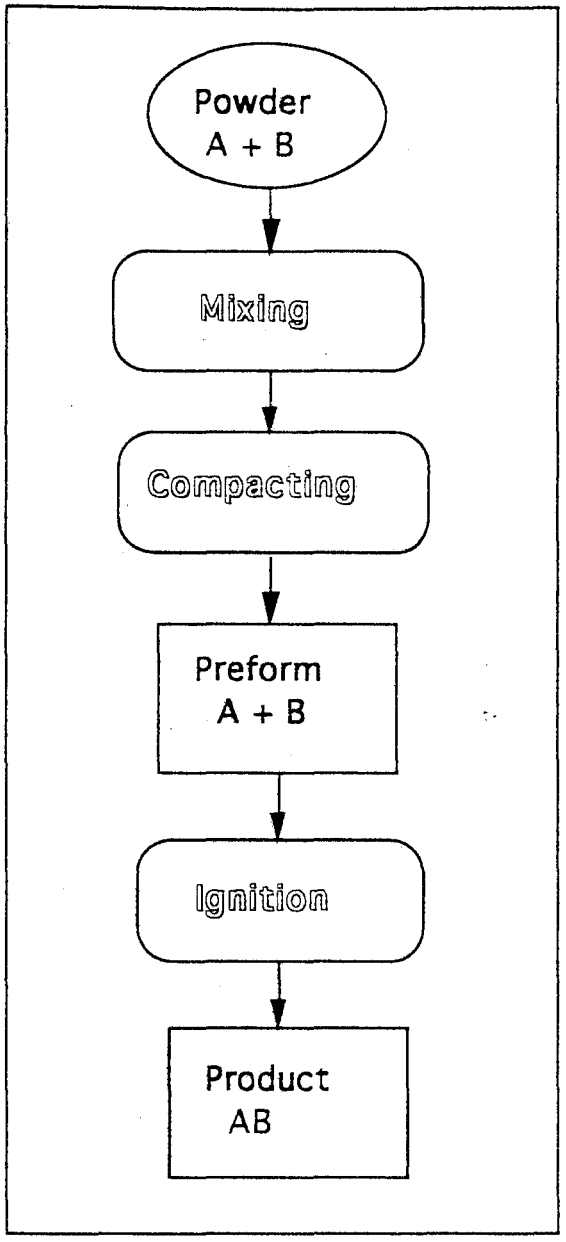

Figure 2.2. Schematic representation of MS processing flow chart

The MS processing starts with a porous compact of an aggregates of reactant particles and/or nonreactant diluents which are based on the required compositions. The reactants are typically

metals and/or transition element powders, powdered mixtures of metals and nonmetals or mixtures of a metal and a metal oxide with a nonmetal or nonmetal oxide.

After forming the compacted preform, reaction is usually initiated at an elevated ignition temperature, (Tig). Propagation of these reactions occur over a zone of about 0.1 - 5 mm in thickness with temperatures often in excess of 2000 °C and rapidly moving combustion fronts (e.g. 0.1 to 25 cm/s) [26-37].

Since propagation from local ignition is a basic aspect of these reactions, it is important to understand parameters controlling such propagation. While such reactions take place in powder compacts, ignition, propagation as well as product character, could be expected to depend on compact microstructures. In order to predict the dynamic behavior of MS systems under different operating conditions, detailed theoretical studies are required. Interest in this method of preparation stems from theoretical as well as practical considerations.

2.1.1.1. Advantages and potential applications

Since forcing by the competitive market to optimize materials and the processing techniques for the broad requirements of technology and society, in the recent years, research activities have been focused on high performance, cost effective and environmentally secure processing techniques.

There is increasing recognition that MS technologies may offer an important opportunity for material processing. As an alternative technique to the conventional fabrication methods, MS promises economic feasibility by conservation of time, energy and raw materials over the rest. It is also very versatile for a wide range of products. In addition to higher purity products, complex or metastable phases [8] and simultaneous formation and densification of the desired products [16, 22-25] can be obtained.

The simple and energy efficient nature of the process may save from costly complicated manufacturing processes and furthermore bring less hazardous environment. Higher purity of the products is the result of the high temperatures associated with the combustion wave along which volatile impurities can be removed. Also formation of metastable phases are possible because of high thermal gradients and rapid cooling rates.

Some disadvantages of MS may include presence of high defect concentrations, nonequlibrium phases [22]. Also large amount of

porosity can be generated by the process because of initial porosity in the reactant compact, volatilization of impurities or reactants and volume differences between reactants and product(s). Therefore additional steps such as active liquid metal exudation [1,5], hot rolling [26], hot pressing [27-31] and sintering [22,31] may be required. Also, the most energetic reaction involves high cost elements like B, Ti etc. In addition, the complex nature of MS is still not understood completely so that much development and uncertainty remains.

Regardless of the above, the MS process continues to generate interest because of current and potential applications. Its wide applications include

Abrasives, cutting tools and polishing powders [1,7,8]
Shape memory alloys [32,33]; TiN, TiPd
Structural alloys and refractory compounds [34-41]; TiAl, NiAl, TiB_2
Coating and welding [17, 42-44]; TiC, TiB_2
Composite fabrication [13,15,16, 45-49]; TiB_2-Cu,
Electrodes and heating elements [1,7,8]; $MoSi_2$, TiB_2

2.1.1.2. Thermodynamic considerations

MS depends on the magnitude of the enthalpy of formation [14,35] and requires relatively high adiabatic temperatures (Tad), to be self sustaining.

Depending on the heat of formation, extremely high reaction temperatures, commonly referred as combustion temperatures (Tc), can be obtained during the reaction. Since the reactions occur in a very short time, the heat loss can be neglected and the maximum combustion temperature (Tc) can be assumed to be the adiabatic temperature (Tad) [10].

By considering the reaction between a solid metal A(s) and a solid nonmetal B(s) to produce compound AB(s), the adiabatic temperature which characterizes the exothermicity of the reaction can be calculated from [14,35]

$$\Delta H^{o}_{T_o} = \int_{T_o}^{T_{ad}} C_p(AB)dT \qquad (2.1)$$

where $\Delta H^{o}_{T_o}$ is the enthalpy of formation of AB(s) at T_o=298 °K (Cal/g) and Cp(AB) is the heat capacity of the solid product (Cal/g °K).

A schematic representation of enthalpy with temperature for reactants and product is shown in Figure 2.3. Figure 2.4. shows the results of calculations of Tad for selected group of compounds [8]. It has been empirically concluded that reactions will not be self-sustaining unless $\Delta H^{o}_{T_o} / Cp_{T_o} \geq 2x10^3$ °K.

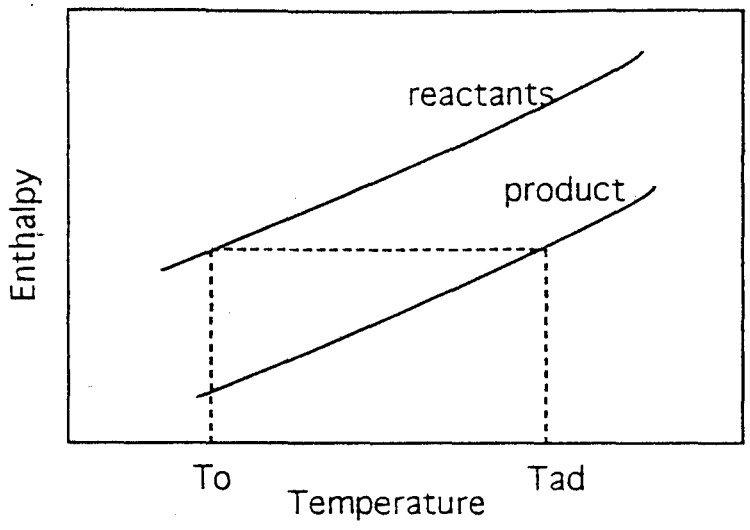

Figure 2.3. A plot of enthalpy as a function of temperature for an adiabatic micropyretic process

The latent heat of fusion and the specific heat capacity of the liquid product should be considered when the adiabatic temperature is greater than the melting temperature of the product.

Measurements of both the maximum combustion temperature [21,37,50] using thermoelectric methods and the heat of formation [51-54] using calorimeter have been done experimentally.

There is lack of agreement between the adiabatic temperature and the experimentally observed combustion temperature values. The calculated adiabatic temperature values are essentially upper limits [10] and can be used as a useful design criteria. The main differences to this lacking agreement are because of assumption incorporated into the theoretical model, strong dependency to processing variables and limitations of measuring techniques.

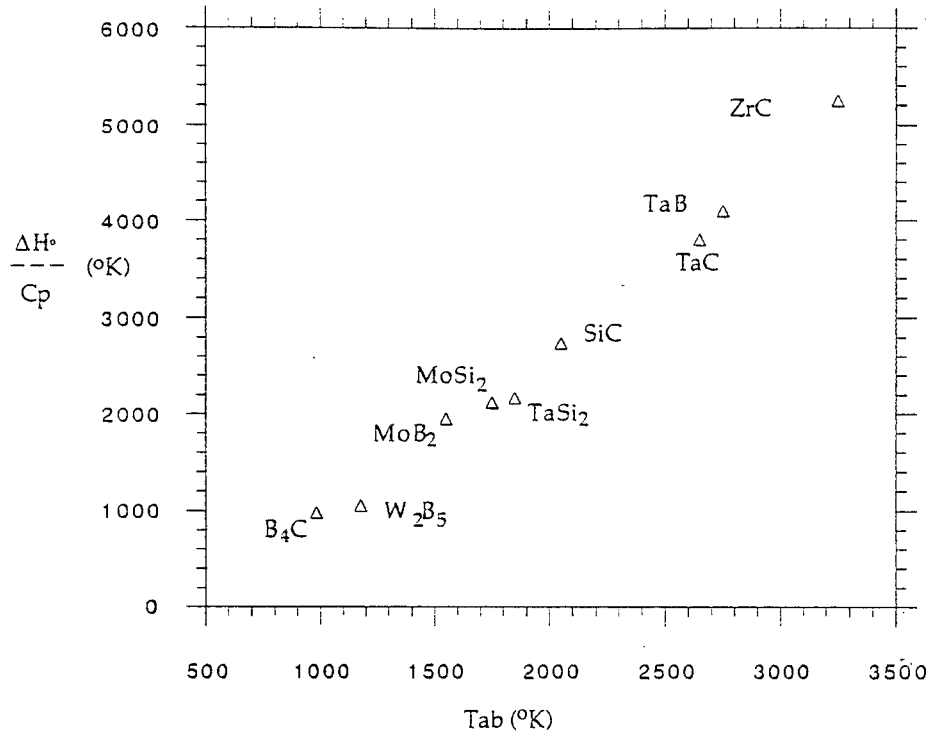

Figure 2.4. Relationship between ΔH^{o}_{To} / Cp_{To} and the adiabatic temperature for selected compounds [8]

2.1.1.3. Processing parameters

The engineering properties of MS components and nature of the reaction are affected by the large number of processing variables that can be classified as material parameters and fabrication technique parameters. The effect of some of these variables on combustion velocity and temperature are given in Figure 2.5. [10].

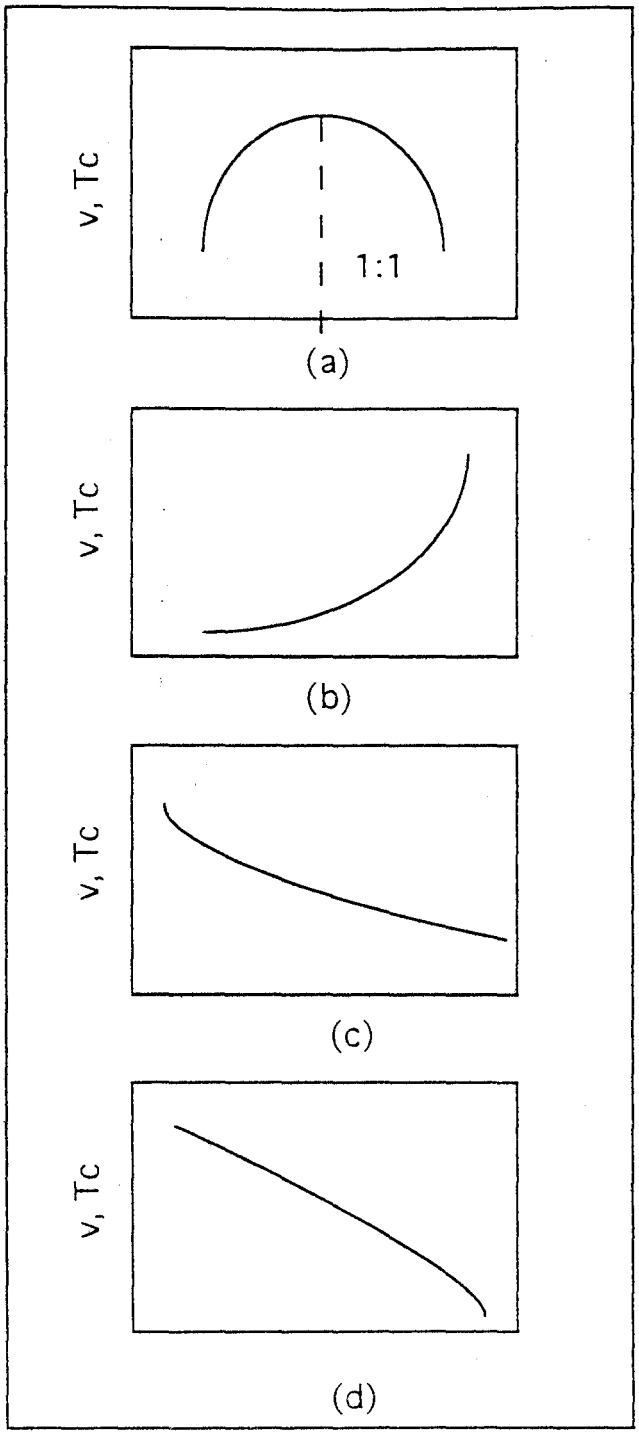

Figure 2.5. Effect of (a) stoichiometry, (b) preheating temperature, (c) particle size and (d) amount of diluent on propagation rate, v and combustion temperature, Tc [10]

2.1.1.3.1. Material parameters

Powder characteristics like size, shape, composition and structure strongly influence the nature of reaction and component properties. Some previously reacted products may also be added as a diluent to the unreacted powder mixtures to slow down the reaction and/or fabricate composite [8,10].

Since the powder particle size and shape determine the diffusion distances, they play a significant role in MS processing. In general, it is desirable to have a broad distribution of particle sizes in the blend because the smaller ones may fill voids among larger ones by increasing packing density and material properties.

Various investigations have been carried out to study the effect of the reactant size. Studies on the Ti +C and Ti + 2B systems showed that the reactant size determines the propagation rate, the degree of reaction completion and the nature of the product [11, 55-57].

Powder purity and structure should also be considered. Undesirable elements should be minimized since readily oxidizable element or oxide layers on particle surfaces can form diffusion barriers which impede the interdiffusion process. Hard particles may also make the compaction process difficult.

2.1.1.3.2. Fabrication techniques and related parameters

The kinetics of solid state reaction are dependent on the homogeneous dispersion and the effective contact area of the reactants. Therefore, mixing, compacting ways, ignition and thermal environment conditions are critical steps in the process.

Studies on the effect of the compact density [8,26,55,56] were carried out in various investigations. It was concluded that there could be an optimum limit for pressurization as shown in Figure 2.6. and HIP [26,27,31] could be useful technique to obtain dense MS product. Rice et al. [26] have investigated titanium based reactions to study the effect of the compact density on micropytretic synthesis. It was found that the maximum propagations rates were at approximately 60% (±10) of theoretical density of the reactant compacts. However, as the density of the reactant compact is further increased, the surrounding unreacted powder provides a high thermal conductivity path to remove heat from the reaction zone. The effect of the thermal environment, ignition ways and different initial preheating temperatures were studied by Yi et al. [10,20]. They investigated the effect of TiO_2 formation on the TiNi synthesis as shown in Figure 2.7. It was found that prior TiO_2 formation triggers the TiNi reactions. They also concluded that higher preheating temperatures lead to higher combustion velocities and temperatures for NiAl and CuAl reactions.

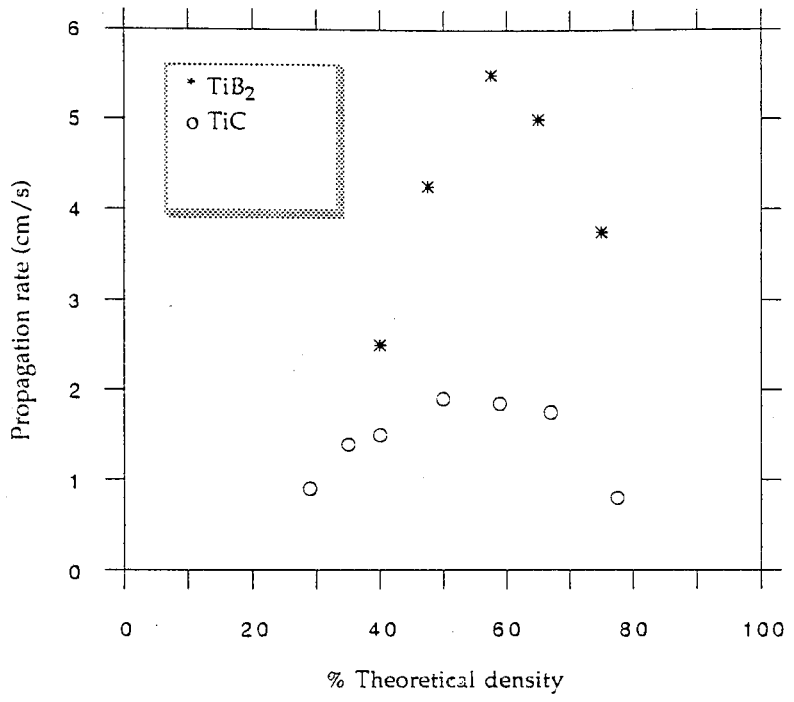

Figure 2.6. Propagation rate vs percent reactant density [26]

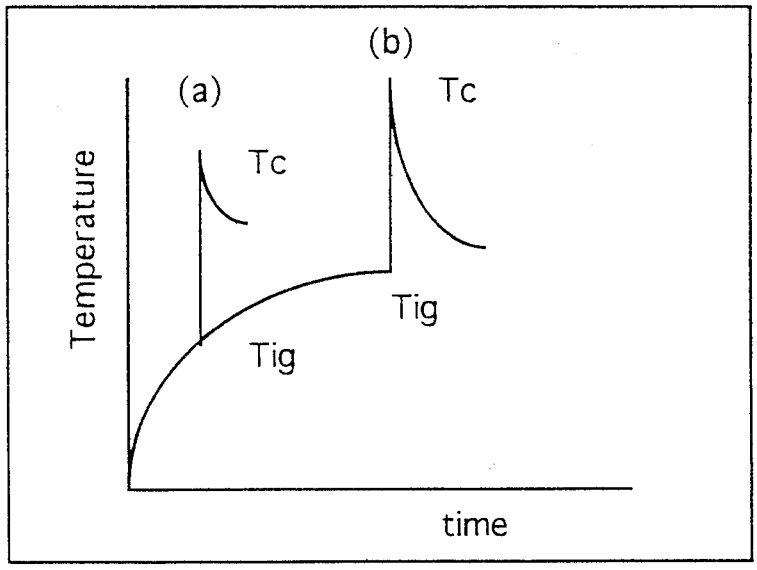

Figure 2.7. Comparison of temperature vs time plots for the combustion reaction conducted in (a) air and (b) argon at the same furnace temperature [20]

2.1.2. Micropyretic Theory and Reaction Mechanism

Properties of combustion wave which is characterized by chemical reactions leading to heat generation with accompanying heat and mass transfer is one of the common mode for a MS reaction. The reaction mechanism through heat generation and dissipation is dictated by thermophysical and heat transfer criteria. As it was mentioned before, these criteria are determined by processing variables.

Since so many parameters involved in the reacting system are co-correlated, it makes difficult to deal with a detailed analysis of model covering whole system. As temperature in the combustion wave changes and a significant chemical conversion is obtained, the material properties vary widely which bring additional difficulties to analysis. In order to predict the dynamic behavior of MS under different processing conditions, detailed theoretical and experimental studies are still required.

Depending on the reacting system parameters, the combustion wave propagations are generally divided into two main classes [23,58], namely homogeneous (steady) and heterogeneous (non-steady) wave forms which lead to structural and property differences in the product.

In homogeneous form of combustion, the temperature and species concentration remains uniform throughout the process and

the combustion wave advances through the reactants at the same velocity and narrow reaction zone as shown in Figure 2.1. However this narrow reaction zone may changes with the activation energy of the system. In other words, wider reaction zones are possible in the reactions which have strong kinetic control [8].

On the other hand, there are both thermodynamic and kinetic reasons which provide the basis for departure from the homogeneous conditions [50, 59-65]. While thermodynamic reasons basically come from the extent of exothermicity of the reaction, kinetic considerations may arise from incomplete reactivity caused by the diffusion barriers, particle size, density and size of the compacted preform, structure and property changes in the reaction zone etc.

The instability of the combustion wave, which leads to the transformation from homogeneous to heterogeneous state, can bring ultimately to the extinction of the combustion. Since instability can come about from insufficient heat generation, weakly exothermic reactions are prime candidates for extinction [11].

In the case of heterogeneous form of combustion, the reactions and heat generation often occur at the phase boundary or in several phases and may be accompanied by phase transition [65]. The rate of heterogeneous form is usually limited by transport phenomena and shows a oscillatory or spin type [8,12,58] nonuniform propagation velocity which causes nonuniform structure and property. In such a case, the heat evolution is not uniform throughout the volume, but

takes place in local regions where the product layer forms, as the components are mixed. The product is formed at the interface and for further reaction the reactants diffuse through the product layer and react, leading to increase in the layer of the product [63,66].

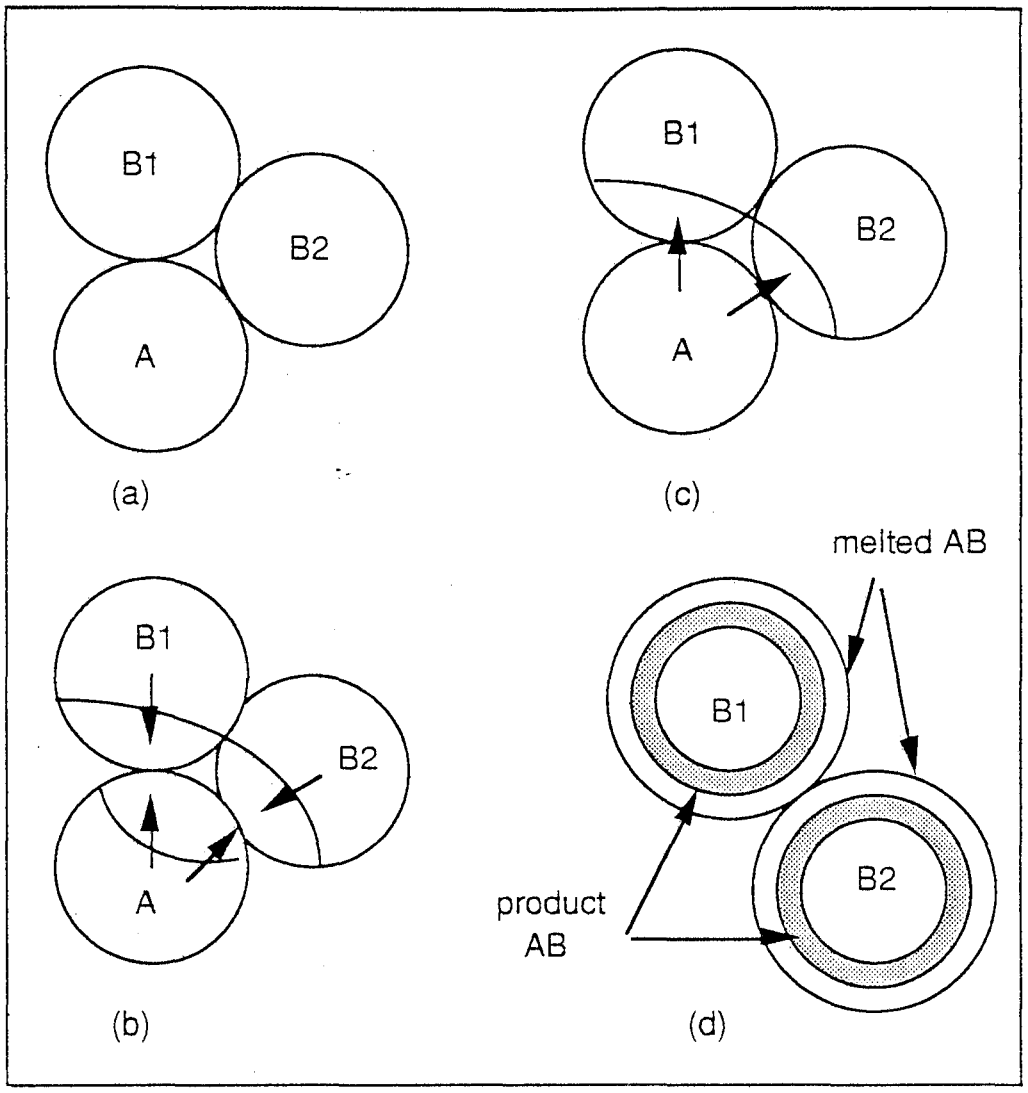

Figure 2.8. Sketches of reactions between particles (a) before reaction, (b) with approximately equal interdiffusion of A and B, (c) A is the only diffusing species and (d) A melts and reacts with B

Possible phase transformation in the reacting system can also affect the combustion form. In most cases, melting of the reactant takes place and once the melting of the low melting component takes place, interdiffusion as well as reaction between the components can occur as shown in Figure 2.8. However the nature of the reaction and hence the propagation velocity will depend on the rate limiting step [66-68]. If the time for diffusion is not a rate limiting step, the reactants are able to interdiffusion and the reaction proceeds homogeneously in the kinetic regime. On the other hand, the reaction becomes heterogeneous and takes place in the diffusion regime if the reaction time less than the interdiffusion time. The theory of heterogeneous combustion wave propagation form involves various complication and is needed to be developed separately for different types of system [65]. The most extensively studied micropyretic process is the homogeneous mode of combustion because it is relatively less complicated and furthermore, for uniform structure and property, especially material processing, homogeneous combustion mode is essential. Therefore, designing the MS systems are needed to be optimized by altering the heat generation and dissipation processes which can be accomplished experimentally through a variety of ways. However, a more complete description of the nature and systematic approach to design of MS systems are still in its infancy. Lack of basic physico-chemical data describing the reacting systems as well as detailed information on reaction kinetics at elevated temperatures does not allow for a quantitatives description of the dynamic behavior of MS systems [46,65,69].

2.1.2.1. Propagation velocity

The study of a homogeneous combustion mode and the determination of conditions under which it is realizable is the principle concern of MS wave propagation theory.

The homogeneous propagation is the result of local initiation of the reaction in a reactant capable of net exothermic reactions whose rate rapidly increases with temperature.

By assuming the thermophysical properties are not strong functions of temperature and also, convective and radiative heat losses are negligible, the equation for the energy balance with a stationary reference frame for a reacting system at which the combustion wave moves in the directions of the coordinate, x, with a constant velocity, v, can be given by [62,70,71]

$$Cp\,\rho\,\frac{\partial T}{\partial t} = K\,\frac{\partial^2 T}{\partial x^2} + q\,\rho\,\frac{\partial f}{\partial t} \qquad (2.2)$$

where Cp is the heat capacity (Cal/g°K), ρ is the density of the product (g/cm^3), K is the thermal conductivity of the product (Cal/cm°Ks), q is the heat of reaction (Cal/g), v is the wave velocity (cm/s), T is the temperature (°K), t is the time (s), x is the dimension along which the wave is propagating (cm) and f is the fraction reacted ($0<f<1$).

Since [62,70,71]

$$\frac{\partial f}{\partial t} = K_o\ (1\text{-}f)^n\ \exp(-\frac{E}{RT}) \qquad (2.3)$$

where Ko is pre-exponential factor, R is gas constant (Cal/g ^oK), E is activation energy (Cal/g), n is the reaction order.

Then equation (2.2) becomes [62,70,71]

$$Cp\ \rho\ \frac{\partial T}{\partial t} = K\frac{\partial^2 T}{\partial x^2} + q\ \rho\ K_o\ (1\text{-}f)^n\ \exp(-\frac{E}{RT}) \qquad (2.4)$$

The solution of equation (2.4) utilizing Arrhenius kinetics, an expression for the velocity of propagation of the combustion is given in the following form [72-75]

$$v^2 = f(n)\ \frac{K}{q\rho}\ \frac{RT_c^2}{E}\ K_o\ \exp(-\frac{E}{RT_c}) \qquad (2.5)$$

where f(n) is a function of the kinetic order which have been calculated for a variety of assumed kinetic processes [8].

However equation (2.5) does not take into account explicitly the effect of the reactant particle size and also ignores heat losses and the possible phase transformation.

The improved expression for the velocity were derived by considering the thermophysical and chemical properties of all product and the reactants [76].

$$v = \sqrt{\frac{1}{f\left(\frac{\rho q}{K}\right)} K_o \left(\frac{RTc^2}{E}\right) \exp\left(\frac{-E}{RTc}\right)} \qquad (2.6)$$

where

$$f\left(\frac{\rho q}{K}\right) = A + B \ln\left(\frac{K_{(r)}}{K_{(u)}}\right) \qquad (2.7)$$

with

$$A = \left(\frac{3\overline{C\rho}(Tc-To)-0.5q(\rho^{(r)}-\rho^{(u)})}{3(K_{(r)}-K_{(u)})}\right) + \left(\frac{(0.5qK_{(u)}(\rho^{(r)}-\rho^{(u)})-q\rho^{(u)}(K_{(r)}-K_{(u)}))((K_{(r)}-K_{(u)})-2K_{(u)})}{2(K_{(r)}-K_{(u)})^3}\right)$$

$$B = \left(\frac{(0.5qK_{(u)}(\rho^{(r)}-\rho^{(u)})-q\rho^{(u)}(K_{(r)}-K_{(u)}))K_{(u)}^2}{(K_{(r)}-K_{(u)})^4}\right) - \left(\frac{3\overline{C\rho}(Tc-To)K_{(u)}}{(K_{(r)}-K_{(u)})^2}\right)$$

$$\overline{C\rho} = 0.5(\rho^{(u)}Cp_r - \rho^{(r)}Cp_u) + 0.33[(\rho^{(r)} - \rho^{(u)})(Cp_r - Cp_u)]$$

where the parameters with the subscripts, (r) and (u), represents reactant(s) and product(s) respectively.

2.1.2.2. Wave characteristics

As mentioned before, the combustion can be changed from one form to other when related parameters change. Many theoretical attempts to explain this phenomenon have been developed.

The results showed that the neutral boundary between homogeneous and heterogeneous form can be defined in terms of the parameter, α, given by [77,78]

$$\alpha = \frac{RT_c}{E}\left[\frac{9.1C_pT_c}{q} - 2.5\right] \qquad (2.8)$$

It is concluded that, according to equation (4), homogeneous combustion form is attained if $\alpha \geq 1$ [77,78].

The nature of heterogeneous combustion depends on the value of the stability parameter, α. As α approaches to 1, the pulses are almost sinusoidal with peaks in temperature and velocity, followed by depression in temperature and velocity. At regions further away from stability, the oscillations become more complex with a number of peaks in each cycle as shown in Figure 2.9 (b).

It was also showed that heterogeneous combustion can be obtained if $(\rho C_p K)_{reactants} > (\rho C_p K)_{products}$ [76].

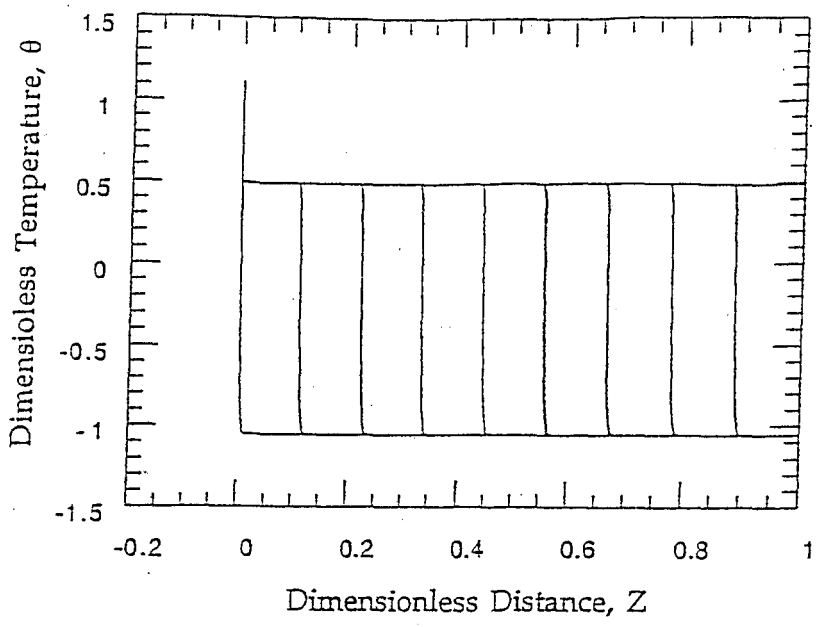

(a)

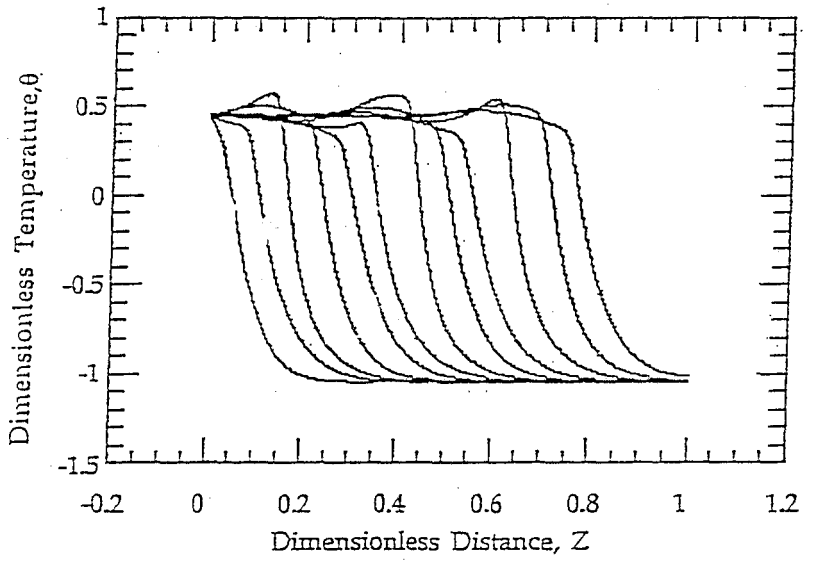

(b)

Figure 2.9. Results of numerical solution of combustion problem (a) homogeneous combustion and (b) heterogeneous combustion [87]

2.1.2.3. Theoretical and experimental studies

The question of the stability and mechanism of combustion has been examined both experimentally and theoretically. In most of the analysis, homogeneous reaction is assumed where the reaction rate is give as in equation (5). For a system satisfying equation (5), the plot of ln(v/Tc) against 1/Tc gives a straight line with a slope equal to E/2R, from which the activation energy for the micropyretic reaction can be obtained. This technique has been used to determine the reaction mechanism for various systems [8, 35, 50, 82, 86].

The theoretical investigations of stability in MS systems for homogeneous mode which in turn have the advantage of admitting on explicit representation of the basic solution that is undergoing a change of stability have been obtained based on equation (4) [62-92]. Numerical solutions of equation (4) have been given for the homogeneous wave propagation and stability problem in condensed phase system [62,76].

Another case that has been studied is the combustion of a heterogeneous system when the components react through solid [63-66] and liquid [67,68] product layer. Analysis of reaction mechanism in the presence of melting has been done by Okolovich et al. [67]. Their model comprises of particles of high melting component distributed among the finely dispersed particles of low melting component. Initially in the preheating zone the particles of one kind melt and spread out uniformly between the particles of the less

fusible component. When the temperature at which the particles of second component melt is reached, interdiffusion of the reactants and their chemical reaction with the formation of a liquid product. They have found out that the starting particle size leads to a significant change in the structure of the combustion front at which an increase in particle size causes to a decrease in the combustion rate.

Neksarov et al. [68] analyzed a similar system to determine how capillary spreading of the molten component over the infusible component affects the combustion wave propagation. Depending on the ratio of volume of the product and the reactants, complete and incomplete conversion of the material in the course of the combustion may appear in the capillary regime. In the incomplete case, as the liquid metal spreads, the metal reacts with the pore wall and the product layer is formed. If the volume of the product is more than volume of the reactants, the layer of the product reduces the pore radius and therefore the flow rate of the liquid metal. Finally the pore may be blocked before the spreading is completed. The combustion rate is related directly to the pore radius and inversely to the particle size. In other words, the combustion rate increases with increasing the reaction time and decreasing the spreading time.

In conditions of complete conversion, since the volume of the reaction product is equal to the volume of the finely disperse reagents, the pore radius remains unchanged throughout the process,

Therefore, in this case, the liquid metal may spread without obstruction until complete conversion is reached. This means that the combustion rate is not dependent on the rate of chemical reaction and is determined mainly by the characteristics of capillary spreading.

In order to confirm this analysis reactions were experimentally carried out for the Ti + C system for different Ti particles and different ignition temperatures for the reactions [37,68,78]. Their results indicate that the velocity, measured with a photorecorder, decreases with increasing particle size. At larger particle sizes, the velocity shows no dependence on the initial temperature, whereas at lower radii, there is an increase in velocity with increasing temperature. These results were experimentally confirmed by Dunmead et al. [37]. They also concluded that at high combustion temperatures, TiC was formed by dissolution of C into liquid Ti and TiC was subsequently precipitated out of solution. On the other hand, at lower combustion temperatures, TiC formation occurs via a carburization type process, where a TiC layer forms around the carbon particles, and further TiC formation to occur, C must diffuse through the product layer.

Recent models and numerical solutions have been directed to detailed analysis of the problem including phase transformations, heat transfer, solidification of the product etc. Puszynski et al. [86] have developed the criteria for stable, unstable and degenerated

combustion, as well as the approximate relations for the velocity of a steady state profile as a function of the heat transfer coefficient.

The case of a phase change leading to a change in the combustion kinetics during the melting of a reactant phase has been considered by Morgolis [69]. Also he has showed that several oscillatory modes of combustion may manifest during the condensed phase micropyretic process.

Recently, Laksimikanta et al. [87] have developed a numerical method of solving the combustion problem by considering provisions for solidification of the product. It was concluded that oscillations can be obtained if thermal activity of the reactants (ρCpK) is more than thermal activity of the product as shown in Figure 2.9.

Experimental in-situ observation of reaction mechanism in the presence of melting has been carried out by Alexandrov et al. [58,84]. Interaction between the reactants in the form of one reactant powder lying in a film of another reactant was observed using an electron microscope. The reaction is initiated by stepped heating of the sample using a high intensity electron beam. They observed that for the system studied, melting of one of the component takes place and the primary product is formed at the interface. Once the primary product reaches a certain thicknesses, the thickness remains constant. At the product-liquid interface dissolution of the primary product occurs and at the product solid interface growth into the solid takes place.

The possibility of obtaining new materials with unique properties and the ability to produce composite materials from cheaper raw materials have provided considerable incentives for increasing the research effort in MS technique.

The main attractiveness of the MS as a process for synthesis of materials are concerned with improvements in process such as the energy savings associated with the use of self-sustaining reactions, simplicity of the process and the possibility for producing high purity products.

However, achieving high product density and tight control over the reaction and product are likely to be a common challenging problems of the processing.

The complex nature of MS and lack of basic physico-chemical data related to the MS systems as well as detailed information on reaction kinetics at high temperatures are still the limitations of a more complete analysis and systematic approach to design of MS systems.

2.2. Slip Casting

The casting of ceramics is usually done by a room temperature operation in which ceramic particles suspended in a liquid, usually water based are cast into a porous mold which removes the liquid and leaves behind a particle compact. The process is commonly called slip casting. The main requirements are ease of formation and good green strength, followed by high strength after firing with little shrinkage.

Slip casting can be used to fabricate shapes that would normally be difficult or impossible to make other processing methods. Typical processing flow chart is shown in Figure 2.10. The process can produce either a solid object or a hollow objet.

There are many advantages of slip casting which makes possible to form thin walled and complex shapes with relatively low capital investment [93-96]. In slip casting, the slurry is poured or pumped into a permeable mold having a particular shape. Gypsum which is hydrated calcium sulfate is commonly used as a permeable mold material with 40-50% porosity [94]. The solids into a cast adjacent to the wall of the mold are concentrated by capillary sanction and filtration through the mold. There are two types of casting modes, solid casting and drain casting. In solid casting, casting is allowed to continue until a solid cast, having the shape of

the mold cavity, formed. Alternatively, the casting interrupted after forming desired wall thickness is called drain casting.

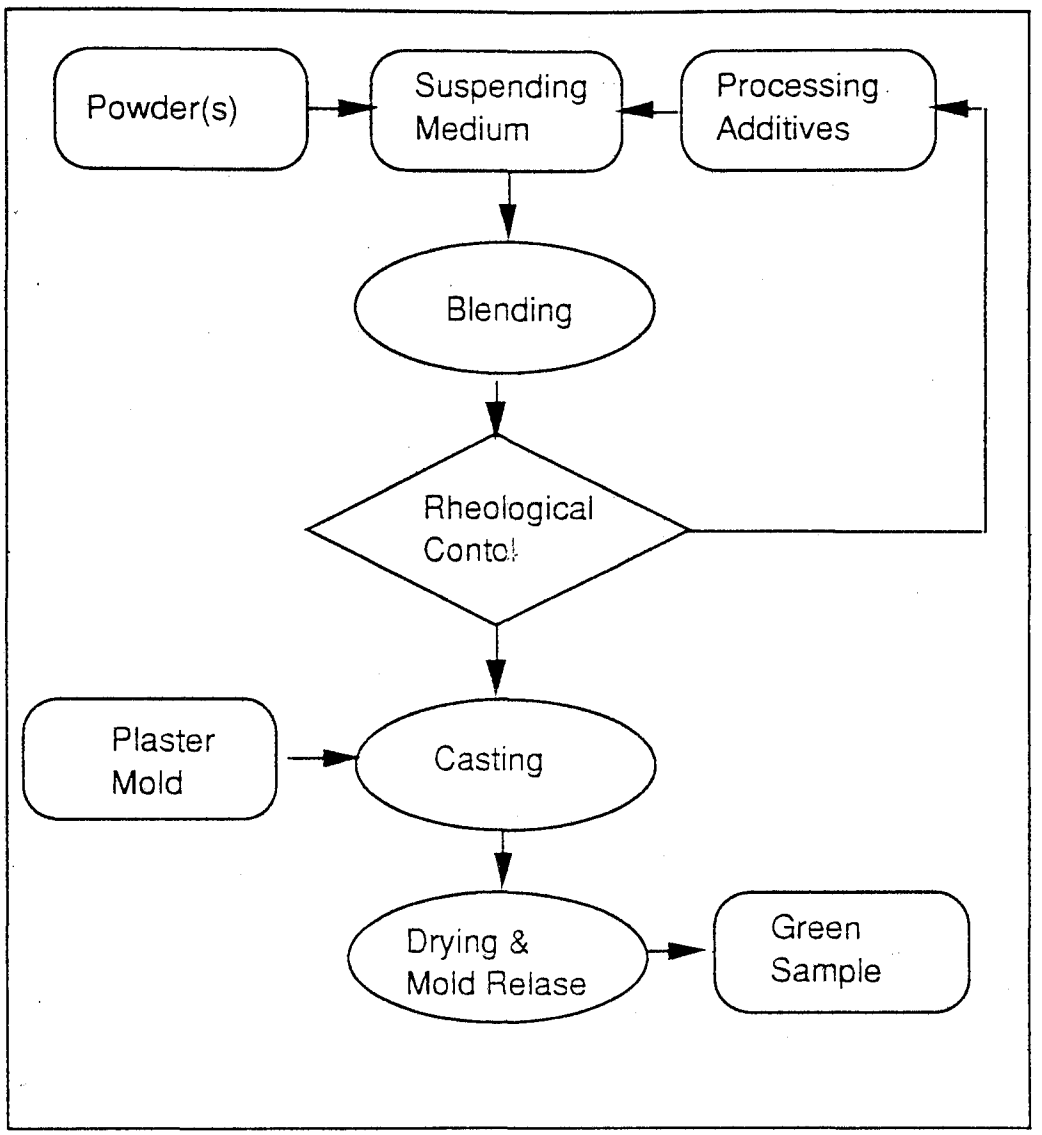

Figure 2.10. Schematic representation of slip casting flow chart

After casting, the cast material is allowed to dry in the mold to provide adequate strength for handling. Some shrinkage occurs in this step and semi-hard solid object is removed from the mold.

2.2.1. Slip Characteristics

Slip casting is considered a diffusion controlled process by which the mold draws liquid from the slip. The cast has a higher moisture stress than adjacent slip and will draw liquid from the slip and transfer it to the mold. The slurry rheology, the casting rate, the cast density and shrinkage are significant factors in processing of slip casting [93-100]. These parameters are mostly function of particle size and distribution, degree of deflocculation, and kind and amount of colloids.

Slurries containing liquids, solids and other processing additives may be prepared in a variety of mixers. Mixing time is dependent on type of mixer used and slip characteristics. Viscosity of casting slurries are formulated low enough for convenient mold filling and escape of bubbles. The viscosity is usually less than 2000 cps at a shear rate of 1-10 sec^{-1} in slip casting [94]. The slurry density should be high enough during the time necessary to make a casting to minimize particle settling in the suspension. The mold material porosity and strength, gypsum formed from the reaction between plaster of paris and water, depends on water/plaster ratio. Higher ratios increase absorption of water and lowers the strength of the mold [94]. Casting time may range from a few minutes to several hours depending on the process. In solid casting, voids due to shrinkage can be eliminated by risering. The excess slurry must drain readily from the surface of the cast, but

the cast must be relatively rigid in drain casting. Separation of the piece normally occurs from the shrinkage on drying.

2.2.1.1. Processing additives

a) solid phase: The solid phases of casting slips can be classified as clay based, refractory oxide, cermets, and powdered materials. Although most slip casting is done with clay slips, the slip casting process is important in the production of complex shapes from a wide variety of prereacted ceramic powders, refractory oxides, cermets, and powdered metals.

Particle size may vary over a wide range depending upon the density of the material and the desired characteristics of the cast product. Generally, the more extended a particle size distribution is, the greater the fluidity of the slip at high solid loadings [101-105].

b) liquid phase: The liquid phase should have relatively low vapor pressure, compatibility with suspended solids, low viscosity, cheap, nontoxic etc. For most slip systems, Distilled or deionized water is used as the liquid phase. Organic liquids may be used but they violate most of the requirements listed above. Their use may be imperative when casting materials that react with water [97].

c) deflocculants: Additives to deflocculate slurries achieve dispersion by absorbing onto and altering the particle surfaces.

Slurries which have not been deflocculated settle rapidly and the for same solids loading have higher viscosities. The solution above the sediment is clear because all the particles, large and small, have rapidly fallen out together. In a well dispersed suspension, the sediment is formed slowly with a high packing density and is more difficult to redisperse.

A number of commercially available deflocculating agents are widely used in slips such as sodium carbonate, silicate borate and phosphates, sodium and ammonium polyacrylates [97, 100, 106-107]. In general, acids and basics are frequently used to adjust deflocculation and pH is used as a control test.

d) binders: Cast products sometimes has poor green strength and it may be necessary to add a binder. Additives to a slip system perform various functions and may behave as rheological aids altering flow, as thickeners that increase the apparent viscosity, as suspension aids capable of retarding settling, and ultimately as a binder imparting green strength in the final body.

Some binders are organic such as natural gums, cellulose ethers, polymerized alcohols, waxes, glycols etc and provide only temporary strength. They have relatively high molecular weight and work by absorbing onto the surface of particles and bridging them together. Others are inorganic such as colloidal particles which may leave residue after firing.

Since viscosity depends on the interaction of molecules in a solution, the size, shape and concentration of binder molecules affect the viscosity of the system. The viscosity may greatly change if a thermal or chemical change in the system occurs as in the case of gelation. Gelation occurs when the molecules cross link into a three dimensional configuration and the solution behaves more like a solid than a liquid.

2.2.1.2. Colloid principles

In slip casting the rheology of particulate suspensions in liquid phase plays a major role. Their colloidal properties are especial significance in the process of slip casting. The structure of the slip, as determined by its degree of dispersion, has also to be controlled by suitable additives. Particle size for slip casting may range from of coarse materials as large as 1 mm to 10^{-3} micron at the lower limit of the colloidal region.

As particles are made smaller, there is a rate change in certain important size related physical properties; for example, the specific surface increases, the diffusion rate increases, the sedimentation velocity slows, the coagulation rate increases, and the solubility increases [108-111].

An important characteristic of disperse system is the large area of the interface between the particle and the surrounding medium, with the consequence that a significant proportion of the

molecules are associated with the micro heterogeneous regions which form the interfaces between the dispersed phase and the dispersion medium. Since the contributions which these molecules make to the thermodynamic properties of the system are different from those made by the ones within each of the bulk phases, the presence of the interface affects the overall thermodynamic state of the system and in particular the free energy [108] which is function both of the surface tension, σ and of the interfacial area, A_i

$$G = \sigma A_i \qquad (2.9)$$

It is clear that a colloidal dispersion represents a state of higher free energy than that corresponding to the bulk material. Passage to a state of lower free energy will therefore tend to occur spontaneously unless there is a substantial energy barrier preventing the elimination of the colloidal state. In the presence of such a barrier the system will be metastable and may remain in that state for a very long time. On the other hand, if conditions are adjusted so that the energy barrier becomes negligibly small or disappears altogether, then the colloid becomes unstable. Thus the whole question of the preparation and stability of colloid system is closely tied with the factors that give rise to free energy barriers of adequate height to prevent the breakdown of colloidal state.

In the case of colloid dispersions the energy necessary to carry a system over the energy barrier comes from the Brownian motion of the particles which results from the random bombardment

of the surface of the particles by molecules of the medium. A situation peculiar to colloid system is that in which the free energy curve has the form of Figure 2.11.

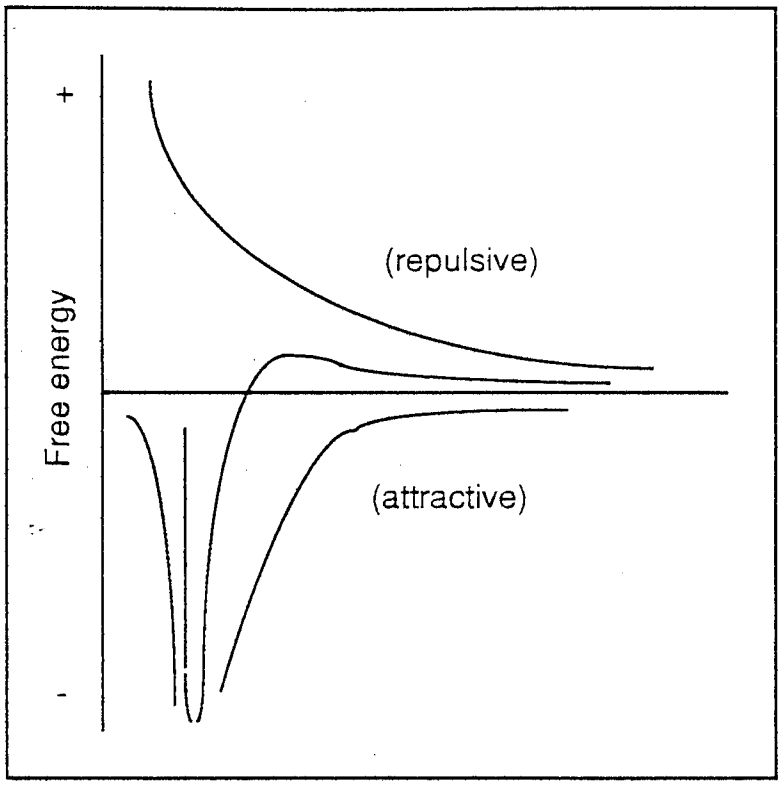

Figure 2.11. Free energy curve for the colloidal system [108]

The apparently random stepwise or zig-zag movement of colloidal particles was first observed by Robert Brown and named after him [108]. Brownian displacement of particles in slip is of particular importance in particle size determination and with respect to coagulation kinetics of suspensions. When a particle is small enough, collisions with individual fluid molecules can displace the particle by measurable amounts. This displacement results in

the random motion of particles and in addition to the external forces such as gravity.

The mean Brownian displacement, X of a particle from its original position along a given axis after time, t given by [108]

$$X = \sqrt{2Dt} \qquad (2.10)$$

where D is diffusion coefficient. The work done in moving a particle through a distance dx against a frictional resistance, Fr due to motion is related to the diffusion coefficient by [108]

$$DF_r = kT \qquad (2.11)$$

where k is the Boltzman constant and T is the absolute temperature. The value of Fr depends upon particle geometry and for a system containing spherical particles of radius, r [108]

$$F_r = \frac{6\pi\eta rN}{R} \qquad (2.12)$$

where R is the gas constant, η is viscosity, r is particle radius and N is Avogadro number.

Figure 2.11. indicates that under certain circumstances the mutual free energy curves of colloidal particles may exhibit a maximum so that when the particles approach the free energy

increases initially, i.e. the particles repel one another, until at the maximum in the curve this repulsion changes over to an attraction.

There are various factors which contribute to the shape of interparticle free energy curves and hence control the stability of dispersion.

(i) intermolecular forces: The existence of attractive forces between non-polar molecules has been recognized since the work of van der Waals. According to the theoretical equations, these attractive forces increase in magnitude as the molecules approach one another, and at a separation of r between the nuclei of the system or the center of mass of roughly spherical molecules they are proportional to the inverse power of the separation. If we choose the energy at infinite separation as the energy zero, then the free energy of attraction between a pair of atoms or molecules at separation d [108]

$$\Delta G^{att} = - \Delta W = - \frac{A}{d^6} \qquad (2.13)$$

The constant A is given by London [108] in the form

$$A = \frac{3}{4} h \psi a^2 \qquad (2.14)$$

where a is the polarisability of the atom, h is Planck's constant and ψ is a characteristic frequency identified with that corresponding to

the first ionisation potential. As the atoms approach one another, the attractive force increases and the free energy becomes increasingly negative. However, at close distances their electron cloud begin to interact. If the electrons are in non-bonding orbitals, this gives rise to a repulsive force and an increase in free energy which becomes effectively infinite when the electron clouds interpenetrate [108].

$$\Delta G^{rep} = \frac{B}{d^{12}} \qquad (2.15)$$

The total potential energy of interaction between a pair of atoms or molecules is assumed to be the sum of the contributions from attractive and repulsive [108]

$$\Delta G = \Delta G^{rep} + \Delta G^{att} = \frac{B}{d^{12}} - \frac{A}{d^{6}} \qquad (2.16)$$

(ii) <u>electrostatic forces</u>: Particle surfaces become electrically charged by variety of mechanisms the more important of which are the following;

a) Ionization of surface groups
b) Differential solution of ions from the surface of a sparingly soluble crystal
c) Isomorphous substitution
d) Charged crystal surfaces
e) Specific ion absorption

The fundamental law of electrostatic expresses the inverse square law of force between two electric charges q1 and q2 separated by a distance d [108]

$$F = \frac{q1q2}{4\pi ed^2} \qquad (2.17)$$

where e is the permittivity of the medium surrounding both charges. The work done in bringing two charges together from infinite separation to a distance d is therefore given by [108]

$$\Delta G^{el} = \Delta W = \int_{\infty}^{d} Fdh = \frac{q1q2}{4\pi ed} \qquad (2.18)$$

and measures the electrical free energy of the system relative to that at infinite separation. The charge q1 may be thought of as producing an electric field at a point d, such that the work needed to bring a unit charge to this point is $\frac{q1}{4\pi ed}$ which is called the electrical potential at d due to the charge q1.

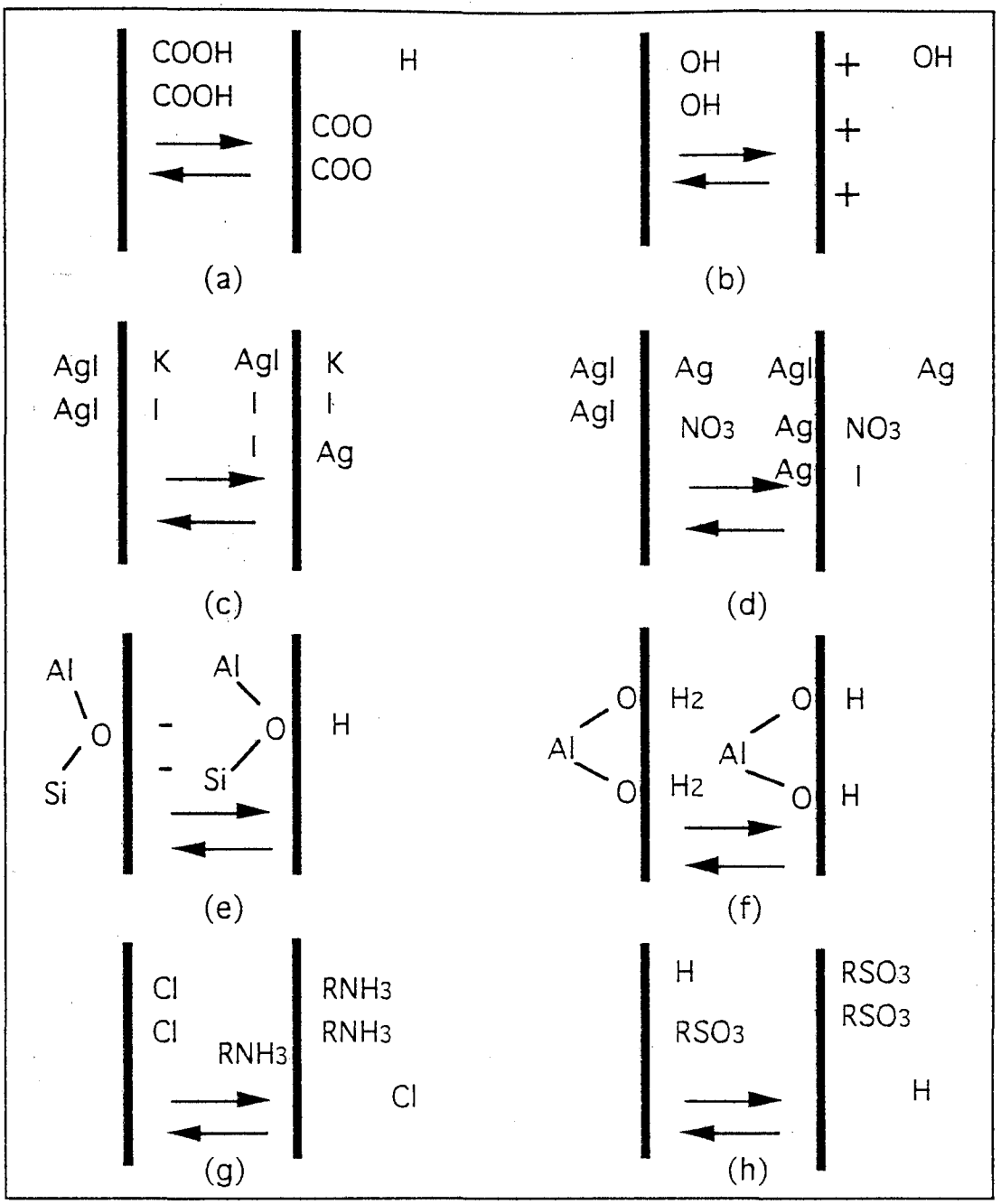

Figure 2.12. Origin of surface charges by (a) ionization of acid groups to give negatively charged surface (b) ionization of basic groups to give positively charged surface (c) differential solution of silver ions from a AgI surface (d) differential solution of iodide ions from a AgI surface (e) isomorphous substitution in a clay surface to give a negatively charged surface (f) breaking a clay crystal to give a positively charged edge (g) specific adsorption of a cationic surfactant (h) specific adsorption of a anionic surfactant [108]

2.2.2. Slip Casting Behavior and Mechanics

The rheological behavior of slips is the dominant factor in the process. The properties of a slip which must be obtained in order that satisfactory casting may be made depend on suitable rheological behavior of the slip. Because of the importance of the rheological behavior of the slips and its dependence on the pH of the dispersing medium, several investigations of the viscosity and pH relations for various systems have been carried out [106, 112-115].

The flow properties of slips shows non-Newtonian fluid characteristics at which the shearing stress as a function of the shear rate is non-linear. There are several types of flow behavior characterized by viscosity changes in response to variations in shear rate and time. The degree of behavior varies considerably and a good slip is one in which the non-linearities are minimized.

Rheological behavior can be altered by deflocculating, diluting and size distributions of particles in the slip. The specific gravity of the slips kept as high as possible consistent with proper viscosity. Increasing the solid loading leads to higher viscosity. A limit for solid loading exists where it is no longer practical since viscosity becomes extensively high to process. In general widening the distribution of particles allows the smaller particles to fill the voids of the larger particles leading to reduction in volume and viscosity.

2.2.2.1. Rheology of slurries

Rheology deals with the flow and deformation of matter. Liquid or suspensions when subjected to shear stress behave in one or two basic ways. If the ratio between the shear rate and the shear stress is constant the fluid is classified as a Newtonian fluid. Where the ratio between the shear rate and the shear stress is not constant, the fluid is considered to behavior in a non-Newtonian manner. Non-Newtonian substances can be further classified according to dependence of the shear rate on the shear stress.

Viscosity is a measure of the resistance of a fluid to flowing. This function becomes apparent when a layer of fluid is made to move in a relation to another layer. Viscosity can be defined by considering the model shown in Figure 2.13. [116].

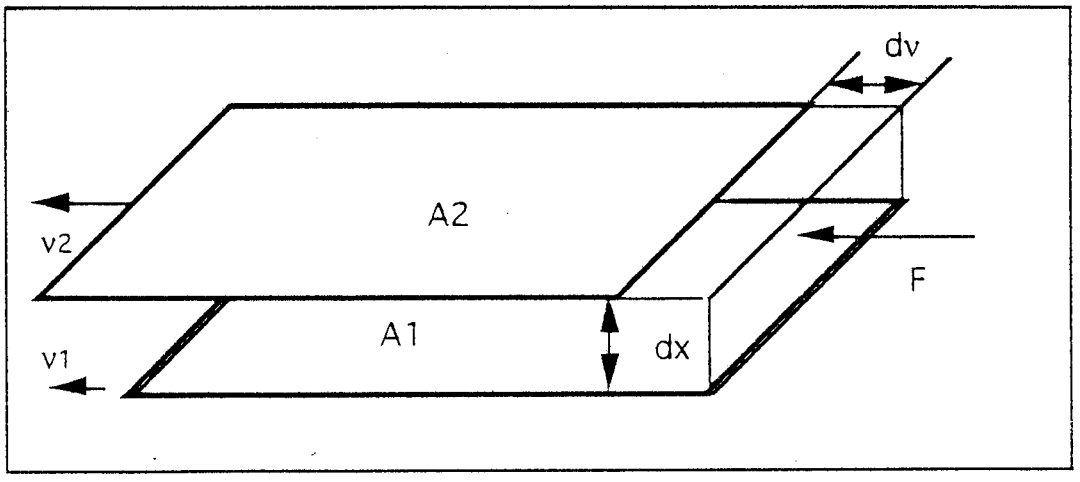

Figure 2.13. Schematic representation of viscosity model

In Figure 2.13., two parallel planes of fluid of equal area, A1=A2, and separated by a distance, dx, are moving in the same direction at different velocities, v1 and v2. The force required to maintain this difference in speed through the velocity gradient [117]

$$F/A=\eta\ (dv/dx) \qquad (2.19)$$

Where η is a constant for a given material and called viscosity. The velocity gradient, dv/dx, is a measure of the speed at which the intermediate layers move with respect to each other and called shear rate (1/sec). The force per unit area, F/A, is required to produce the shearing action and called shear stress (dynes/cm^2).

A non-Newtonian fluid shows that the relationship between shear stress and shear rate is a straight line and viscosity remains constant as shear rate increased as shown in Figure 2.14. (a-b).

A Newtonian fluid is broadly defined as one for which the relationship between shear rate and the shear stress is not constant. The viscosity of such fluids changes as the shear rate varied. Type of flow behavior is characterized by the way of viscosity changes in response to variations in shear rate and time. The effect of shear rate a non-Newtonian fluids causes two types of behavior, pseudoplastic and dilatant. Pseudoplastic, also called shear thinning, fluid displays viscosity decrease with increasing shear rate. Opposite effect is observed in dilatant fluid which is also called as shear thickening as shown in Figure 2.14. (c-d).

Some fluids shows a change in viscosity with time under constant shear rate. There are two categories of this type of fluid, thixotropic and rheopectic. While thixotropic fluid displays a viscosity decrease with time, rheopectic undergoes a increase in viscosity with time as shown in Figure 2.14. (e-f).

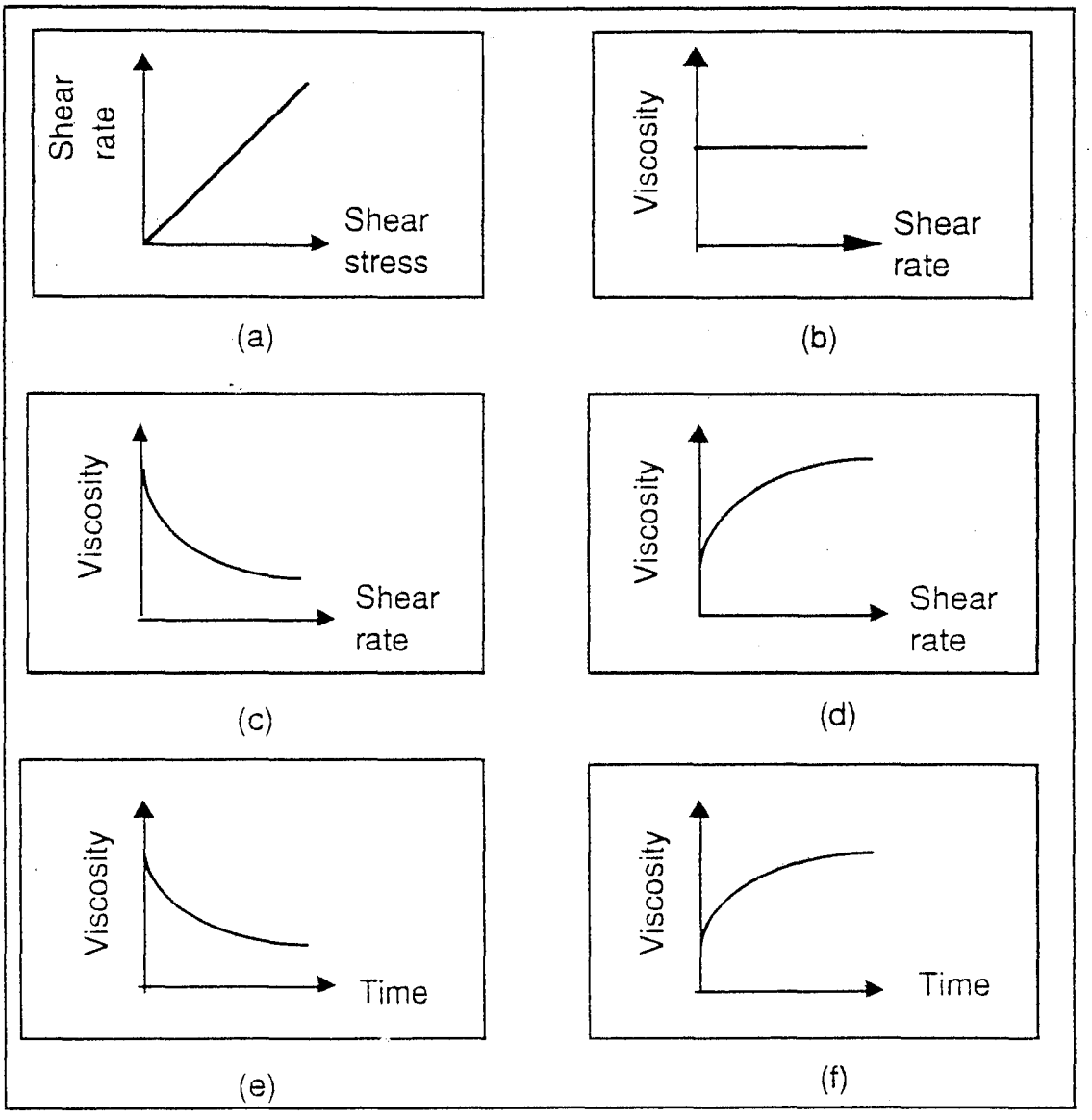

Figure 2.14. Effect of shear rate and time on viscosity for Newtonian and non-Newtonian fluids

It is important not only to have a slip that has minimum viscosity, but also the rheological properties should be suitable for casting. The term rheology denotes the science of the deformation and flow of matter. The flow properties of slurries are illustrated by graphs showing the shear stress as a function of the shear rate. For slips, such a curve is usually nonlinear. The degree of nonlinearity varies considerably and good slip is one in which it is minimized. The control of these effects is largely a matter of proper liquid content and optimum deflocculation.

2.2.2.2. Deflocculation theory

There is no single unified theory that accounts for all the observed characteristics of slips. Most theorists agree that solid particles, when suspended in a liquid medium, become electrically charged.

The control of casting slips requires an intimate knowledge of the interaction between solid particles, suspending fluids and additive chemicals. The aggregation of particles within an aqueous slip results from complicated combinations of electrokinetic interactions, stearic hindrance, and hydrodynamic and gravitational forces [94, 97, 107]. The main effect within a slip system will result from interparticle forces. The solid particles in suspending medium become electrically charged. These charges are of like sign and produce forces of electrostatic repulsion between particles. If

it is sufficient to overcome attractive van der waals forces, the system goes to defloculation. The state of defloculation is not unique but varies in degree according to the magnitude of the repulsive forces. This leads to various viscosity characteristics of a slip.

The overall charge on oxide particles is usually negative however the charge may not be symmetrically distributed overall surfaces. Oxide surfaces have a marked acid-base character. It has been found with a number of oxides that the surface contains a definite number of ionizing sites from which H^+, acid dissociation or OH^-, basic dissociation may be released, giving rise to the net surface charge [94, 97]. The state of ionization of the surface depends on the nature of the oxide and the pH of the dispersing phase with which it is in equilibrium. The electrically charged solid particles attract other charges from the suspending liquid. In aqueous system, H^+ or OH^- ions are attracted to the particles. If and acid such as HCl is added to the liquid, a layer of Cl^- ions is formed adjacent to the layer of H^+ ions [94, 97]. In general, it is found that there is an optimum charge on the particles that will bring proper dispersion.

Oxides were considered to absorb hydrogen ions at low pH in aqueous system and develop a positive surface charge with ions of acid functioning as counter ion cloud [94, 97]. At specific pH value for the particular oxide, a maximum zeta potential coincided with a minimum slip viscosity. As pH value is increased, the double layer

contracts and zeta potential drops, therefore, slip viscosity is decreased. On the other hand, if pH value is increased, surface charge dropped to zero, slip viscosity is reached its maximum. As pH is raised further, the particles develop a negative surface with ions of basic functioning as the counter ion cloud and the zeta potential reaches its second maximum leading to viscosity decrease.

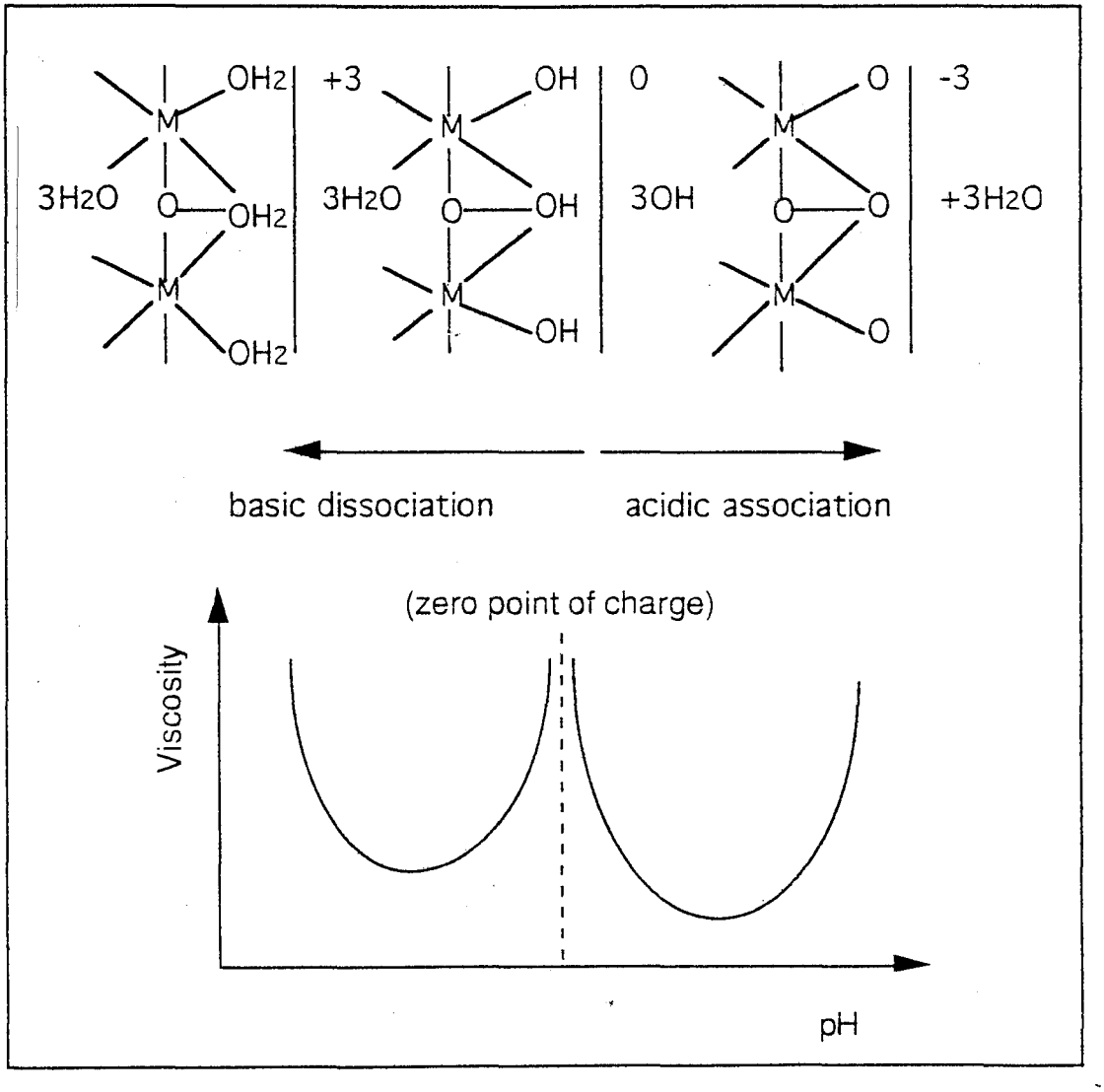

Figure 2.15. Simplified diagram showing how the surface of metallic oxide particles charges in amount and sign when pH is changed monovalent acids and bases [94]

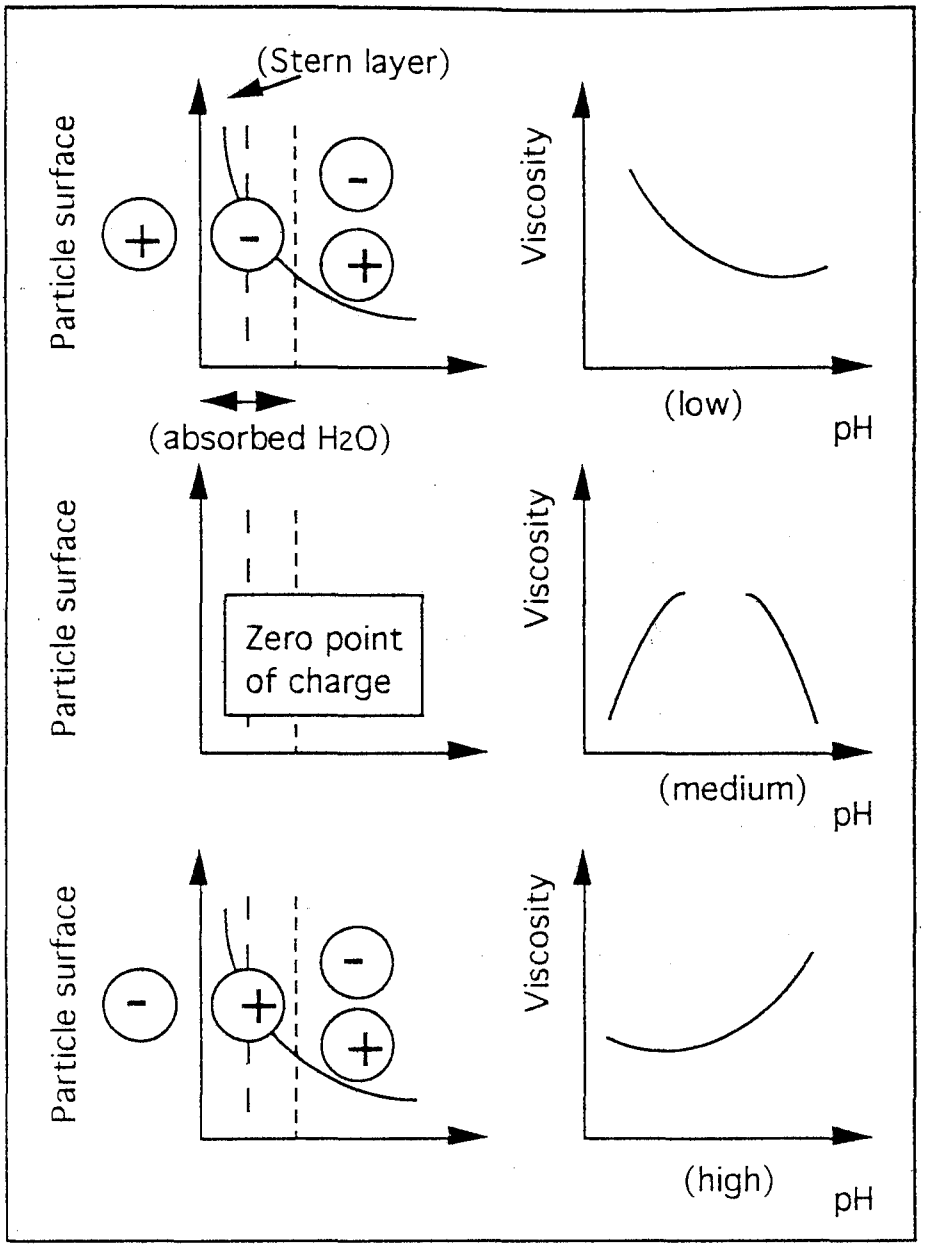

Figure 2.16. The effect of pH on the surface charge of metal oxide which can be deflocculated in water [94]

The negative charge originates from dissociation of surface hydroxyl groups when the pH of the slip is greater than the pH of zero point of surface charge. Where pH is lower than the zero point

of surface charge, the surface becomes positively charged by proton addition to the neutral aqua-complex [94].

2.2.2.3. Casting mechanism

Investigation of mechanism of formation of solid cast from slips have shown that it is a diffusion controlled process and amounts to a simple dewatering of the slip. The fine pores of mold exert a suction on water of the slip thereby drawing the dispersed particles together and forming a semi hard structure, which grows as water moves through the cast into the mold. When a ceramic powder is suspended in water, particles are influenced by a variety of forces, as shown in below Figure 2.17., that arise from the following sources:

gravity (C)-drag (D) [118]

$$\frac{dy}{dt} = \frac{V_p (\rho_s - \rho_l) g}{6n\eta(2r)} \qquad (2.20)$$

where Vp is volume of particle, ρ_s is density of solid, ρ_l is density of liquid, g is gravitational constant, η is viscosity and r is particle radius.

thermal agitation (E) [108, 118]

$$D = \frac{k T}{6n\eta(2r)} \qquad (2.21)$$

where D is diffusion coefficient due to thermal agitation, k is Boltzmann's constant and T absolute temperature.

fluid transport (A) [109-111, 118]

$$J_f = -\left[\frac{1}{A}\right]\frac{dV_S}{dt} = -\left[\frac{\varphi}{\eta}\right]\frac{dP}{dy} \qquad (2.22)$$

where A is crossectional area, dP/dy is pressure gradient and φ is permeability.

interparticle potential (E) [108, 118]

$\Delta G = \Delta G(\text{attractive}) + \Delta G(\text{repulsive})$

$$\Delta G = \left[\frac{32\ e\ (2r)\ k^2\ T^2\ \gamma^2}{e^2\ z^2}\right] \exp\ (-\kappa\ d) + \frac{-(H\ (2r))}{12\ d} \qquad (2.23)$$

where e is permittivity, z is charge of dissolved ionic species, d is distance from particle, H is Hamaker's constant, γ is distance between inner and outer Helmholtz planes, K is conductivity, ζ is zeta potential and $1/\kappa$ is double layer thickness.

streaming potential (B) [118]

$$E_s = \frac{e\ \rho\ \zeta}{\eta\ K} \qquad (2.24)$$

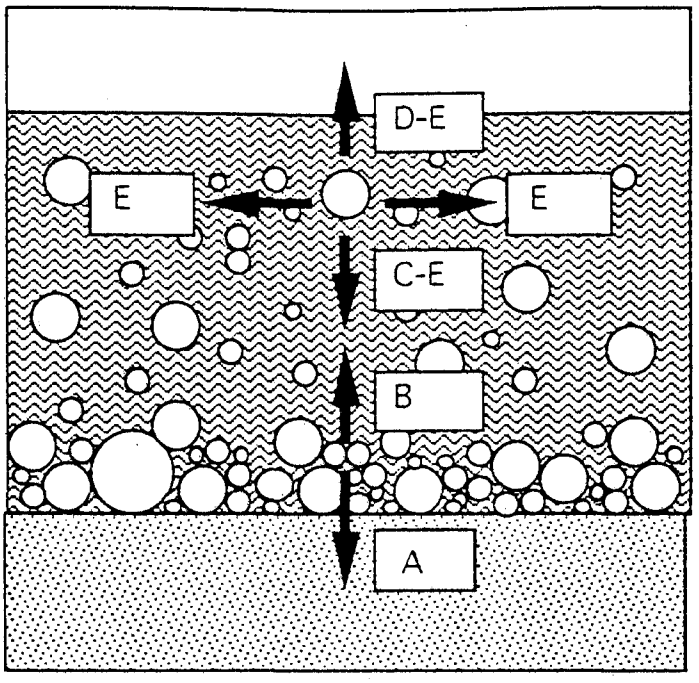

Figure 2.17. Schematic representation of forces effecting on particle

Most theoretical approaches found in the literature to slip casting kinetics are based on simple mathematical models of the process to which casting kinetics is usually presented by cast layer versus time plots.. It has been shown that the rate of cast formation which is parabolic can be quantitatively determined from equation (14) by [94, 97]

$$\frac{L^2}{t} = \frac{2\,P\,g\,\omega^3}{5\,S^2\,\eta\,(y-1)\,(1-\omega)^2} \qquad (2.23)$$

where L is the thickness of the cast layer, t is time, P is the suction pressure, ω is the void fraction, S is the surface area of solid particles, n is the viscosity, y is the volume of slip containing volume $(1-\omega)$ of solids and g is acceleration due to gravity [94, 97].

Similar investigations to the cast formation rate have been developed by solving the Carman-Kozeny equation of filtration [109, 117-119].

2.2.2.4. Particle packing

The degree of packing density in slip casting mainly depends on deflocculation level, solid concentration and particle size distribution. Theoretically, spheres of uniform sizes may be packed up to 0.74 packing volume fraction (e.g. FCC and HCP arrangements). Since there are voids in the packing of particles, smaller particles may enter without changing the overall volume of the cast. Lower viscosity has been observed to be related in some way to the optimum packing of particles of various size distributions and solid concentration of suspensions [94, 103-104, 113, 121]. Several investigations have been done on particle packing. The relationship that is the most applicable to the ceramic raw materials is the Andreasen-Funk equation which describes a size distribution produces optimum packing efficiency at n=0.37 [102, 103]

$$\frac{CPFT}{100} = \frac{(2r)^n - (2r_s)^n}{(2r_L)^n - (2r_S)^n} \qquad (2.26)$$

where CPFT is cumulative percent finer, r is any particle radius, r_L is the largest particle and r_S is the smallest particle radius in the distribution.

In relation with viscosity, Einstein first described the viscosity of a dilute dispersion of rigid spheres as a function of solid concentration by [121,122]

$$\eta_r = 1 + 2.5\left(\frac{\text{vol\% solid}}{100}\right) \qquad (2.27)$$

where η_r is relative viscosity (= viscosity of suspension/viscosity of solvent), vol% solid is percent solid in dispersion and O is term of order.

For concentrated monodisperse system, many investigators [105, 121-125] have applied Einstein equation in modified forms (in the original equations, the term, packing factor was substituted the term (1-w));

R.D. Sudduth [122]

$$\ln(\eta_r) = -2.5\,(1-\omega)\ln\left(\frac{100(1-\omega) - \text{vol\% solid}}{100(1-\omega)}\right) \qquad (2.28)$$

M. Mooney [123]

$$\eta_r = \exp\left(\frac{2.5(\text{vol\% solid})(1-\omega)}{100(1-\omega)-(\text{vol\% solid})}\right) \qquad (2.29)$$

where η_r is relative viscosity (= viscosity of suspension/viscosity of solvent) and ω is void (pore) fraction.

D. Quemada [124]

(for Newtonian systems)

$$\eta_r = \left(1 - \frac{\text{vol\% solid}}{100(1-\omega)}\right)^{-2} \qquad (2.30)$$

For equation (2.28), (2.29) and (2.30), Newtionian behavior is assumed and intrinsic viscosity is closely associated with void fraction and related to the structural state of the system, $2/(1-\omega)$.

D Quemada [125]

(for non-Newtonian systems)

$$\eta_r = \left(1 - \frac{1}{2}\,\tilde{\eta}\ \text{vol\% solid}\right)^{-2} \qquad (2.31)$$

where $\tilde{\eta}$ is intrinsic viscosity, $\tilde{\eta} = \tilde{\eta}$ (vol% solid, shear rate)

D. Quemada [124] showed that many data on polydisperse systems, exhibiting Newtonian behavior, have been in better agreement with equation (2.30) than (2.29). He also extended the relative viscosity-volume concentration relationship to the description of non-Newtonian behavior [125]. Chanyavanich [121] analyzed submicron sized and bimodal spherical silica particles in an organic media to determine the rheological behavior of concentrated suspensions. It has been also concluded that the equation of Quemada most nearly describes the variation of η_r with vol% solid and ω.

3. STATEMENT OF THE PROBLEM

Amongst the various forming processes, dry powder pressing has received the bulk of attention while casting techniques have not been used for micropyretic synthesis. In this study, the processing of slip cast micropyretically synthesizable materials is studied for the first time. This thesis is aimed towards developing an optimized processing methods to obtain a refractory composite by means of micropyretic synthesis of slip cast preforms.

Various metals and alloys have been prepared for several decades by metallothermically reducing the oxides [13]. Highly exothermic reactions which take place during such reactions may be utilized to form refractory composites. In this study, the exothermic reactions which were studied were all used for the synthesis of $SiC\text{-}Al_2O_3$ composites by utilizing combustible mixtures of SiO_2, Al, C, and Cr_2O_3. In the reactions, aluminum is used as the reducing metal. With the simultaneous production of multiple phases in the aluminothermic reduction, $SiC\text{-}Al_2O_3$ composite were formed by reacting carbon with the product metal to form SiC. Two reactions, reaction 1 and reaction 2, were predominantly employed at stoichiometries

Reaction 1: $3SiO_2 + 4Al + 3C \Longrightarrow 3SiC + 2Al_2O_3$ (3.1)

Reaction 2: $3Cr_2O_3 + 6Al + 4C \Longrightarrow 2Cr_3C_2 + 3Al_2O_3$ (3.2)

The phase diagrams for the systems Al_2O_3-Al, Si-C, Cr-C and Cr-Si are given in appendix A [126]. The plot of entalphy as a function of temperature for reaction 1 at adiabatic condition is given in appendix A [127]. The reaction can attain an adiabatic temperature higher than 2000 °C at which both aluminum and silicon are liquid. This may lead to densification in the synthesized product. However, the heat generated by the reaction may not be sufficient enough to full conversion, therefore, the reaction 2 may be introduced as a trigger reaction. This study is related to the preparation of slip cast refractory compounds, particularly, to the methods of preparing alumina with a high volume content and the silicon carbide and chromium carbide reinforcement. The method of preparing the refractory composite is by means of micropyretic synthesis of slip cast preforms. Details of the slip preparation, cast formation and synthesis will be investigated. This area of research has not previously been investigated. Some of the expected advantages over traditional way of fabrication are complex shape possibility, lower cost and controlled property. For the investigation, colloidal silica was used as the main suspending medium as well as the combustion source in the slip to achieve a high uniform packing density. In regard to micropyretic synthesis, the role of colloids in final microstructure and property is also planned to determine the feasibility of the process.

The experimental procedures and the variables affecting the process in relation to slip casting and micropyretic synthesis are discussed in the following chapters.

4. EXPERIMENTAL PROCEDURES

4.1. Raw Materials

Powders and additives used in this study are listed together with their sources in Table 4.1. All powders were used in the as received condition. Although manufacturer's grade for all powders were -325 mesh, powders were irregular in shape and the average particle size and distribution were differs widely. The average particle size ranges for SiO_2, Al, graphite and Cr_2O_3 powders were 2-3, 5-10, 10-15 and 0.5-1 microns respectively. A scanning electron micrographs for powders used in the experiments is shown in Figure 4.1. As shown from Figure 4.1., all powders are irregular in shape and a non uniform size distribution.

X-ray diffraction performed for powders is shown in Figure 4.2. The main inclusions according to the Johnson Matthey Catalogue for powder specifications; for aluminum, inclusion was Al_2O_3 (0.5 wt%) which exist on the surface of the particles; for silica powders, Fe_2O_3 (0.044 wt%), Al_2O_3 (0.027 wt%), and CaO (0.027 wt%) and loss on ignition was 0.463 wt%; for graphite, moisture and volatiles were 0.2-0.6 wt% and ash was < 0.5 wt%. Colloidal silica used in the experiments which has multifunctional behavior and/or as suspending medium, binder, dispersant, viscosity modifier had 30 wt% solid content with around 14 nanometer particle size. Manufacturer's name for colloidal silica was 1430AT™.

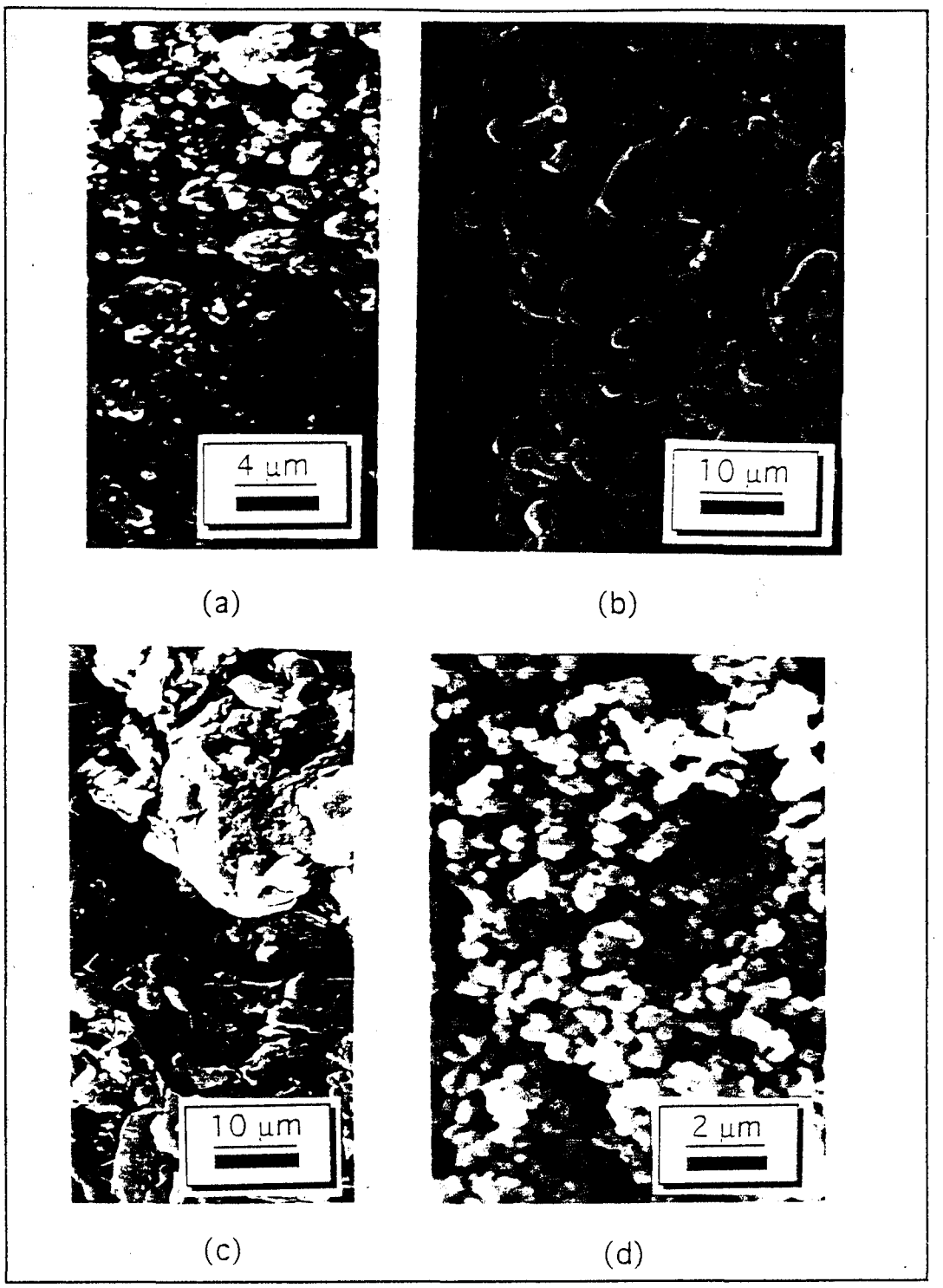

Figure 4.1. SEM micrographs for reactant powders (a) SiO2, (b) Al, (c) C and (d) Cr2O3

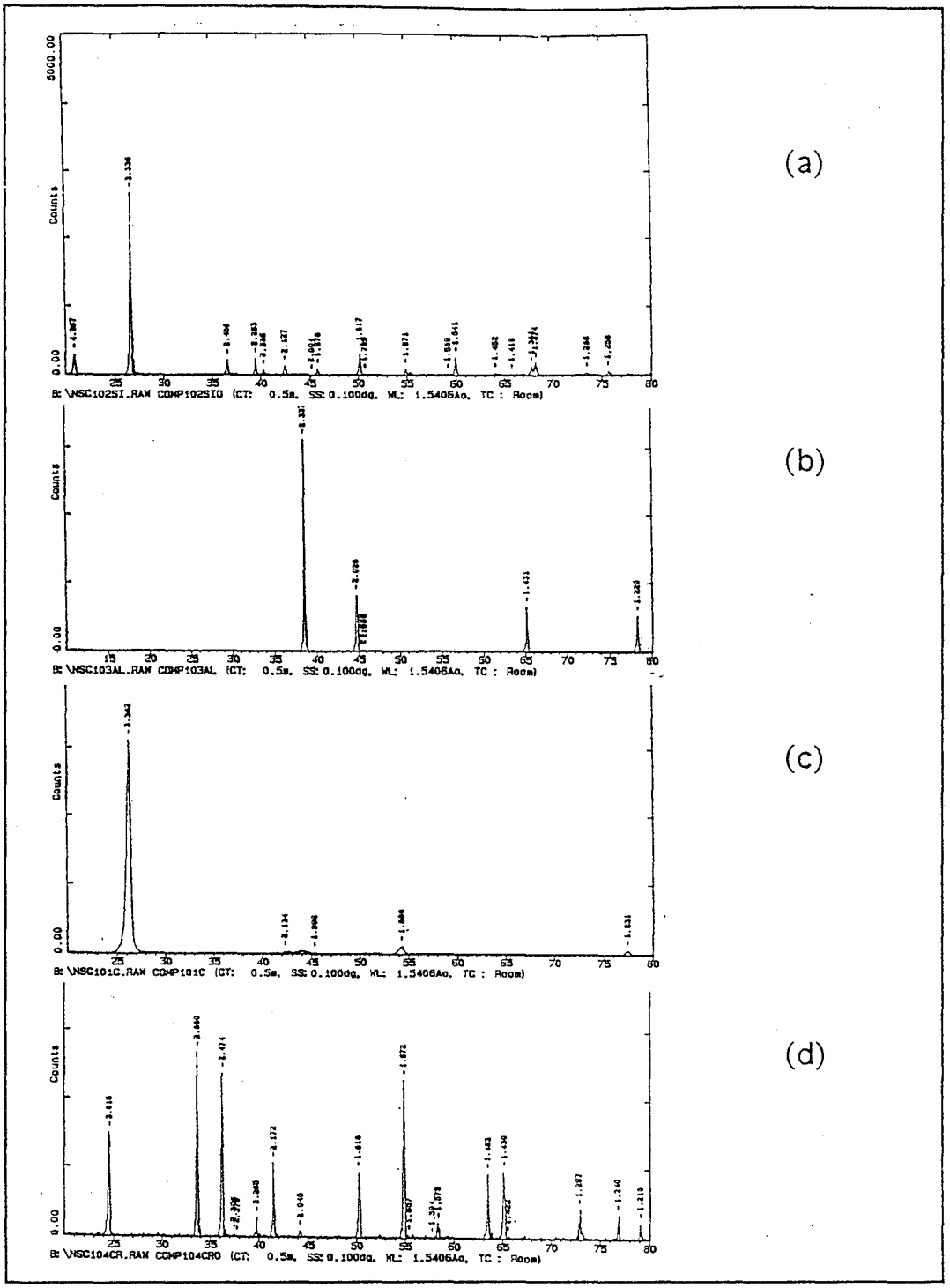

Figure 4.2. X-ray diffraction patterns for reactant powders (a) SiO2, (b) Al, (c) C and (d) Cr2O3

This particular product had been chosen because it was stable in wide pH range, pH= 3 to 11. For distilled water suspended slips, polyvinly alcohol was used as a binder.

4.2. Sample Fabrication

The green preform of samples were fabricated by slip casting into plaster mold. The traditional processing, compaction, was also studied for comparison. Figure 4.3. shows the schematic representation of both forming processes, slip casting and compaction. All compositions for both cast and compacted samples are given in Tables 4.2. to 4.7. The compaction samples were obtained by mixing powders with polyethylene glycol(PEG) and 1430AT™ binders and compacting the blend under pressure, 10,000 psi, into shape. Both solid casting and drain casting modes of slip casting were studied. After forming the cast preforms by slip casting, the preforms were combustion synthesized. The processing route for sample fabrication are briefly explained in sections 4.2.1. through 4.2.4.

4.2.1. Mold Making

Molds were prepared by standard techniques using plaster of paris ($CaSO_4.1/2H_2O$), DURABOND™, using the ratio of 2 parts of water to 3 parts of plaster by weight. Three pieces of mold were employed for easy mold release. The 8.5x12x60 mm sized pattern was employed to form half of the mold cavity. Molds were dried

thoroughly before use. The SEM micrograph of mold surface is shown in Figure 4.4-c. For solid casting, to eliminate shrinkage defects a cylindrical riser was used. Drain casting at which mold cavity was cylindrical was used for casting time determination. The side and top view of the mold is shown in below Figure 4.4-a and b.

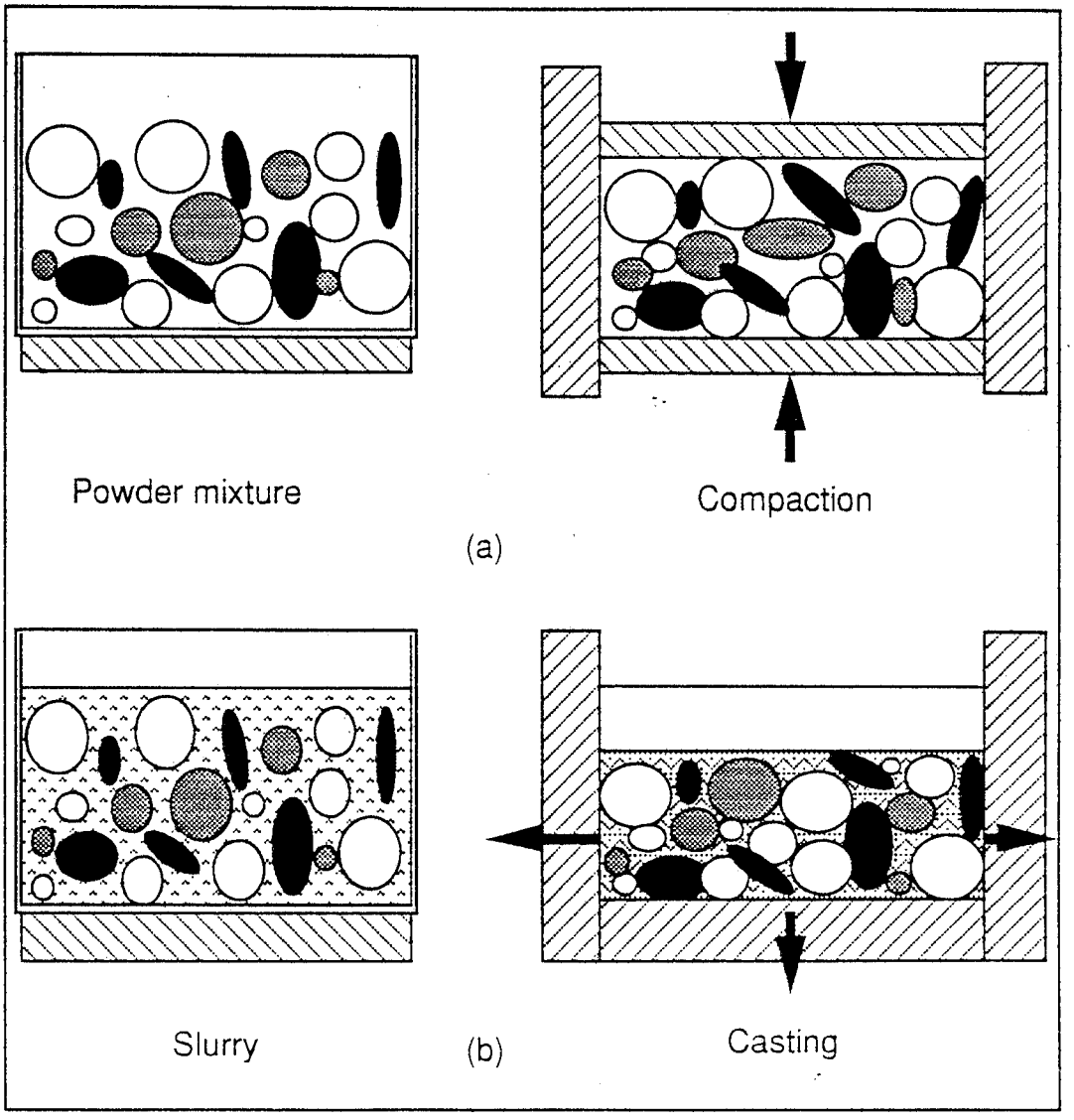

Figure 4.3. Schematic representation of forming processes, compaction (a) and slip casting (b)

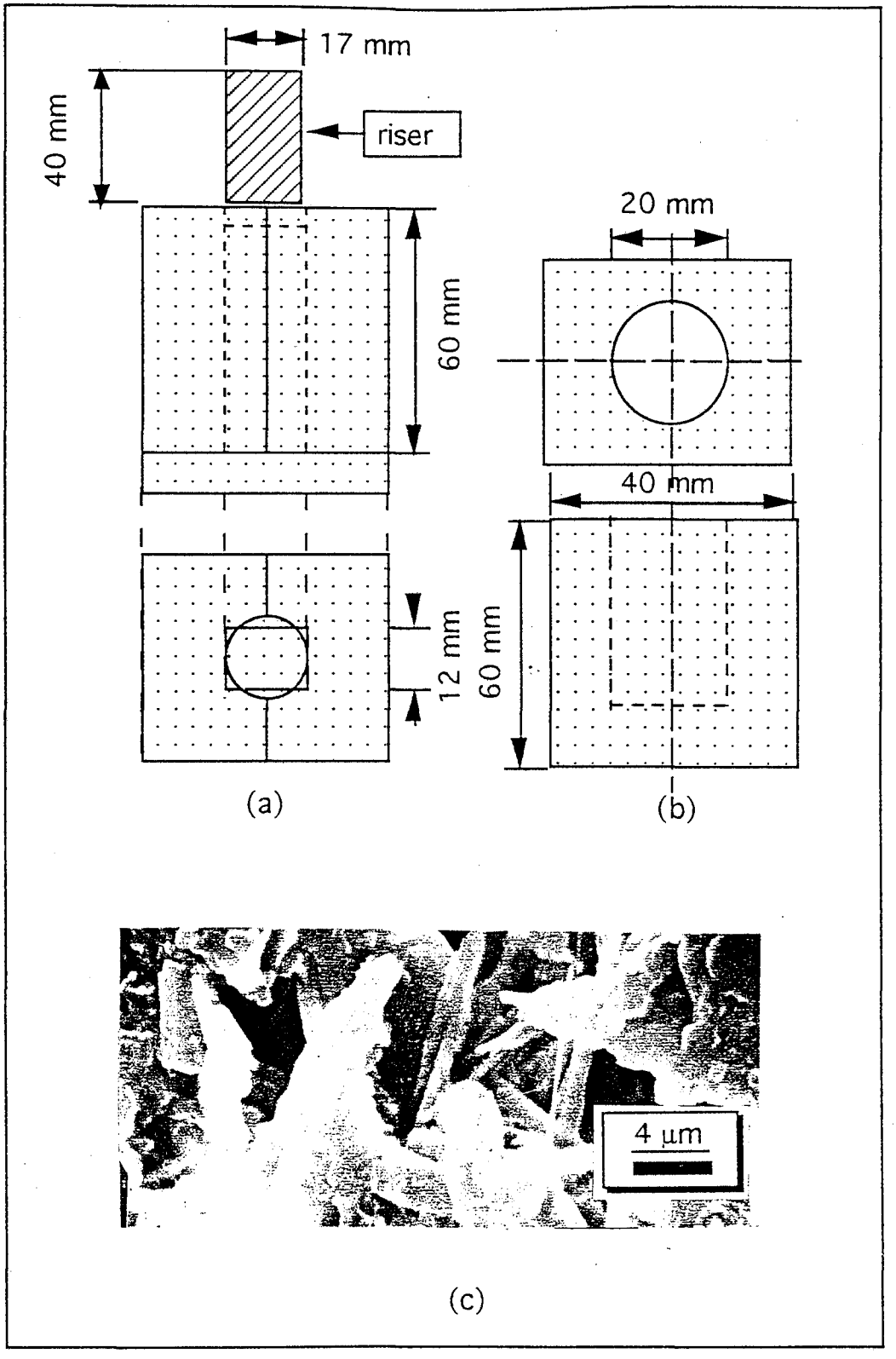

Figure 4.4. Plaster molds (a) solid casting, (b) drain casting and (c) SEM micrograph of mold surface

4.2.2. Slurry Preparation

Reactant powders were weighted at required amount for the compositions shown in Tables 4.2. to 4.7. into a 1000 cc plastic container and blended for 30 minutes using roller mill. The combustion powder source; for the reaction consisting of SiO_2, Al and C in the weight ratio of stoichiometry was 55.55 wt%, 33.33 wt% and 11.11 wt% respectively; for Cr_2O_3, Al and C was 68.47 wt%, 24.32 wt% and 7.21 wt% respectively.

The suspending medium, colloidal silica, distilled water and other additives, were prepared separately. For colloidal silica suspended slip, the procedure was relatively straight forward. Since the slip did not require any binder and dispersant, colloidal silica was directly added to the slip system. The amount of colloidal silica was varied in the slip by substituting the amount of colloidal silica with -325 mesh SiO_2 powder to keep the powder stoichiometry. The solid concentration of the slip, vol% solid, was varied by diluting colloidal silica with distilled water. For distilled water suspended slips, binder and dispersant were Polyvinyl alcohol (PVA) and DARVAN-C™. In order to prepare the binder system, 20 wt% PVA powder was first dispersed in cold distilled water using sufficient agitation to wet out all particles with water. The solution temperature was raised to 95 °C and hold for 30 minutes to cook and then the suspending medium solution was prepared by placing the required wt% of distilled water and dispersant to the binder, 20 wt% PVA. Both mixtures, powders and suspending

medium, were mixed together at required ratios to give the particular solid concentration in the slip and slip were prepared by hand mixing, until smooth consistency was obtained. After dispersing, the suspensions pH adjustments were done both acidic and basic sides to find out optimum slip viscosity. pH value was decreased by drops (~0.025 gr) of 25 vol% distilled water diluted HCl to avoid local flocculation.

pH and viscosity measurements were done using CORNING-107 pH meter and BROOKFIELD-LVTDV-II digital viscometer respectively. The details of pH adjustment and viscosity measurements are given in characterization section.

Table 4.1. Powders and binders used in the experiments

POWDER	MESH SIZE	PURITY %	COMPANY
Cr_2O_3	-325	99.5	Johnson Matthey
SiO_2	-400	99.5	Johnson Matthey
SiC	-325	99.0	Electro Ceram.
Al	-325	99.5	Johnson Matthey
C	-325	99.0	Johnson Matthey
BINDER	MANUFACTURER NAME		
Polyethylene glycol(PEG)	300 NF™		Union Carbide
Polyvinly alcohol(PVA)	AIRVOL 205™		Air Product
SUSPENDING MEDIUM			
Colloidal silica	1430AT™		Nycol

Table 4.2. Slip compositions used in the experiments

slip compositions (wt%)	samples							
	A10	A11	A12	A13	A14	A15	A16	A21
SiO_2	19.38	21.86	25.07	29.39	34.09	35.52	35.52	23.15
Al	21.07	21.11	21.15	21.21	21.27	21.31	21.31	22.35
C	7.02	7.04	7.05	7.07	7.09	7.10	7.10	7.45
Cr_2O_3								
SiC								
submicron SiO_2 from 1430AT™	15.75	13.33	10.19	5.97	1.38			14.11
suspending medium from 1430AT™	36.76	31.10	23.78	13.94	3.23			32.93
suspending medium from distilled water		5.57	12.75	22.41	32.92	34.77	34.59	
PVA						1.30	1.30	
DARVAN-C™							0.13	
vol% solid	40.4	40.4	40.4	40.4	40.4	40.4	40.4	44.4

Table 4.3. Slip compositions used in the experiments (continue)

slip compositions (wt%)	samples							
	A22	A23	A24	A25	A26	A27	A31	A32
SiO_2	26.54	31.11	33.41	36.07	36.29	36.29	25.07	28.74
Al	22.39	22.45	22.48	22.51	21.77	21.77	24.21	24.24
C	7.46	7.49	8.04	7.51	7.26	7.26	8.07	8.08
Cr_2O_3								
SiC								
submicron SiO_2 from 1430AT™	10.79	6.32	4.07	1.47			15.29	11.68
suspending medium from 1430AT™	25.17	14.75	9.51	3.42			27.36	27.26
suspending medium from distilled water	7.64	17.87	23.03	29.03	33.38	33.22		
PVA					1.31	1.31		
DARVAN-C™						0.15		
vol% solid	44.4	44.4	44.4	44.4	44.4	44.4	51.0	51.0

Table 4.4. Slip compositions used in the experiments (continue)

slip compositions (wt%)	samples							
	A33	A34	A35	A36	A37	A41	A42	A43
SiO_2	33.66	36.15	39.00	39.41	39.41	26.13	29.95	35.08
Al	24.29	24.32	24.34	23.64	23.64	25.23	25.27	25.32
C	8.10	8.11	8.12	7.88	7.88	8.41	8.42	8.44
Cr_2O_3								
SiC								
submicron SiO_2 from 1430AT™	6.84	4.41	1.58			15.93	12.17	7.13
suspending medium from 1430AT™	15.96	10.29	3.70			24.28	24.17	16.64
suspending medium from distilled water	11.14	16.72	23.25	27.45	27.26			7.39
PVA				1.42	1.42			
DARVAN-C™				0.18	0.35			
vol% solid	51.0	51.0	51.0	51.0	51.0	55.0	55.0	55.0

Table 4.5. Slip compositions used in the experiments (continue)

slip compositions (wt%)	samples							
	A44	A45	A51	A54	B10	B11	B12	B20
SiO_2	37.65	40.63	27.36	40.98		12.85	6.70	
Al	25.33	25.36	26.42	24.58	18.89	18.14	18.89	19.59
C	8.45	8.46	8.81	8.19	5.90	5.66	5.89	6.06
Cr_2O_3					30.57	29.34	30.56	35.47
SiC								
submicron SiO_2 from 1430AT™	4.59	1.65	16.68	4.99	13.39		6.70	11.66
suspending medium from 1430AT™	10.71	3.85	20.71	11.66	31.25		15.62	27.20
suspending medium from distilled water	13.26	20.04		9.58		32.57	15.62	
PVA						1.32		
DARVAN-C™						0.11		
vol% solid	55.0	55.0	60.0	60.0	40.4	40.4	40.4	51.0

Table 4.6. Slip compositions used in the experiments (continue)

slip compositions (wt%)	samples						
	B30	AB1	AB2	D10	D20	D30	D40
SiO_2		12.70	20.22				
Al	20.57	22.19	23.15	14.18	16.17	14.55	16.73
C	6.30	7.10	7.60	4.42	5.04	4.46	5.12
Cr_2O_3	42.26	23.57	12.50	22.94	26.16	29.91	34.38
SiC				16.75	9.55	21.84	12.55
submicron SiO_2 from 1430AT™	9.26	10.33	10.95	10.05	11.46	6.55	7.53
suspending medium from 1430AT™	21.60	24.10	25.56	23.45	26.74	15.29	17.57
suspending medium from distilled water				8.17	4.86	7.39	6.10
PVA							
DARVAN-C™							
vol% solid	55.0	55.0	55.0	40.4	40.4	51.0	51.0

Table 4.7. Slip compositions used in the experiments (continue)

compact compositions (wt%)	samples					
	P1	P2	P3	P4	P5	P6
SiO_2	46.29	50.50	45.00	41.96	35.90	31.36
Al	27.75	30.27	30.30	30.30	30.30	30.30
C	9.25	10.09	10.10	10.10	10.10	10.10
submicron SiO_2 from 1430AT™			5.50	8.54	14.60	19.13
suspending medium from 1430AT™			6.36	6.36	6.36	6.36
PEG	16.66	9.09				

For samples of Aij, SiO2-Al-C reaction was studied for different conditions for slip such as overall solid concentration in the slip (vol% solid), volume percentage of submicrometer SiO_2 from colloidal silica in the slip (vol% submicron SiO_2) and/or weight percentage of submicron SiO_2 from colloidal silica in solid content of slip (wt% submicron SiO_2), type of binder, dispersant etc. To compositions A1j, A2j, A3j, A4j and A5j (i=0 to 5); vol% solid were varied 40.4 %, 44.4 %, 51.0 %, 55.0 % and 60 % respectively; wt% submicrometer SiO_2 of 1430AT™ in solid were varied from 0 to 24.91 % as j increased 1 to 5 by keeping the overall stoichiometry fixed and balancing the silica concentration with -325 mesh SiO_2 powder substitution. To compositions A15-A16 (vol%=40.4), A26-A27 (vol%=44.4) and A36-A37 (vol%=51.0), PVA which was added as a binder 2 wt% with respect to the powder and DARVAN-C™ which was added as a dispersant.

For samples of Bij, the effect of Cr_2O_3-Al-C reaction to SiO_2-Al-C reaction was studied for different conditions for slip such as overall solid concentration in the slip (vol%), volume percentage of colloidal silica in the slip, vol% submicron SiO_2, type of binder, dispersant etc. To compositions B10, B20 and B30, vol% were also varied 40.4 %, 44.4 % and 51.0 % respectively and vol% submicron SiO_2 were varied 10.80 %, 10.06 %, 8.90 % respectively. To compositions, B11 (vol%=40.4), PVA which was added as a binder 2 wt% with respect to the powder and DARVAN-C™ which was added as a dispersant. For sample B12 (vol%=44.4), amount of colloidal silica was decreased comparing to the sample B10 from 10.80 vol%

submicron SiO_2 to 5.40 vol% submicron SiO_2 by keeping the overall solid concentration same and balancing the silica content in powder as 55.55 wt% with -325 mesh SiO_2 powder substitution. For compositions AB1 and AB2, the vol% solid and vol% submicron SiO_2 were 51.0 % and 8.90 % respectively. The weight ratio of Cr_2O_3-Al-C reaction to SiO_2-Al-C reaction for samples AB1 and AB2 were 0.91 and 0.35 respectively.

For samples of C10 and C20 series of the compositions, SiO_2 and Al powders alone were studied with colloidal silica suspension at 51.0 vol% solid. On the other hand, C and Cr_2O_3 could not be prepared for the same loadings due to extreme agglomeration.

Along the D series, Cr2O3-Al-C reaction system with colloidal silica suspension and SiC dilution was investigated for two different particle sizes and weight percentages of SiC with 40.4 vol% and 51.0 vol% solid.

4.2.3. Casting

Both solid and drain casting were studied. The pH and viscosity adjusted slip were directly cast into the mold at room temperature (18-24 °C). Solid casting was done by risering at which casting shrinkages were eliminated and the porosity level of green form were also determined. Drain casting was used for casting time determination. The schematic representation of cast formation is shown in Figure 4.5. Since mold release was readily obtained for all

colloidal silica employed samples, mold releasing agents was not required. After casting, mold was dried for 24 hours in air and cast preforms were released from the mold. The excess parts due to risering were removed and the inhomogenities due to mold mismatches were grinded by polishing. The 12x17x60 mm cast preforms were cut into several pieces for further operations.

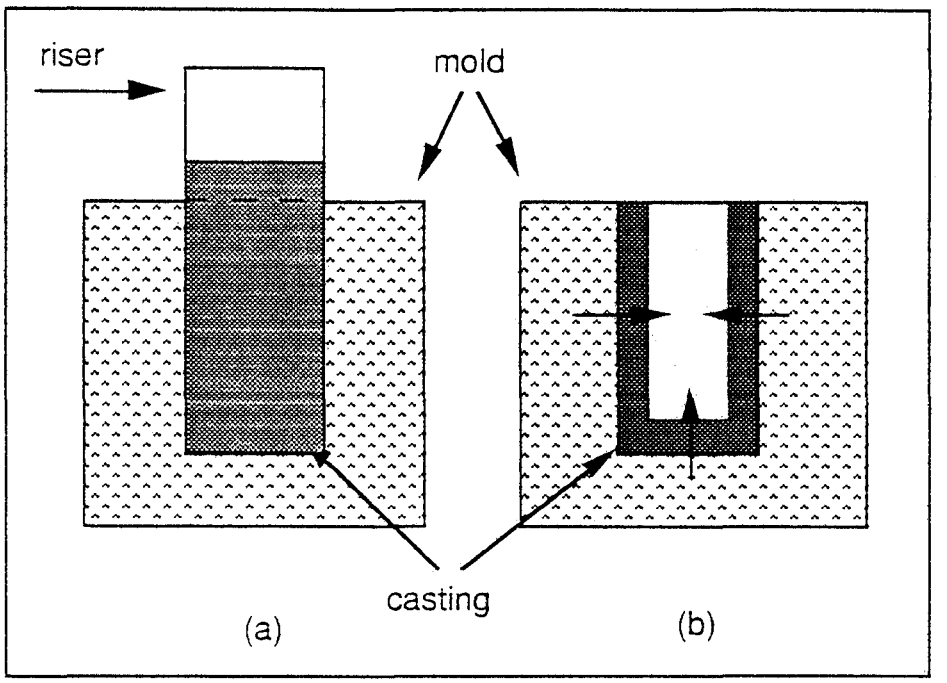

Figure 4.5. Schematic representation of cast formation (a) solid (b) drain casting

4.2.4. Synthesizing

After mold release, sample were calcined at 250 °C for 15 minutes for removing hydrated water. The samples were synthesized using both modes of combustion, wave propagation and thermal explosion as shown schematically in Figures 4.6. and 4.7. For wave propagation mode, combustion was carried out by igniting

one end of the sample which was 12x17x30 mm with a propane torch after preheating the sample.

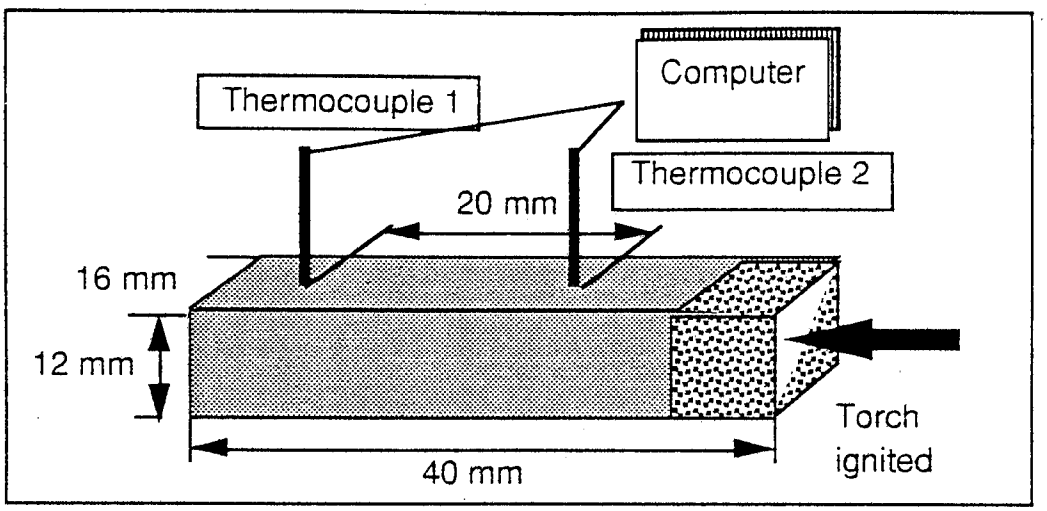

Figure 4.6. Combustion velocity measurement setup for wave propagation mode

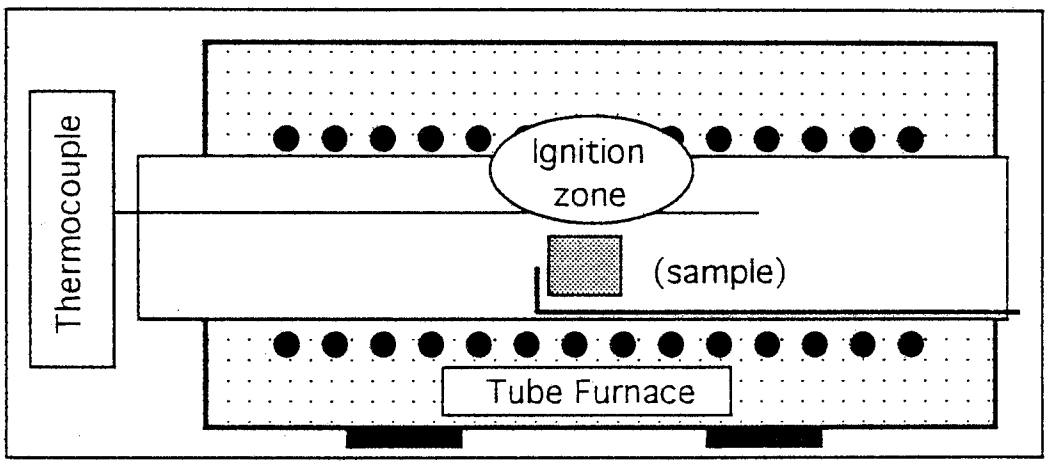

Figure 4.7. Furnace configuration for thermal explosion mode of combustion

Two different furnace temperature, 700 °C and 1000 °C, were employed in thermal explosion mode to which the sample which was 12x17x10 mm was placed and kept for 5 minutes in the furnace.

4.3. Characterization

4.3.1. Rheological

Rheological behavior of the slurries in the experiments were analyzed by Brookfield LVTDV-II digital viscometer. Viscosity changes as a function of spindle speed, pH and time were recorded using #4 spindle of LV series and 100 ml beaker as a sample container. The measurements were done at room temperature, 22 ± 2 °C. The typical schematic of viscosity measurement is shown below in Figure 4.8.

Starting at lowest spindle speed, the viscosity readings at each successively higher speed were recorded until the reading goes off scale. A graph of these readings is the up curve of the plot. Without stopping the viscometer, spindle speeds were decreased incrementally to the starting point by noting the reading at each speed. These readings were formed the down curve of the graph. The time interval between each spindle speed change was 15 seconds. Both down and up curves were measured five times and then average of each point was taken.

Where up and down coincide, the slurry is called time independent and then pseudoplastic and dilatant behavior of the slurry are analyzed. If they do not coincide, slurry shows time

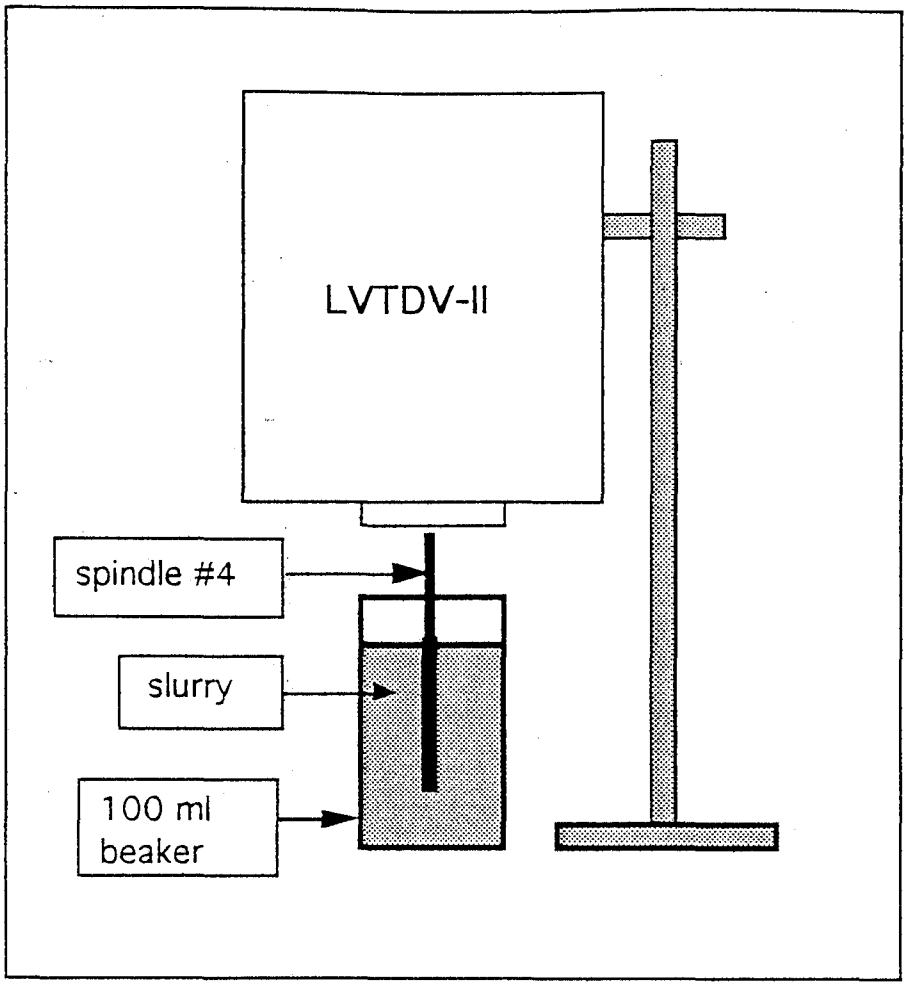

Figure 4.8. Schematic representation of viscosity measurement setup

dependent behavior at which thixotropic and rheopectic flows were considered. The slurry is called thixotropic when the up curve indicates a higher viscosity than the down curve.

The effect of pH on viscosity of the slips were examined by addition of drops (~0.025 grams/drop) of 25 %vol distilled water diluted hydrochloric acid using a pipet. After dropping the deflocculant, the slurry was stirred thoroughly, and the variations

for the pH and the viscosity were noted. The same procedures were repeated until a pH value of 2 to 3.

The time dependent analysis was also done by plotting viscosity vs time using #4 spindle and at 12 RPM of spindle speed. The viscosity measurements were taken each 15 seconds after the rotation of spindle begins.

4.3.2. Propagation Velocity

Combustion velocity of samples were measured by data acquisition system using type C thermocouple, tungsten - 5% rhenium (+lead) and tungsten - 26% rhenium (-lead).

Kaleida Graph™ software was used for analyzing all the data. The data acquisition system were set up with a Macintosh SE computer, 16 bit data acquisition card (ACSE-16-8), terminal panel (T51) and the Analog Connection Workbench™ software.

The thermocouples were placed into the sample with 2 cm distance by embedding in a 0.5 mm dia, 5 mm deep hole which was drilled into the sample. The thermocouples were connected to the data acquisition system which recorded the temperature every 0.1 second. The sample was synthesized by igniting one end with a propane torch after preheating the sample. The temperature against time data collected were plotted using Kaleida Graph Software. The time passed for the combustion wave from the first thermocouple to

the second was measured from the plot. Since the distance between the two thermocouples, 2 cm, was known, the combustion propagation velocity along the sample was calculated using $X_{bt}=V_c t$.

4.3.3. Porosity

Powder packing by slip casting leads to a porous preform and this initial porosity level further increased after combustion mainly due to the density differences between reactants and products. The porosity levels of both the preform and the final product were calculated. The external volume of the samples were calculated from the measured thickness, height and width. The true volume of the samples was measured using Helium pycnometer, model AccuPyc1330, Micromeritics Co. The porosity level was calculated from (external volume - true volume) / external volume. The porosity level of preform was also calculated for solid cast sample by measuring the shrinkage value from the riser.

4.3.4. X-ray diffraction

X-ray diffraction was done to identify the phases formed in combustion synthesized samples. The Siemens diffractometer which is Ni filtered Cu tube operating at 40 KV and 30 mA with a wavelength of 0.154051 nm, model D500, was employed for X-ray diffraction work.

All samples were placed in 99.5% alumina mortar and powdered into -100 mesh by 99.5% alumina pestle. X-ray analysis was done on powdered samples in the range of 2θ from 20 to 80 with a scanning speed of 0.05 degree/seconds.

4.3.5. Microscopy

In order to study the morphology, the longitudinal and transverse sections were cut and polished with 600 grit SiC polishing paper. Further polishing was done with diamond pastes to a 0.25 micrometer finish. The sample surfaces were viewed under both a optical microscope and a Cambridge Stereoscan 600™ electron microscope (SEM) with an energy dispersive X-ray analysis and elemental mapping facility. For SEM analysis, the samples were sputtered with gold (200 °A). The electron diffraction patterns were obtained using Philips CM12™ transmission electron microscope (TEM).

5. DESIGN MODELING OF SLIP CAST MICROPYRETICALLY SYNTHESIZABLE MATERIALS

One of the objective of this work is to study the changes in porosity level of slip cast preforms with slip processing variables such as vol% solid loading, particle size distribution and deflocculation level. Further such variables can be related to reaction kinetics and final porosity level at the synthesized product. Both of the processes, slip casting and micropyretic synthesis, have often been observed to exhibit rather complex and seemingly unpredictable mechanisms.

There are no fully established universal models for any of them. However, there are several simplified analytical and experimental relationships for casting and reaction kinetics.

From the literature survey, the equations (2.28-2.31) which relates viscosity with vol% solid loading and porosity have been found to have a common derivative form and are not far different from the Einstein equation. However, the Quemada's equation has been applied successfully for many poyldisperse suspensions and showed better agreement with most experimental data [121, 124-125]. In order to relate slip casting parameters with casting and reaction kinetics, the Quemada's equation will be chosen in the model. D'Arcy's law [117] and propagation velocity expression by Lakshmikantha et al [76] will also be used for casting and reaction kinetics analysis consideration of the Quemada's equation.

The models chosen for cast formation and reaction kinetics consideration were solved using experimental data. The results and discussions were given in the following sections.

The method of analysis are based on the assumptions due to the constraints and required simplifications

1. Concentrated polydisperse systems studied exhibit Newtonian behavior.

2. Viscosity and porosity data were obtained Brookfield, LVDTV-II viscometer at 12 rpm and Micromeritics, AccPyc 1330 respectively.

3. Castings were made at the minimum slurry viscosity at pH=5.

4. Solid particles accumulate at the mold surface during casting process.

5. The heat generation due to the exothermic reaction creates a narrow reaction zone which propagates along the sample.

6. Full conversion is obtained during the reaction

5.1. Porosity Formation and Casting Kinetics

Modeling of casting kinetics deals with consolidation of solid particles at the mold surface in the one dimensional case for casting process which is schematically given in Figure 5.1. The motion of liquid portion of the slurry is due to the capillary suction pressure.

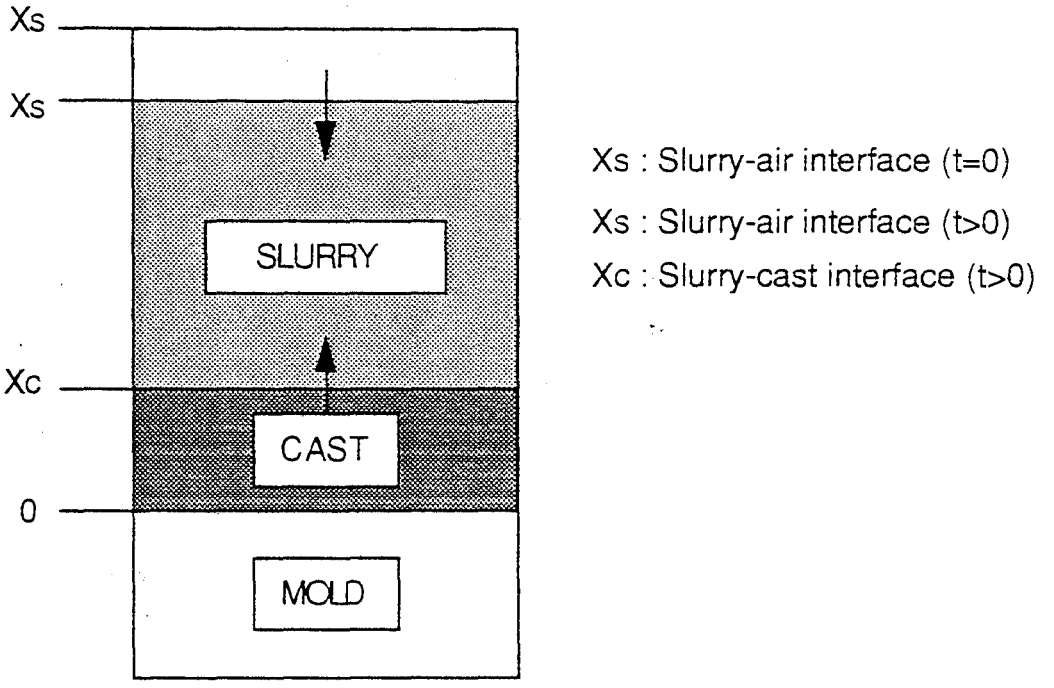

Figure 5.1. A Schematic model for cast formation

The linear flux of the filtrate in one dimensional case may be written based on Figure 5.1. [109]

$$J = \left(\frac{1}{A}\right)\frac{dV_s}{dt} \qquad (5.1)$$

where J is flux, V_S is volume of slip, A is area and t is time.

Since $dV_f = - Ad(X_s^o - X_s)$, equation (5.1) becomes [109]

$$J = \frac{d(X_s)}{dt} \tag{5.2}$$

From D'Arcy's law [117]

$$J = \frac{\varphi}{\eta} \frac{dP}{dX_c} \tag{5.3}$$

where φ is permeability, dP/dXc is pressure gradient and η is viscosity.

Viscosity of the slurry can be written using equation (2.30) considering the solid concentration and casting porosity.

$$\text{Since } dX_c = \frac{(\text{vol\% solid})}{100(1-\omega)} dX_s \tag{5.4}$$

Then equation (5.2), (5.3), (5.4) and (2.30) together

$$\varphi \frac{dP}{dX_c} = \left[\left(\frac{100(1-\omega)}{\text{vol\% solid}}\right) \eta_s \left(1 - \frac{\text{vol\% solid}}{100(1-\omega)}\right)^{-2}\right] \frac{dX_c}{dt} \tag{5.5}$$

where η_s is suspending medium viscosity.

5.2. Reaction Kinetics

Modeling of reaction kinetics deals with the equation considering non-melting reactant radius and the different thermophysical and chemical properties of reactants and products which has been derived using a diffusion kinetics equation by Lakshmikantha et al [76].

$$v = \sqrt{\frac{1}{f\left(\frac{\rho q}{K}\right)} K_o \left(\frac{RTc^2}{E}\right) \exp\left(\frac{-E}{RTc}\right)} \qquad (5.6)$$

where

$$f\left(\frac{\rho q}{K}\right) = A + B \ln\left(\frac{K_{(r)}}{K_{(u)}}\right) \qquad (5.7)$$

with

$$A = \left(\frac{3\overline{C\rho}(Tc-To) - 0.5q(\rho_{(r)}-\rho_{(u)})}{3(K_{(r)}-K_{(u)})}\right) + \left(\frac{(0.5qK_{(u)}(\rho_{(r)}-\rho_{(u)}) - q\rho_{(u)}(K_{(r)}-K_{(u)}))(K_{(r)}-K_{(u)}) - 2K_{(u)})}{2(K_{(r)}-K_{(u)})^3}\right)$$

$$B = \left(\frac{(0.5qK_{(u)}(\rho_{(r)}-\rho_{(u)}) - q\rho_{(u)}(K_{(r)}-K_{(u)}))K_{(u)}^2}{(K_{(r)}-K_{(u)})^4}\right) - \left(\frac{3\overline{C\rho}(Tc-To)K_{(u)}}{(K_{(r)}-K_{(u)})^2}\right)$$

$$\overline{C\rho} = 0.5(\rho_{(u)}Cp_r - \rho_{(r)}Cp_u) + 0.33[(\rho_{(r)} - \rho_{(u)})(Cp_r - Cp_u)]$$

The average thermal conductivities and densities for reactants and products are calculated fro the sum of the product of volume fractions and properties of each component. Consideration of porosity in the calculations of thermophysical properties was given in the literature [76]. These properties can be redefined considering Quemada's equation

$$K = \left[\frac{2 \text{ vol\% solid}}{300\left(1 - \sqrt{\frac{1}{\eta_r}}\right) - \text{vol\% solid}}\right] \prod V f_i K_i \qquad (5.8)$$

$$\rho = \left[\frac{\text{vol\% solid}}{100\left(1 - \sqrt{\frac{1}{\eta_r}}\right)}\right] \prod V f_i \rho_i \qquad (5.9)$$

Equation (5.6) assumes the reacting system in which the reactants give rise to the products in a single step. However, there are at least two possible sequential reactions in the aluminothermite based reaction (reaction 1), reduction of SiO_2 to form Si and interaction of reduced element with C to form SiC [13]. According to this model, the adiabatic temperature exceeds melting point of Al and the decomposition of SiO_2 precedes interaction between silicon oxide and aluminum film to form Al_2O_3 and Si. The formation of SiC may be due to carburization type process since the melting point of SiC is well above the adiabatic reaction temperature, therefore, the dissolution of C in Si and the precipitation of SiC out of the solution may not be possible.

6. RESULTS

6.1. Experimental Results

The data of each sample for rheology, cast formation and reaction kinetics under different processing condition are given in tabular form in Tables 6.1.-6.5. Examples of the plots of combustion temperature against time from which reaction rates were obtained were also given in appendix B. Detail analysis and discussions on the results are made in the next section.

pH in relation to rheological properties of slurries from Table 4.2. to 4.6. were studied. Viscosity of slip was found to be very sensitive to the pH changes and vol% solid loading. The viscosity showed a characteristic minimum at a particular value of pH as

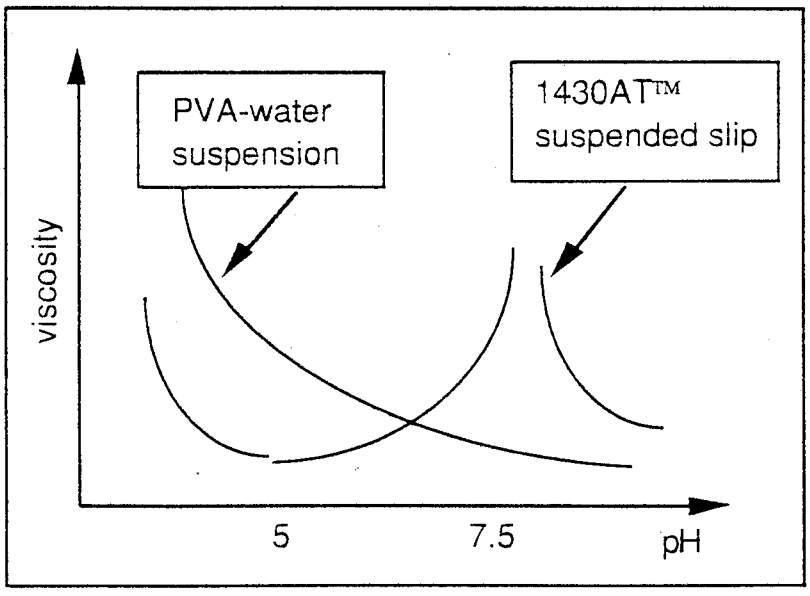

Figure 6.1. Schematic representation of viscosity-pH relationship

Table 6.1. Experimental results

			vol% solid = 44.4			
sample code			A24	A23	A22	A21
wt% submicrometer SiO2 in solid			6.04	9.39	16.06	21.05
viscosity	pH	5.0	< 100	150	200	262
(cps)		7.5	350	551	601	726
porosity (green)	pH	5.0	43.1	42.8	41.9	40.5
(percent)		7.5	43.5	43.2	42.9	42.1
combustion velocity (mm/second)			3.35	3.75	3.88	4.10
porosity (combusted) (percent)			55.3	54.6	53.7	53.5
volume change during combustion (percent)			-18.3	-18.6	-19.0	- 21.5
weight loss during combustion (percent)			2.9	3.5	3.6	3.9

Table 6.2. Experimental results (continue)

			vol% solid = 51.0			
sample code			A34	A33	A32	A31
wt% submicrometer SiO2 in solid			6.04	9.39	16.06	21.05
viscosity	pH	5.0	240	264	650	701
(cps)		7.5	750	902	2,500	
porosity (green)	pH	5.0	40.6	38.9	37.5	34.9
(percent)		7.5	41.7	40.8	40.4	
combustion velocity (mm/second)			3.71	3.94	4.67	4.90
porosity (combusted) (percent)			52.5	51.0	50.8	50.5
volume change during combustion (percent)			-18.6	-19.7	-19.9	-24.3
weight loss during combustion (percent)			3.0	3.2	3.4	3.7

Table 6.3. Experimental results (continue)

			vol% solid = 55.0			
sample code			A44	A43	A42	A41
wt% submicrometer SiO2 in solid			6.04	9.39	16.06	21.05
viscosity	pH	5.0	1,360	1,420	1,850	2,560
(cps)		7.5	2,100	3,960	4,500	6,160
porosity (green)	pH	5.0	36.8	34.5	33.2	32.3
(percent)		7.5	37.3	36.8		
combustion velocity (mm/second)			4.68	5.09	5.69	5.85
porosity (combusted) (percent)			48.4	47.9	47.6	47.4
volume change during combustion (percent)			-19.9	-20.3	-22.4	-23.9
weight loss during combustion (percent)			3.1	3.1	2.7	3.0

Table 6.4. Experimental results (continue)

			vol% solid= 60.0		=51.0	
sample code			A54	A51	AB1	AB2
wt% submicrometer SiO2 in solid			6.04	21.05	13.60	14.70
viscosity	pH	5.0	7,050	7,320	1,360	2,030
(cps)		7.5			10,350	22,265
porosity (green)	pH	5.0	32.8	31.6	33.29	33.44
(percent)		7.5				
combustion velocity (mm/second)			5.32	6.10	11.7	8.90
porosity (combusted) (percent)			47.3	47.5	58.2	53.5
volume change during combustion (percent)			-23.9	-22.7	-33.2	-29.1
weight loss during combustion (percent)			3.3	4.5	9.2	7.0

Table 6.5. Experimental results (continue)

	compaction samples			
sample code	P1	P3	P4	P5
wt% submicrometer SiO2 in solid	0.00 (PEG)	6.04	9.39	16.06
porosity (green) (percent)	45.8	38.0	37.5	37.1
combustion velocity (mm/second)	3.4	4.2	4.6	4.9
porosity (combusted) (percent)	58.2	52.5	52.9	53.3
volume change during combustion (percent)	-22.8	-23.3	-24.6	-25.4
weight loss during combustion (percent)	0.4	0.5	0.9	0.8

shown schematically in Figure 6.1. Note that, for the colloidal silica suspended slip, the minimum viscosity is realized below pH 7 and for the distilled water suspended slip, the minimum shifts to region where pH is more than 7. For 1430AT™ suspensions of reaction 1 at pH=5, Figure 6.2. shows viscosity against vol% solid plot at different wt% submicron particle content.

Both viscosity vs pH and viscosity vs shear rate (spindle speed) measurements were performed. All slurries showed time dependent behavior and shear thinning where viscosity decreased with increasing shear rate (see section 7.1.2). However, at higher solid loadings and at pH = 5, less time dependency for the slips were noted.

The cast preforms and synthesized samples are shown in Figure 6.3. The porosity level at the green cast preform were also measured. The results indicate that the sample with high colloidal silica and solid content has predominantly less porous and smaller pore size structure. The measured porosity levels for both process, slip casting and compaction were comparable. It is also noted that submicron sized particles from colloidal silica, 1430AT™, increases combustion rate as well as conversion efficiency of the reaction.

The data obtained from compaction practices are comparable to slip cast route. Since there are no plastic deformation, powder blend of reaction 2 could not be compacted without binder addition. The sample P1 to which binder was PEG showed the highest porosity level at green form after binder removal. The porosity levels for samples P3, P4 and P5 were close to the slip cast samples with 51.0 vol% solid loading. However conversion efficiency of the reaction for the compaction samples was relatively higher than the slip cast samples.

The shape change (dimensional) was minimal (± 1 %) for slip cast samples during combustion synthesis. However, compaction samples showed up to 10 % expansion in the dimension parallel to the compaction direction. Li and Sekhar [41] have concluded that dimensional changes are strongly influenced by the porosity of synthesized product which also affects the mechanical properties. Although none of the mechanical test measurements was employed,

the fracture toughness of the slip cast samples were qualitatively comparable with the compacted samples. The main reason for not doing any mechanical test was the casting defects such as cracks, shrinkage defects etc. which were not be eliminated totally in the process. These problems primarily arises from drying and design practices of casting.

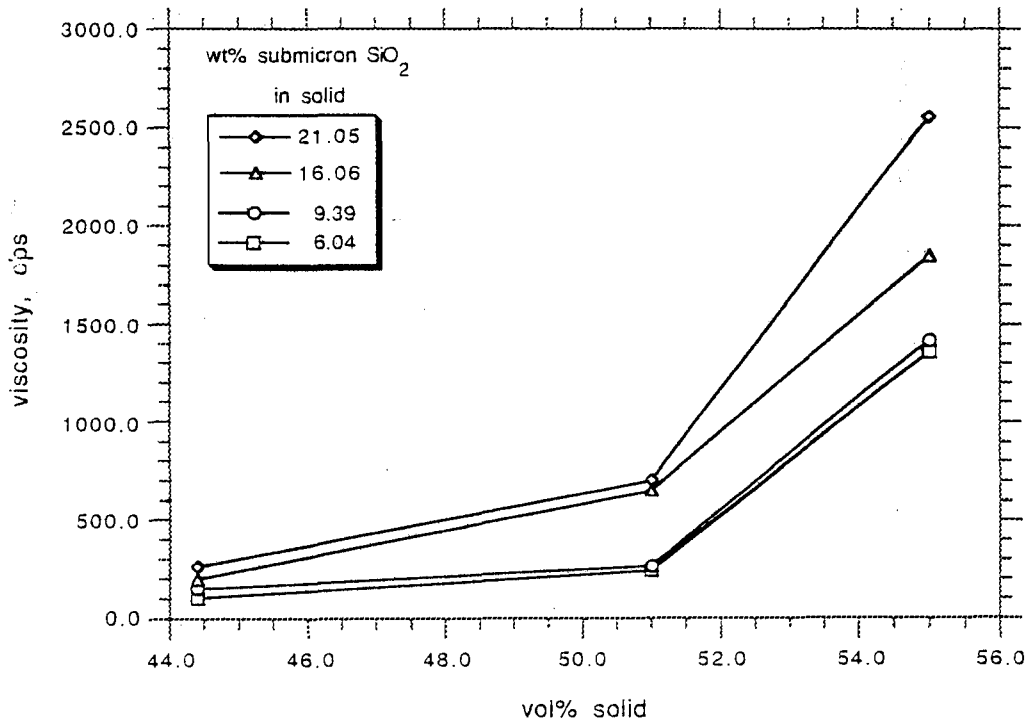

Figure 6.2. Viscosity as a function of vol% solid loading

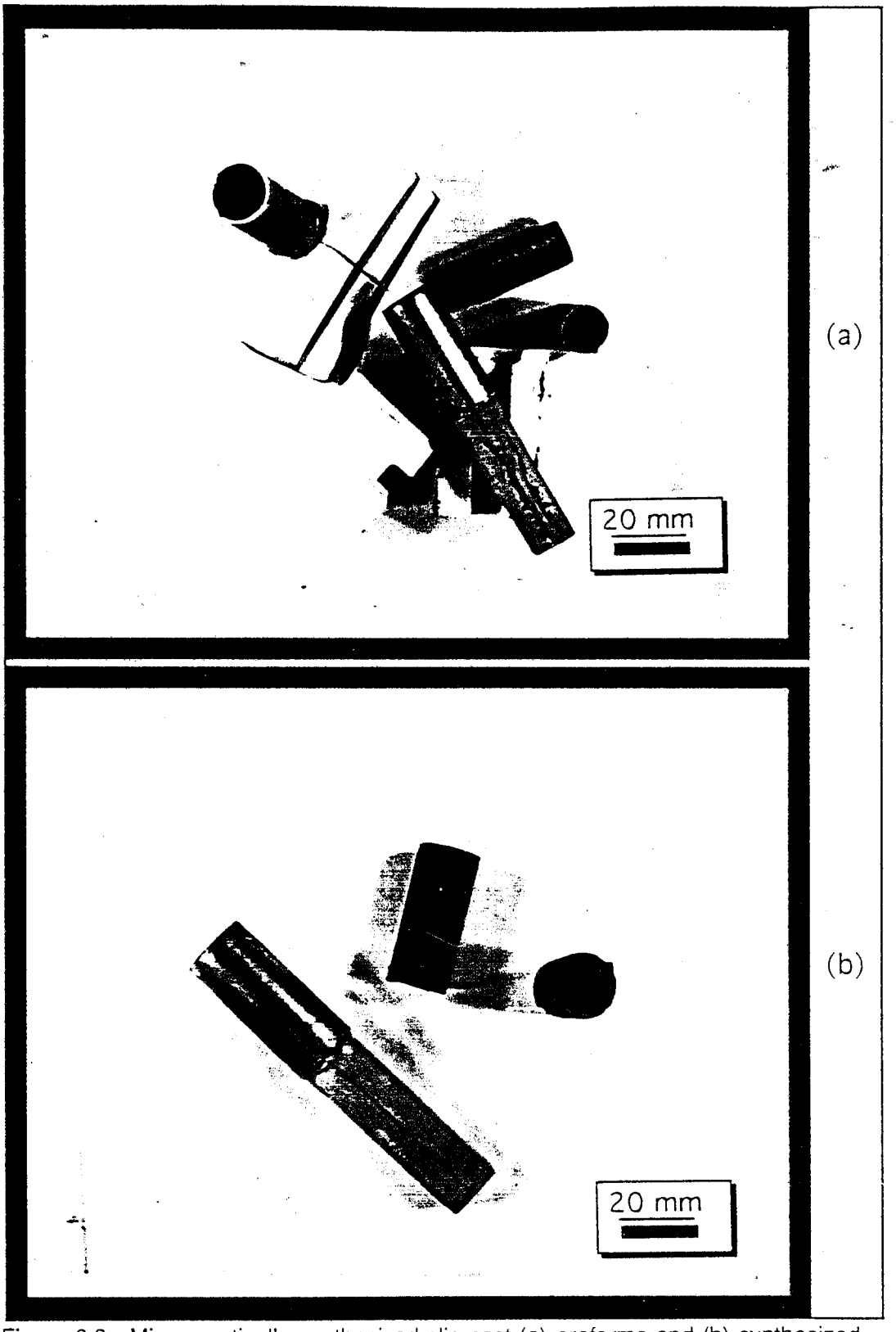

Figure 6.3. Micropyretically synthesized slip cast (a) preforms and (b) synthesized samples

6.2. Model Results

By using the data from Table 6.1-3., the values of η_r calculated from Quemada's equation [124], $\eta_r = (1 - (\text{vol\% solid}/100(1-\omega)))^{-2}$, and then both η (experimental) and η_r (Quemada's equation) plotted against vol% solid as shown in Figure 6.2. and 6.4 respectively. Table 6.6 summarizes the relative viscosity values calculated from Quemada's equation at different solid loadings and submicron particle size concentrations. At 44.4 vol% solid and different submicron particle concentrations, experimentally measured values for casting thicknesses as a function of time are presented in Table 6.7. Using these data, Cast thickness as a function of time was plotted as shown in Figure 6.6. By using the data from Table 6.1 and 6.7, the values of $\varphi dP/dXc$ were calculated from casting kinetics equation, equation (5.5), and then plotted against Xc as shown in Figure 6.7. Xc (slurry-cast interface) values were calculated using the equation (5.4). Xs was measured experimentally by monitoring the slurry-air interface.

Table 6.6. Relative viscosities calculated from Quemada's equation

	wt% submicon SiO_2 in solid											
	6.04			9.39			16.06			21.05		
vol% solid	44.4	51.0	55.0	44.4	51.0	55.0	44.4	51.0	55.0	44.4	51.0	55.0
porosity%	43.1	40.6	36.8	42.8	38.9	34.5	41.9	37.5	33.2	40.5	34.9	32.3
η_r	20.7	50.0	59.4	20.0	36.6	45.3	18.0	23.4	32.0	15.5	21.3	28.4

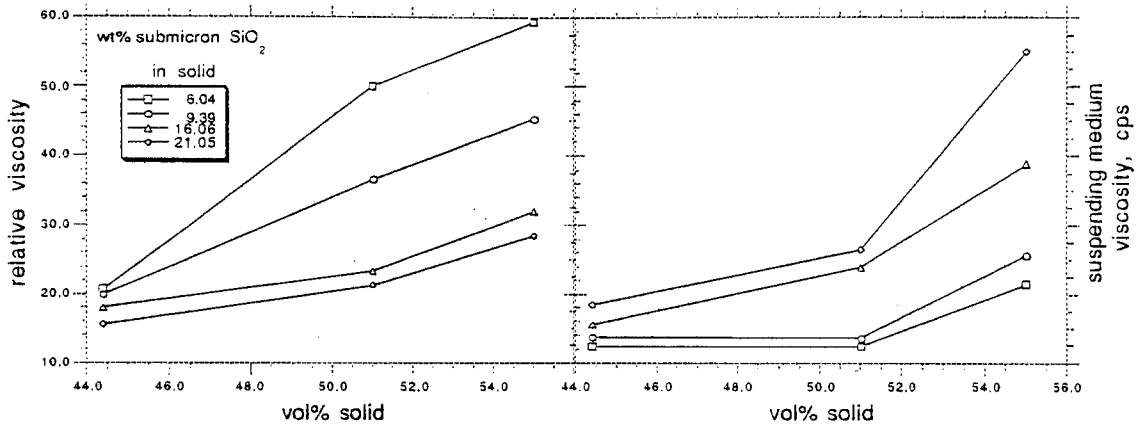

Figure 6.4. Relative viscosity as a function of vol% solid calculated from equation (2.30)

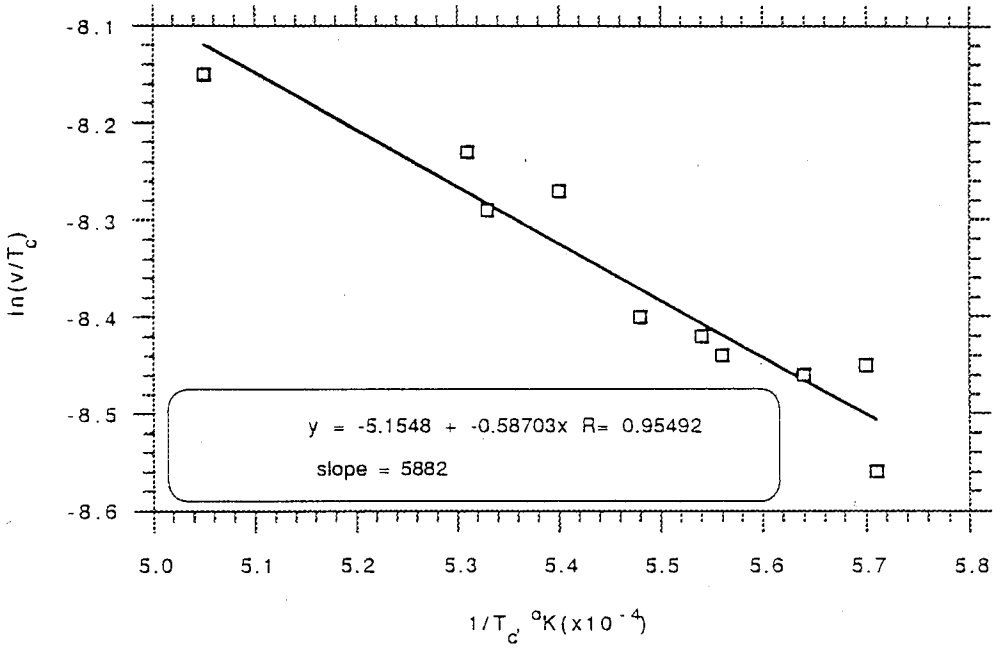

Figure 6.5. Plot of ln(v/Tc) against 1/Tc to obtain the activation energy for reaction 1

Table 6.7. Data for cast formation at vol% solid= 44.4, (pH=5.0)

time after casting, sec.		30	60	120	300
		Xc, cm	Xc, cm	Xc, cm	Xc, cm
wt% SiO_2	6.04	0.280	0.467	0.779	0.966
	9.39	0.330	0.590	0.797	0.959
	16.06	0.367	0.662	0.865	0.974
	21.05	0.394	0.739	0.943	0.982

Table 6.8 shows the thermochemical and physical data used in the analysis for reaction 1. The values for $K_{(u)}$, $K_{(r)}$, $\rho_{(u)}$, $\rho_{(r)}$ and $\overline{C\rho}$ have been calculated using equations (5.8-9) and the data from Table 6.1-4 and Handbook of Thermophysical Properties of Solid Material by Goldsmith et al [128,129]. The activation energy for the reaction 1 has not been previously reported. In order to obtain the activation energy, E, of the system, the velocity and the temperature of the reaction were experimentally measured. From the plot of ln(v/Tc) against (1/Tc) as shown in Figure 6.5., the activation energy was calculated. For reaction 1 with 21.05 wt% submicron concentration, the pre-exponential factor, K_o, was chosen in the range of 2.0×10^5 to 6.0×10^5 to which calculated combustion velocities approximates to experimentally measured combustion velocities. Reaction kinetics equation, equation (5.6), is solved for different vol% solid loading at 21.05 wt% submicron powder in solid and then, combustion velocity against vol% solid loading was plotted as shown in Figure 6.8.

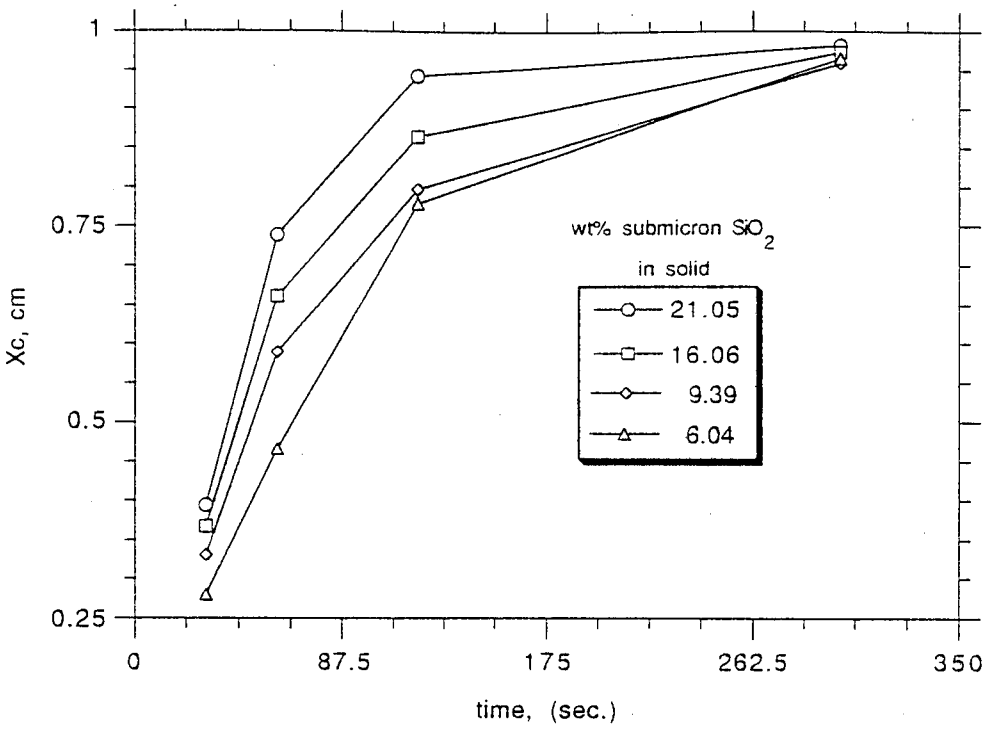

Figure 6.6. Cast thickness as a function of casting time

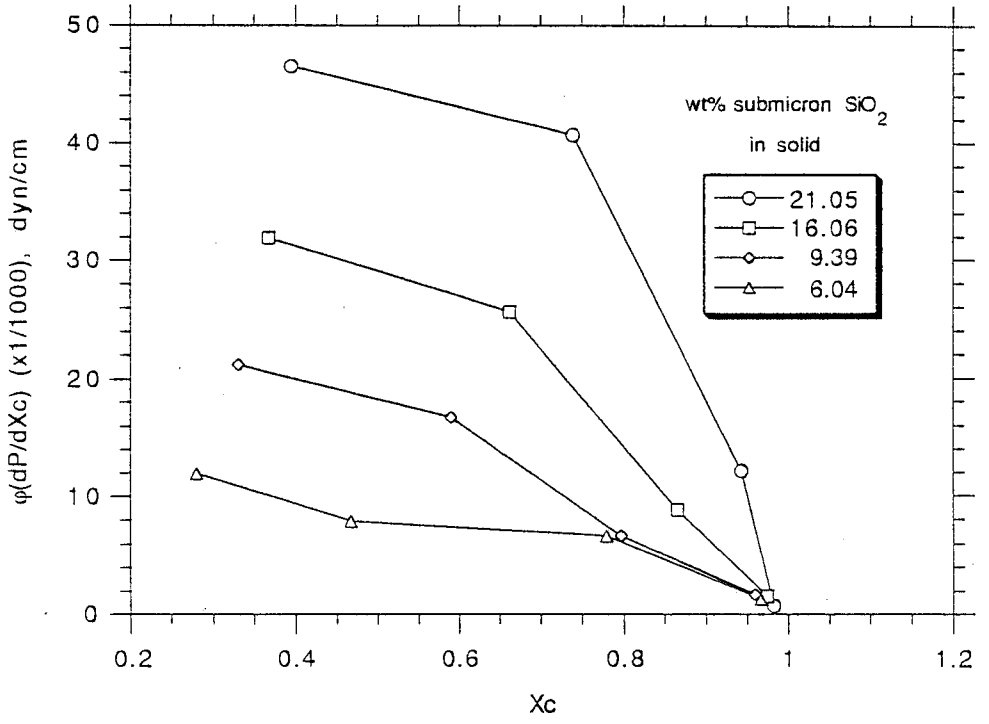

Figure 6.7. Permeability-pressure gradient as a function of casting thickness

Table 6.8. Thermochemical and physical data for reaction 1

		Tc	$K_{(u)}$,	$K_{(r)}$	$\rho_{(u)}$	$\rho_{(r)}$	$\overline{C\rho}$
		°K	J/msec°K		kg/m^3	kg/m^3	J/m^3K
vol% solid	44.4	1823	45.43	23.27	1553	1706	1.98e+6
	51.0	1848	50.89	25.07	1699	1817	2.14e+6
	55.0	2023	53.52	26.97	1767	1930	2.25e+6
q, J/kg	2.64e+06		To, °K		873		
E, J/mole	97,811						

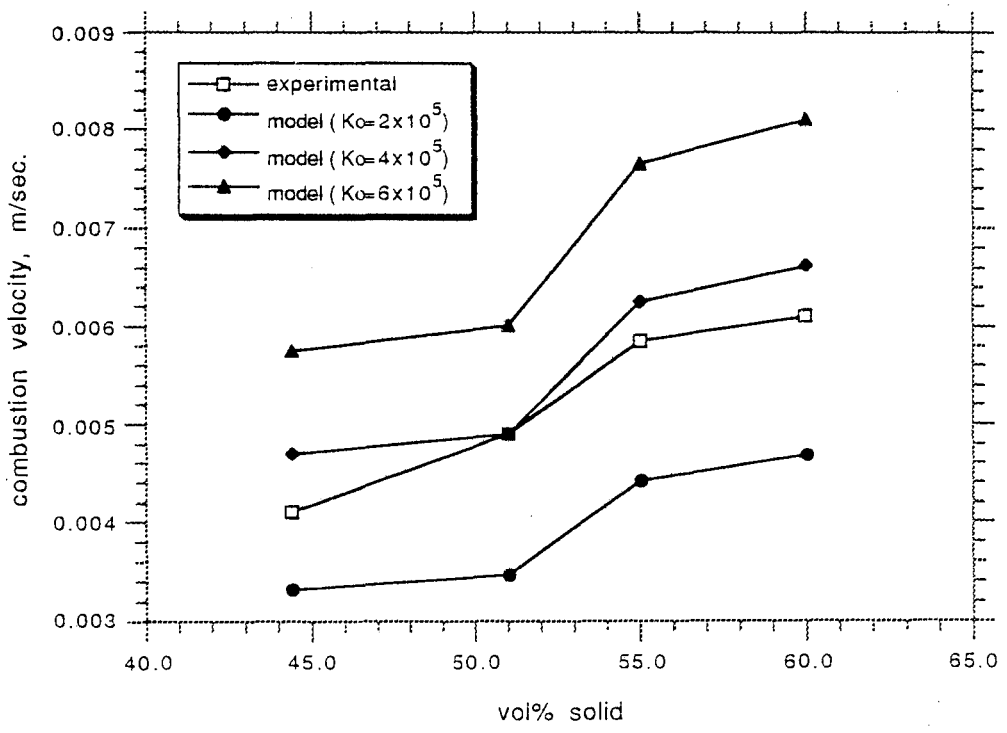

Figure 6.8. A plot of calculated and experimental combustion velocity as a function of vol% solid for samples Ai1 for different Ko values

7. DISCUSSION OF RESULTS

7.1. Rheology of Slurries and Cast Formation

The state of the particulate dispersion is mainly affected by the vol% solid loading, pH and particle size distribution. The viscosity of the suspensions increases drastically when the vol% solid in the suspension is increased beyond a critical value. All compositions suspended with 1430AT™ showed thixotropic behavior and were able to deflocculated at moderate acidity. It is also experimentally observed that wt% submicron powder concentration in solid increases slurry viscosity. It also appears that the initial trends in both the casting rate and the values of $\varphi dP/dXc$ show an increase with wt% submicron concentration and fail to provide consistency with the higher packing densities due to fine particles as shown in Figure 6.3 and Figure 6.6-7. After the initial transient, both the casting rate and the values of $\varphi dP/dXc$ show a relative decrease for the suspensions higher fine particle concentration. This indicates that the suspensions with higher fine particle concentration have agglomeration and possibly lose some colloidal size particles into the mold at the beginning of the casting process. As the casting process proceeds, the permeability and the casting rate decrease and densification in the cast was developed by further filtration of the suspension from the riser. For better understanding of the complex nature of colloidal consolidation, a zeta potentiometer and further experiments are needed to monitor the evolution of the rheology of suspensions during casting process. It

has been shown that the bulk attracting force for particles of colloidal dimensions is greater than that of non-colloidal particles because of the multiplicity of points of contact, even though the actual force of attraction between two individual colloidal particles is less than that between two non-colloidal particles. Thus, there exists a general tendency that the finer the particles, higher the suspension viscosity and lower the permeability [94]. In addition to that submicron particles from 1430AT™ could facilitate the nucleation of the gel network, therefore, increasing the viscosity [130].

7.1.1. Relationship between viscosity and pH

7.1.1.1. Effect of binder type and particle size

The feasibility of the suspending medium, 1430AT™, on dispersion of the powders involved in the reaction 1 and 2 was planned to determine. The slip behavior of each reactant powders of SiO_2, Al, C and Cr_2O_3 suspending with colloidal silica, 1430AT™, were investigated separately. The suspensions of SiO_2 and Al were prepared with 51 vol% solid loading with the following compositions:

a) 79.82 grams of SiO_2 and 50 grams of colloidal silica
b) 81.32 grams of Al and 50 grams of colloidal silica

After homogeneous mixing of the slip, the pH was lowered and the viscosity at each level was measured. Aluminum slip showed

much lower viscosities than silica slip in the entire acidic range as shown in Figure 7.1. The maximum viscosity for the silica slip was observed to occur at around pH = 7. As pH of the slip was lowered, the viscosity decreased and reached to the minimum at around pH = 5. Further decreases in pH caused the viscosity to increase. For pH values above 7, The viscosity was again seen to decrease with increase in pH. However the basic side of the system was not studied completely since colloidal silica was not stable in that range. Since the colloidal silica particle surfaces were alumina treated, in all cases, the pH values which corresponds to zero point of surface charge (zpc), and hence the maximum viscosity, slightly shifted from given pH values in the literature for zpc of all oxides studied. The pH at zpc for oxides Al_2O_3, SiO_2 and Cr_2O_3 are 9.0, 2.2 and 7.0 respectively [94]. Because of this special affect of colloidal silica (pH=9), aluminum slip at which aluminum particles which had 0.5 wt% alumina at surface exhibited very low viscosities in wide pH range. However viscosity increased as pH approached to 9 which is pH at zpc for alumina and also another increase in viscosity was observed as pH lowered to the pH where SiO_2 reaches to zpc. Similar behavior was observed for SiO_2 slip. The maximum viscosity which was expected at pH 2.2 was around 7. The reason for this is the particles are being covered by the cloud of colloidal silica and the slip is behaving like alumina slip conditions due to the surface treatment for colloidal silica powders. The slip of C and Cr_2O_3 for the same solid loading and colloidal silica suspension could not be prepared because of the extreme agglomeration. In the case of Cr_2O_3, it was clear that pH value for slip was the pH at around zpc

for Cr_2O_3. For carbon, it is believed that agglomeration was due to the high polarizibility of carbon powders which causes particles to attract one another to form strong agglomerates [107].

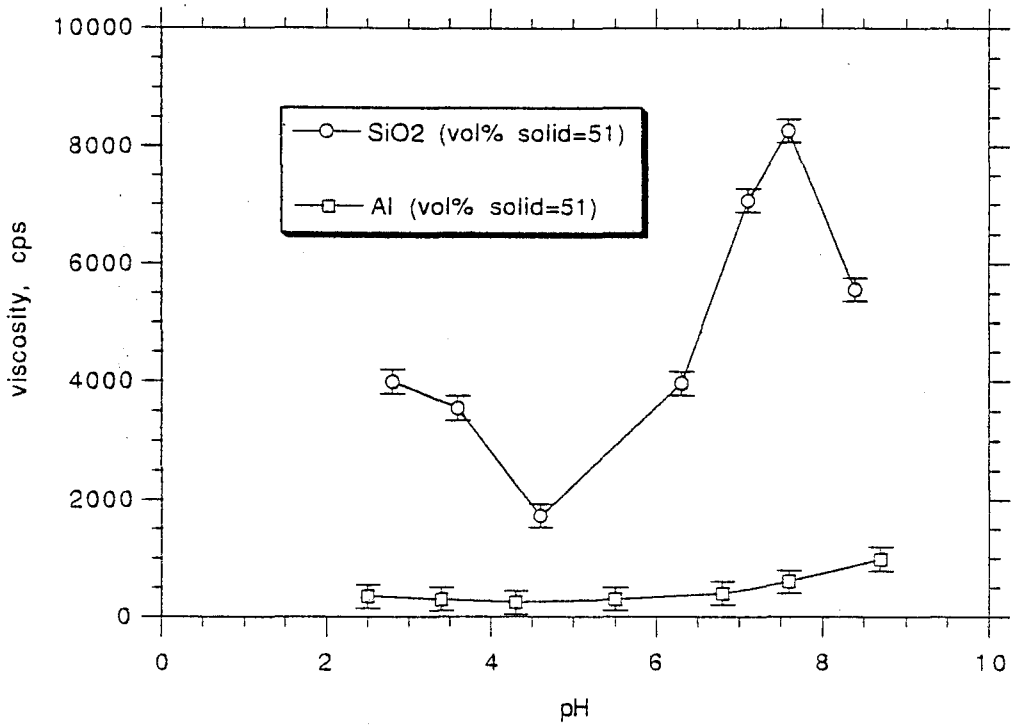

Figure 7.1. A plot of the viscosity as a function of pH for samples SiO2 and Al slips suspended with colloidal silica

The effect of dispersant, binder and deflocculation were also planned to determine if 1430AT™ was compatible for the slip compositions as given in Table 4.2-7. Samples A21, A26, and A27 correspond to 44.4 vol% solid. Samples A32, A36, A37, and A33 correspond to 51.0 vol% solid. Samples B10, B11, and B12 correspond to 40.0 vol% solid. The effect of suspending medium (distilled water and 1430AT™), binder (PVA and 1430AT™) and dispersant (DARVAN-C™ and 1430AT™) were investigated. For both

suspensions, A21 and A27 to which wt% submicron SiO_2 are 21.05 and 0 respectively. However, the rheogical behavior of suspensions are entirely different. Suspension A21 displayed thixotropic behavior while A27 did not. Without dispersant DARVAN-C™, sample A26 couldn't be deflocculated, although it showed a substantial viscosity decrease at low pH values. It is also interesting to note that the response of viscosity to pH changes for slip prepared with distilled water and 1430AT™ is in different manner. The viscosity of distilled water suspension with DARVAN-C™ dispersion, sample A27, increases while the viscosity of 1430AT™ suspension, sample A21, approaches its minimum as pH is lowered. Similar patterns for the viscosity values were obtained at higher solid loadings as shown in Figure 7.3.

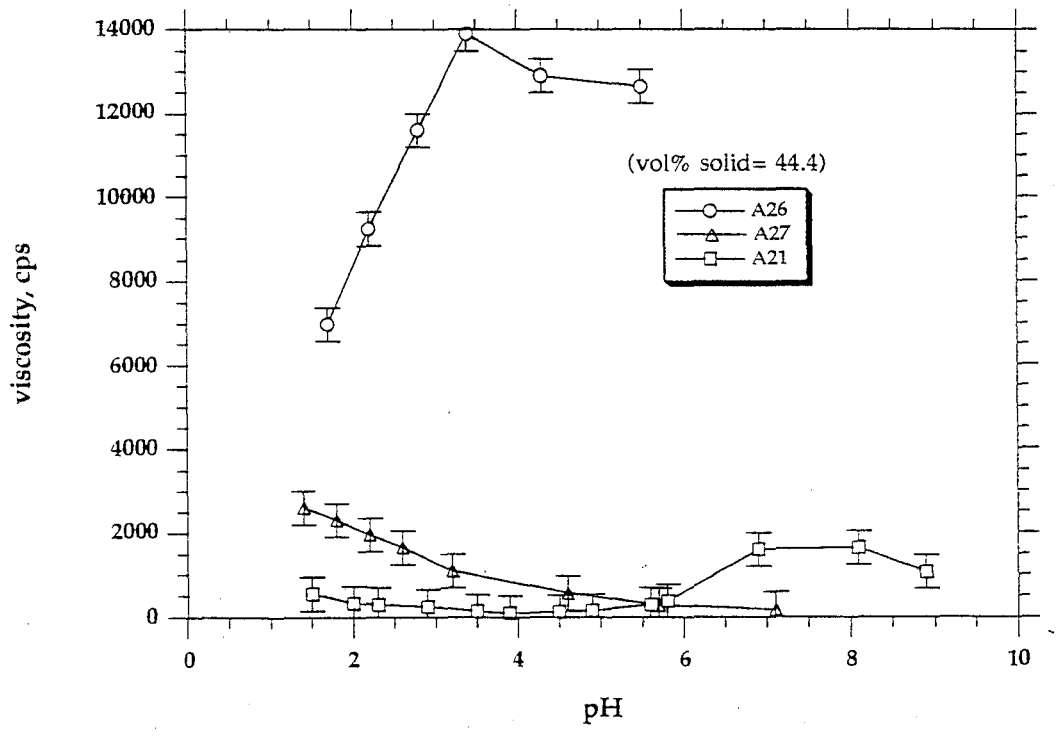

Figure 7.2. A plot of the viscosity as a function of pH for samples A21, A26 and A27

However, relatively much higher viscosities were noted in case of higher solid loadings. The relative viscosities of suspensions, A36 and A37, with 0.18 and 0.35 wt% dispersant were investigated at various pH values as shown in Figure 7.3. The suspension dispersed with 0.18 wt% DARVAN-C™ showed lower viscosities than sample A37 in the entire pH range. The suspension A33 for which submicron SiO_2 content was 9.39 wt% in solid showed lower viscosities at high pH values while higher viscosity at low pH values when compared to the suspension, A32, with 16.06 wt% submicron concentration of solid.

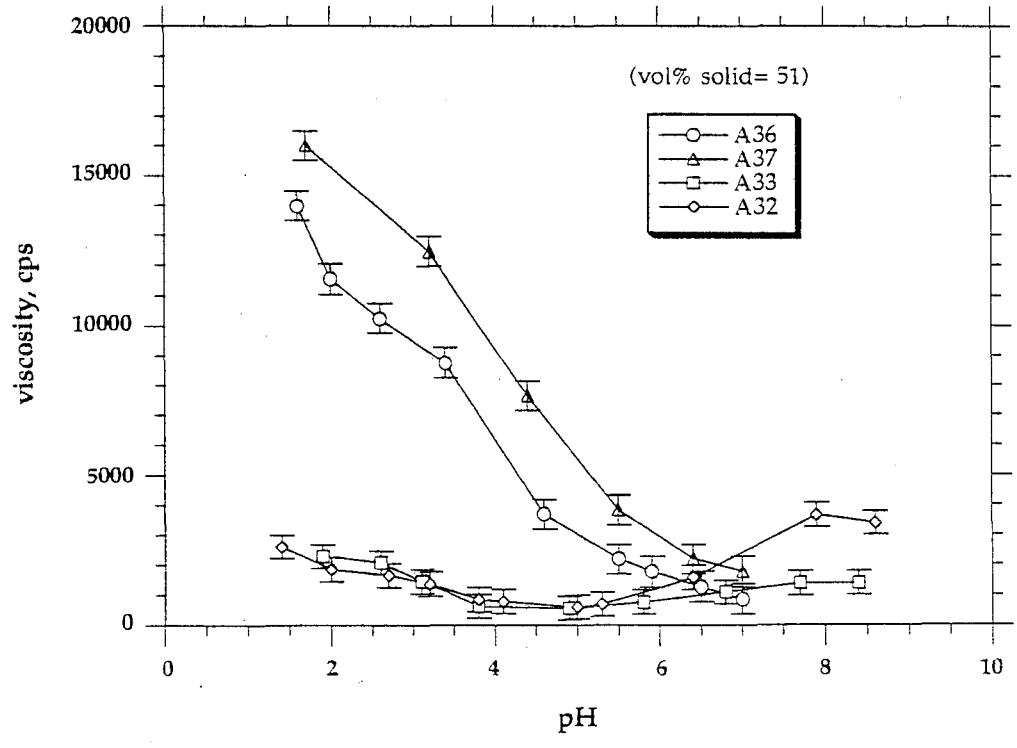

Figure 7.3. A plot of the viscosity as a function of pH for samples A32, A36, A37 and A33

This behavior could be explained with large surface introduced by submicron particles from 1430AT™ which causes increase in viscosity at the pH values (7.5-8.0) closer to the zpc of SiO2.

The Cr_2O_3-Al-C system was also investigated for both distilled water and 1430AT™ suspensions as shown in Figure 7.4. However, the distilled water suspended suspension couldn't be deflocculated possibly because of incompatibility of DARVAN-C™ with this particular system. On the other hand, the 1430AT™ suspension gives reasonable deflocculation and viscosities levels comparable to the

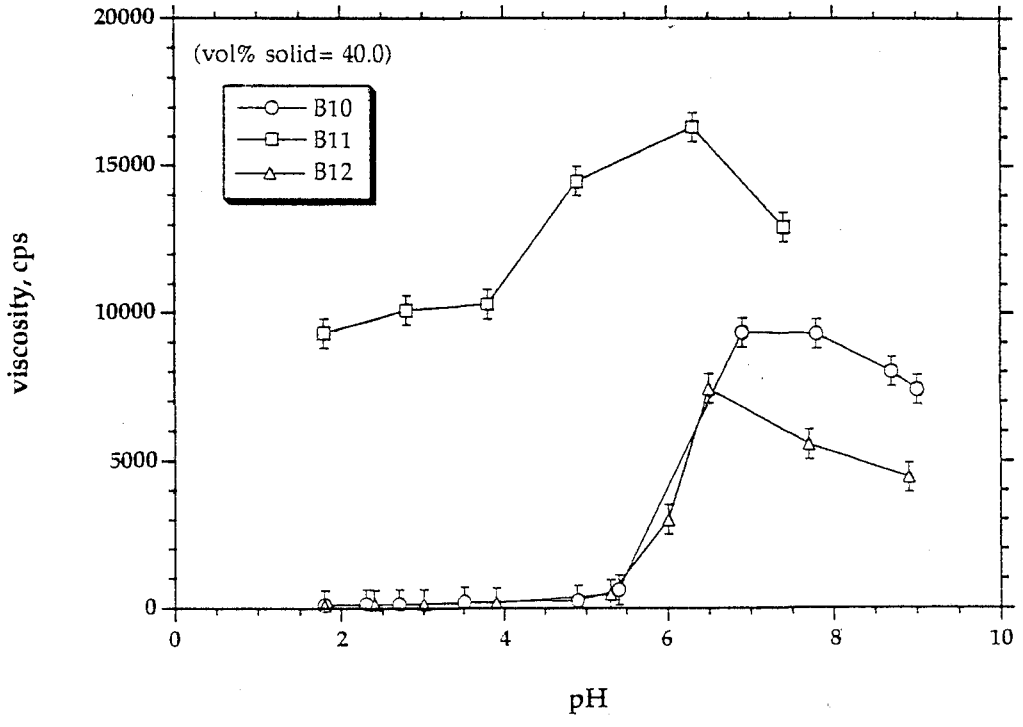

Figure 7.4. A plot of the viscosity as a function of pH for samples B10, B11 and B12

reaction 1 as wt% SiO_2 increased. Figure 7.4. shows that distilled water suspended the Cr_2O_3-Al-C powder system was similar to both colloidal silica suspended the Cr_2O_3-Al-C and the SiO2-Al-C powder systems. However relatively high viscosities were observed along the acidic slips.

7.1.1.2. Effect of solid concentration

The effect solid loading concentration of the suspension, vol% solid, on the rheology and cast formation for both the Cr_2O_3-Al-C and the SiO2-Al-C powder systems as well as their combinations

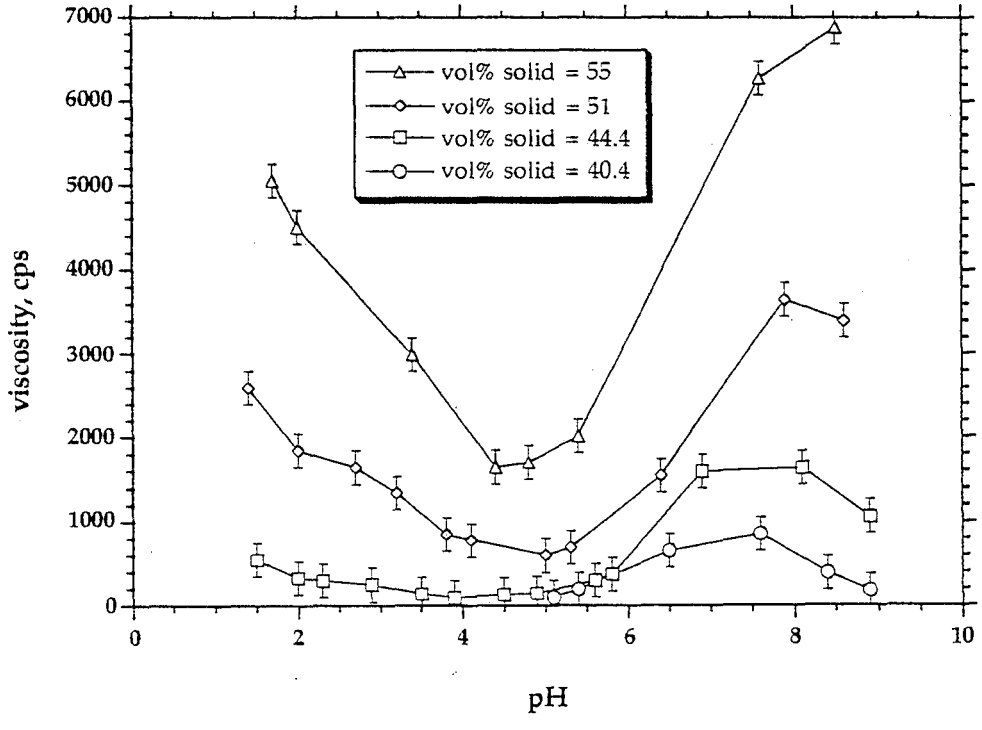

Figure 7.5. A plot of the viscosity as a function of pH for samples A10, A21, A32 and A43

were studied as shown in Figures 7.5., 7.6. and 7.7. The Cr_2O_3-Al-C combustible powder system was also studied with SiC dilution at different solid loadings as shown in Figure 7.8.

All powder systems showed the characteristic behavior of colloidal silica suspended slips. In general at higher solid loadings, higher viscosities were obtained. It is noted that, in all cases as expected, the pH value where highest viscosity is obtained decreases as solid loading increases. Also pH ranges which correspond to lowest viscosities are very sensitive to the vol% solid loading.

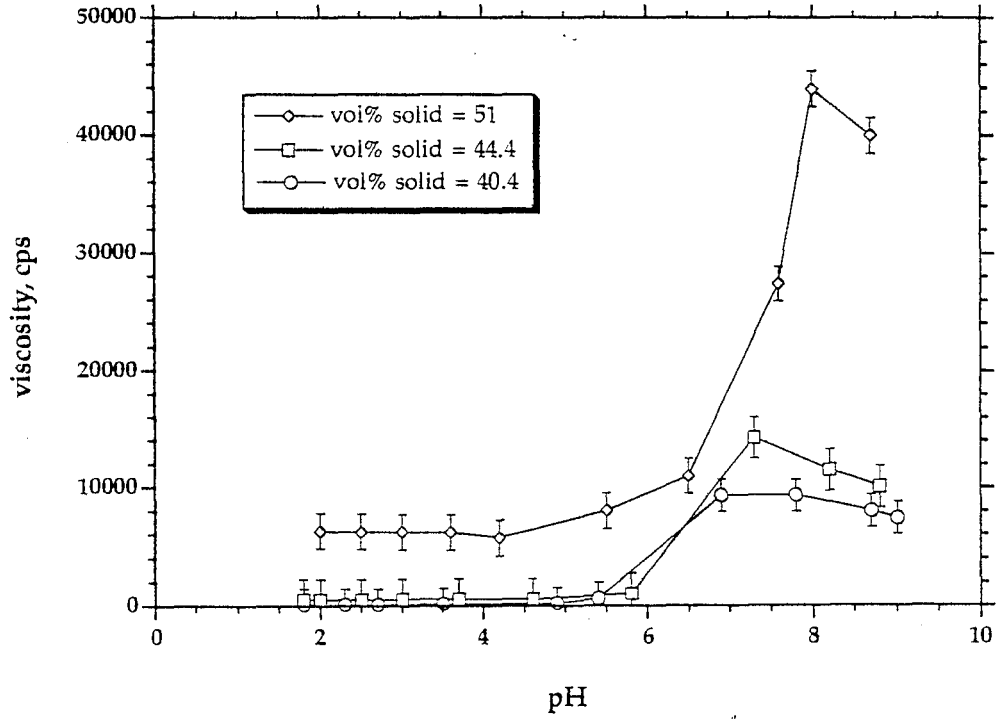

Figure 7.6. A plot of the viscosity as a function of pH for samples B10, B20 and B30.

The state of the particulate dispersion is affected mainly by the suspension of the solid concentration. The viscosity of the

suspensions increases drastically when the solid concentration is increased beyond a critical value. Figure 7.5. shows the rheological behavior at several pH values for the SiO2-Al-C and colloidal silica system. As the pH of the basic slip is decreased the viscosity falls rapidly to a minimum at pH values between 4 to 6 and then rises again.

From the point of view of casting, the desirable suspension would appear to be one for which the pH value of which falls between 4 and 6. The density of the slip should be chosen to suit the particular application, but should contain between 45 and 55 vol% solid for these system.

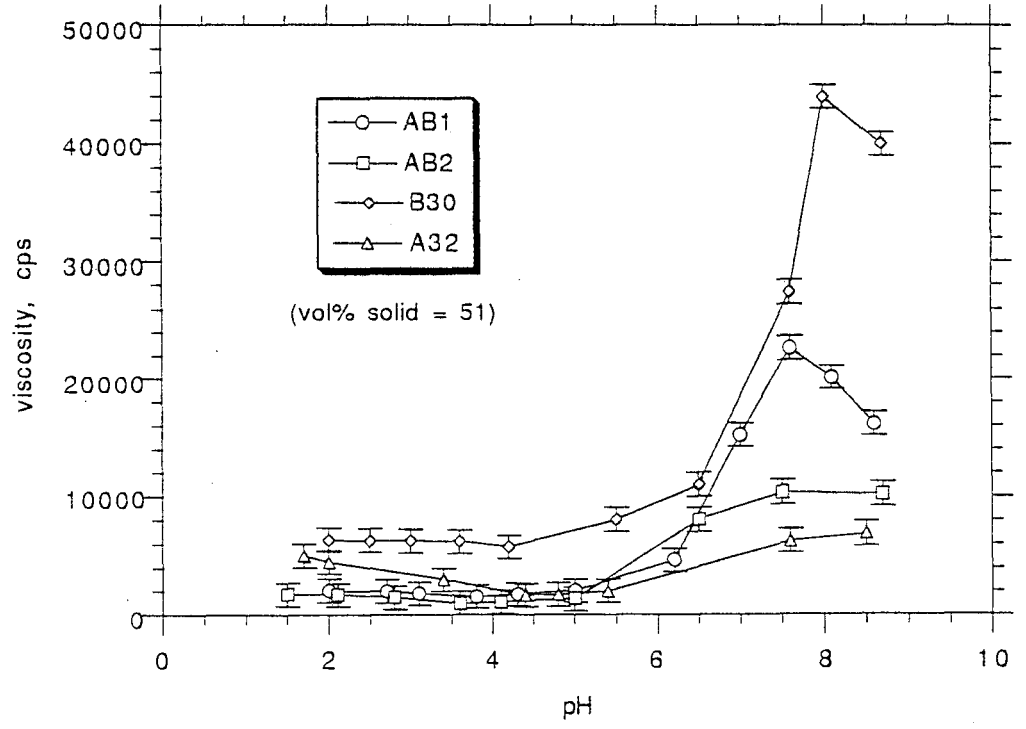

Figure 7.7. A plot of the viscosity as a function of pH for samples A32, AB1, AB2 and B30

For the solid concentration above 55 vol% solid, the slips are out of castability range with very high viscosities. For solid concentration below 44 vol% solid, the suspensions had high settling tendency.

The Cr_2O_3-Al-C powder system exhibited relatively higher viscosities than the SiO_2-Al-C system. As wt% of the Cr_2O_3-Al-C in the SiO_2-Al-C slip increases, pH ranges widens for low viscosities. The Cr_2O_3-Al-C slurry system also exhibited no viscosity change below pH 6. However, viscosities rises rapidly with density and is

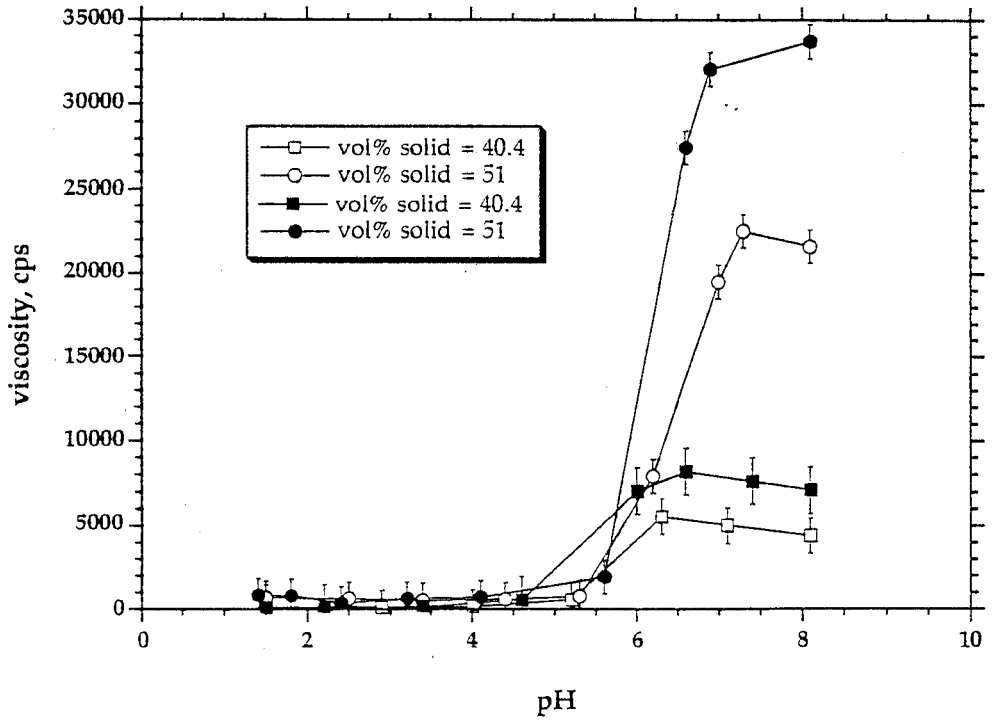

Figure 7.8. A plot of the viscosity as a function of pH for samples D10, D20, D30 and D40

most noticeable in suspensions containing more than 44 vol% solid indicating possibility of more interconnected or agglomerated

structure. One of the reasons for this phenomena could be the particle size of Cr_2O_3 which is in the range of 0.5 to 1 microns. At 51 vol% solid, the extreme viscous characteristic of this system totally changes when it is used together with the SiO_2-Al-C system at different concentrations.

Addition of SiC dilutent to the Cr_2O_3-Al-C slurry system brought full deflocclation for entire acidic range with very low viscosities. The reason for this behavior could be the SiO_2 impurity content of SiC powders, which is on the powder surface.

The processing diagram of reaction 1 for the suspension viscosity at full deflocculation (at minimum viscosity) as a function of processing parameters is given in Figure 7.9. Using such diagrams is helpful to search the optimum condition for the process. Generalization of such diagrams is unlikely, therefore, it must be developed separately for each particular system. The bar codes, on the right hand side of the plot, indicate the level of the viscosity of the suspensions.

In summary, The minimum viscosity for 1430AT™ suspension is realized using HCl at moderate acidity. Upto 55 vol% solid loading with 20 wt% submicron concentration in solid gives suitable conditions for slip casting purposes.

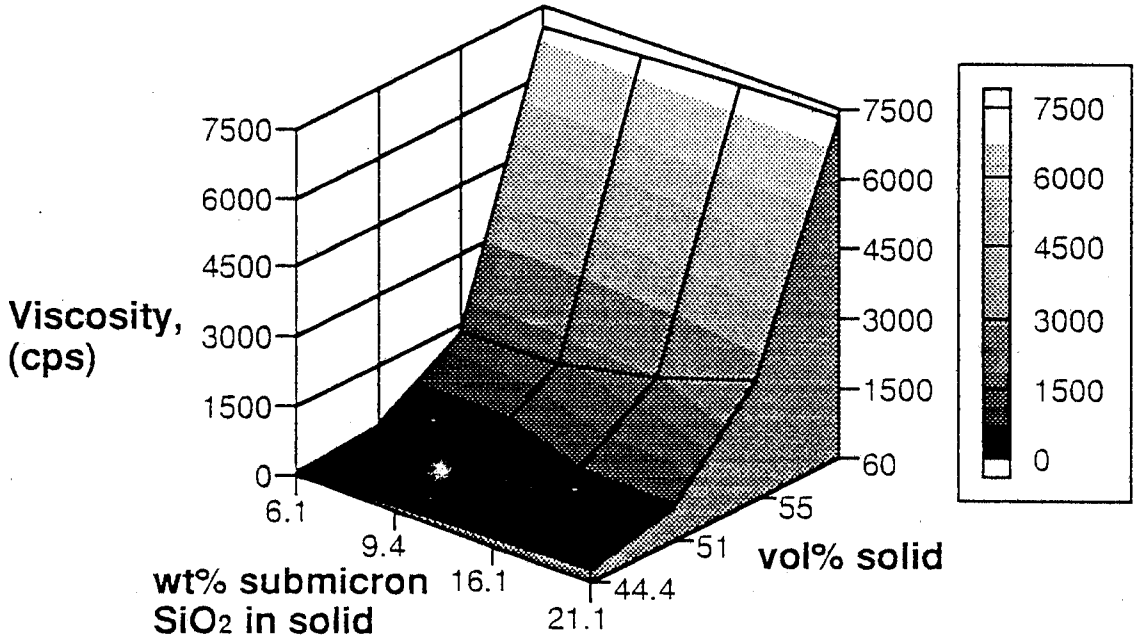

Figure 7.9. A plot of the viscosity as a function of vol% solid and wt% submicron SiO_2 in solid

7.1.2. Relationship Between Viscosity and Spindle Speed

The viscosity changes were recorded with changing spindle speed (RPM) and the up and down curves of viscosity were noted for the slips of compositions A10, A21 and A32. The effect of spindle speed, RPM, on the viscosity readings are shown in Figures 7.10-a, 7.10-b and 7.11 respectively. All these blended samples show an decrease in viscosity with the shear rate.

Figure 7.12 indicates the viscosity changes as a function of time for composition A32. It is noted that time dependent behavior under constant shear rate, 30 RPM, shows slight decrease in viscosity with time. However, viscosity appears to increase after some time (~ 30 minutes) possibly due to corrosion of aluminum and gelation.

There exists a general trend that higher the solid loading and submicron concentration, less change in viscosity with time. This must be primarily due to reduced settling tendency and thixotropy [94,121]. In all the cases the up curve showed a higher viscosity than the down curve which indicates that slurries were thixotropic. However thixotropic behavior decreases as vol% solid increases. It is also noted that the lowest viscosities were obtained for all three suspensions at pH = 5 where thixotropy also decreases and/or the suspensions approach to Newtonian behavior.

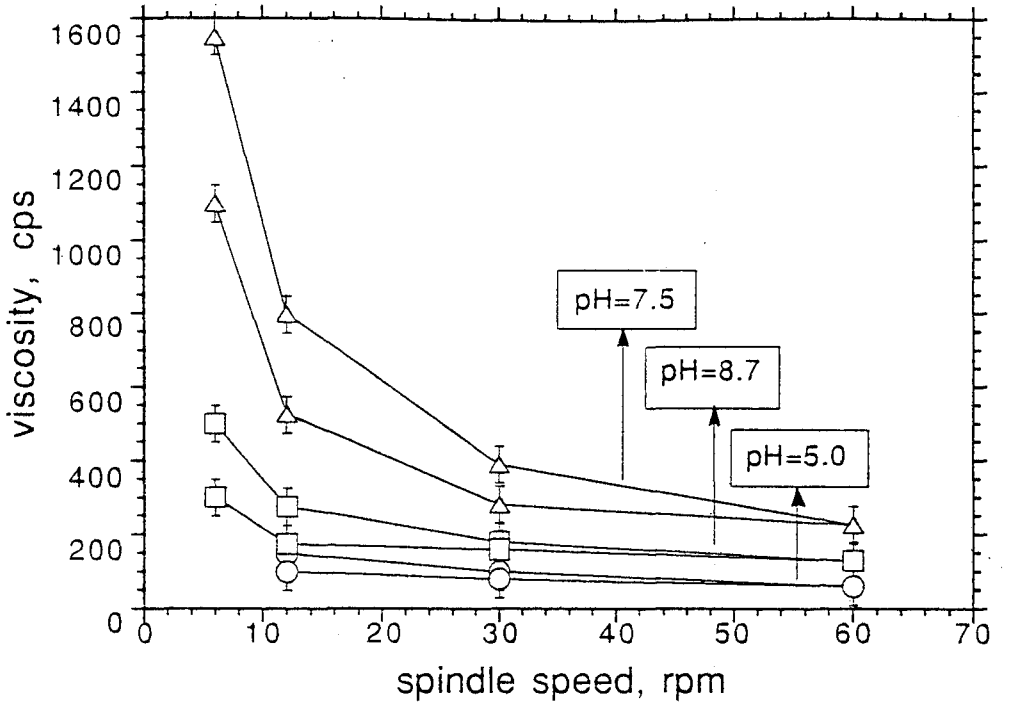

(a)

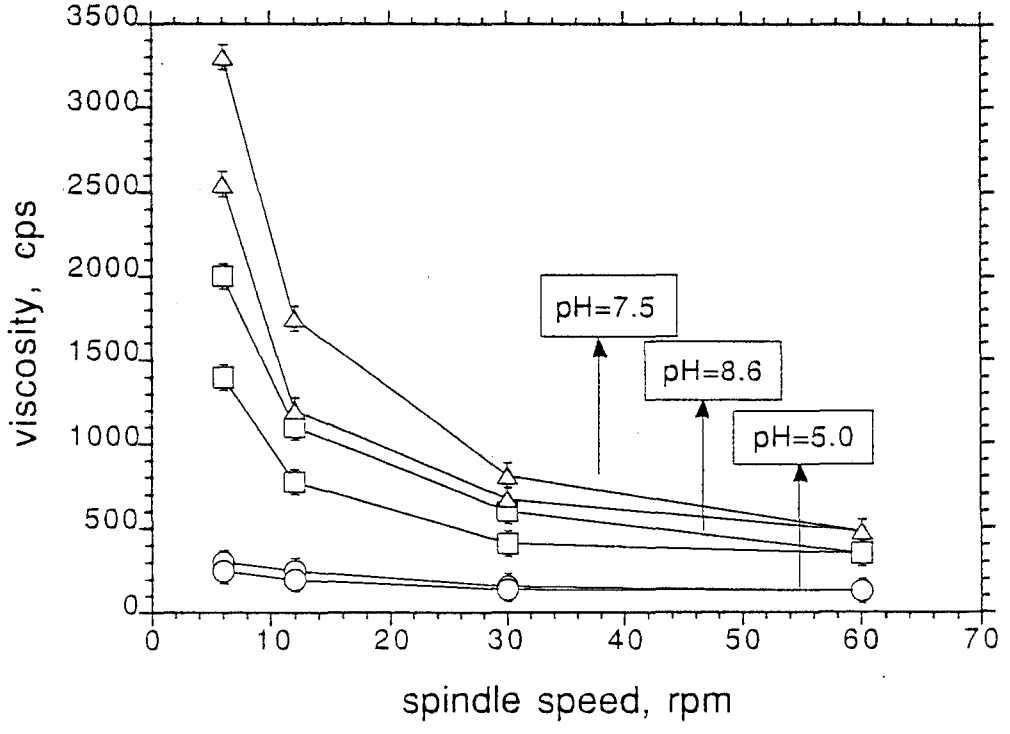

(b)

Figure 7.10. A plot of the viscosity as a function of spindle speed, rpm, for samples (a) A10 and (b) A21

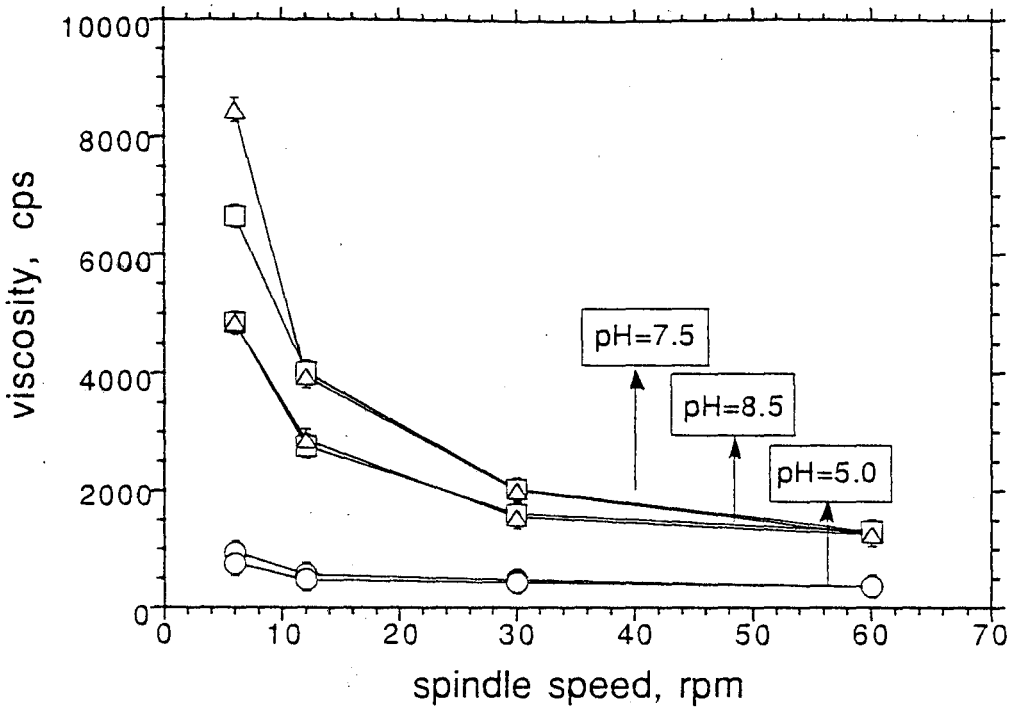

(a)

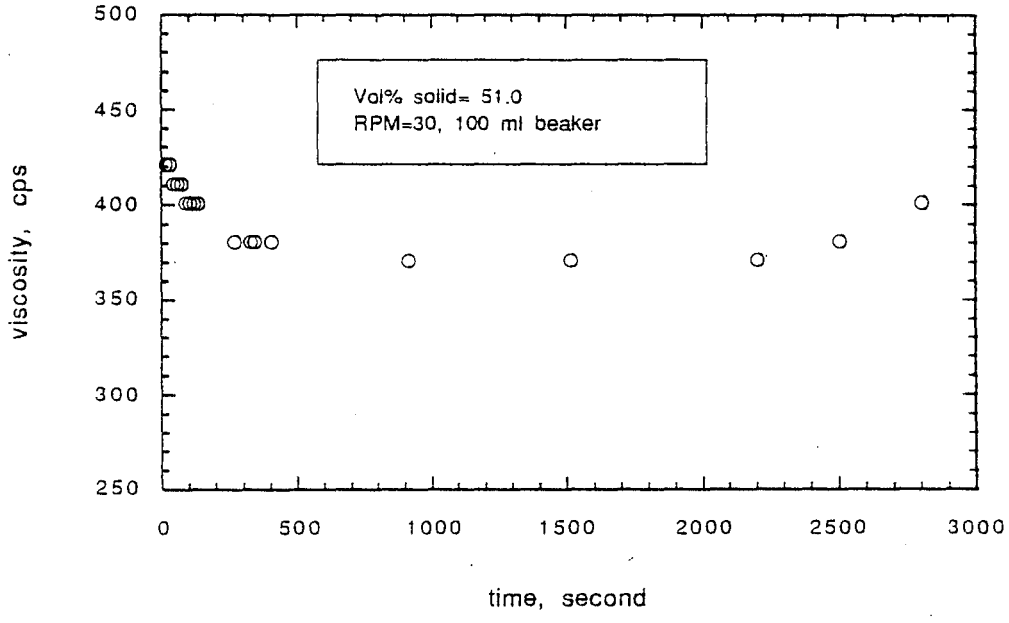

(b)

Figure 7.11. A plot of the viscosity as a function of (a) spindle speed, rpm, (b) time, sec., for sample A32

7.2. Packing Density

The effect of submicron particle size and solid concentration on particle packing have been studied at different deflocculation levels. The slip compositions investigated in this section is shown in Table 4.2.-7.

Quemada model, presented in the Section 5, for the relative viscosity and packing factor is examined and compared with the experimental results. Viscosity of the suspending medium, 1430AT™ with distilled water, is around 10-15 cps. The comparison is noted to be close agreement with the data of low solid loading suspensions at the moderate shear rate. However, a poor agreement is observed at the solid loadings higher than 50% and wt% submicron concentration lower than 21.05%. The effect of submicron concentration was also poorly represented by the model since it is simply based on vol% solid and void fraction of the cast.

Verification of these results need to be backed up by a sound theoretical basis and require strict definition of experimental condition. All experimental data used in this study were obtained using Brookfield LVTDV-II digital viscometer at moderate shear rates with spindle #4 and 100 ml sample container. Finally, in order to take into account non-Newtonian effects, the non-Newtonian extension of the relation may be required [124,125].

Particle size effect on porosity formation for the samples fabricated by compaction was also investigated as shown in Figure 7.12. Using 1430AT™ binder, average of 37.5% porous green preforms were obtained with the compaction pressure of 10,000psi. At 0 wt% submicron concentration, high porosity% was due to the narrow particle size distribution and the removal of the organic binder, PEG.

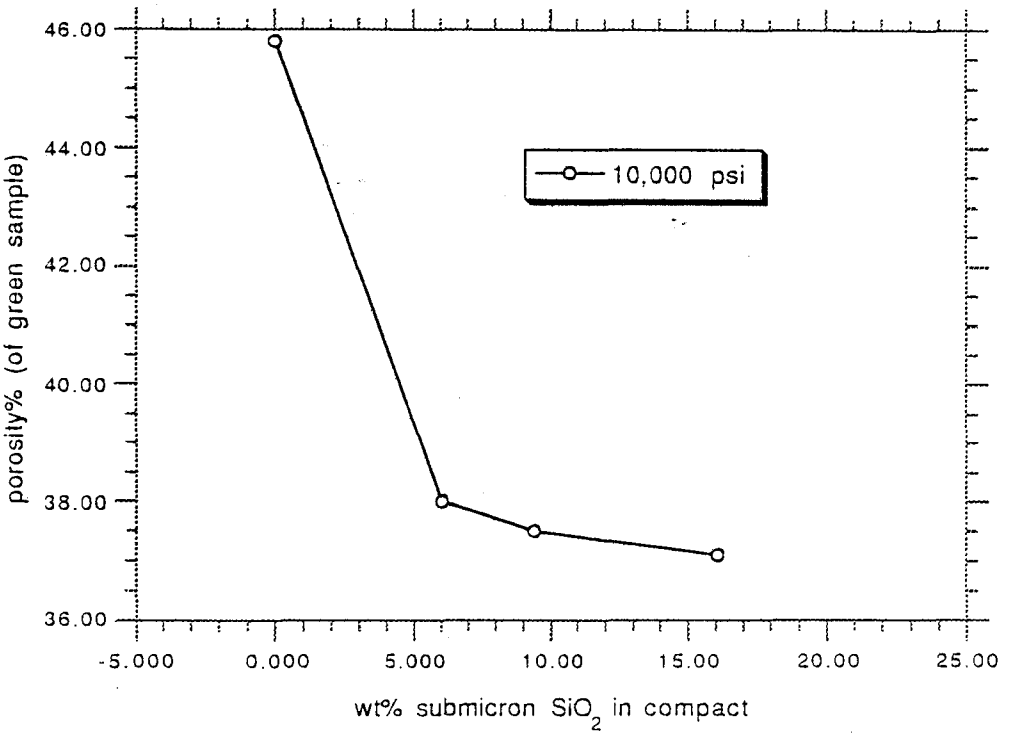

Figure 7.12. Effect of submicron powder concentration on the porosity level of green compact for compacted samples; P1, P3, P4 and P5

The compositions A14, A25, A35 and A45 to which submicron particle size concentration in powder are 2.16% could not be removed from the mold. These samples showed very low green strength due to the low colloidal silica content. Sufficient green

strengths for handling purposes were obtained with submicron concentration higher than 6%.

7.2.1. Effect of pH

The slurries, A2j and A3j, were casted at pH values 5 and 7.5 which are correspands to deflocculated and agglomerated ranges for the slurries as shown in Figure 7.13. As pH increases from 5 to 7.5, the packing density decreases by 1-10% at a given vol% solid and wt% submicron SiO_2. At higher submicron sized powder concentration, the variation in packing density was more sensitive to pH changes since fine particles caused higher viscosities to the slips at the same pH levels.

7.2.2. Effect of Particle Size

The submicron silica powder concentrations in powder were varied from 21.05 wt% to 6.04 wt% through the compositions as shown in Figures 7.13 and 7.14-a. As submicron size concentration increased, packing density increases up to 15% as shown in Figure 7.13-b. It is expected that increasing the fine particle concentration would lead to increase in the packing density. Since widening the distribution of particles allows the smaller particles to fill the voids of larger sized particles, therefore, packing density can be improved by optimization of distribution of particle size.

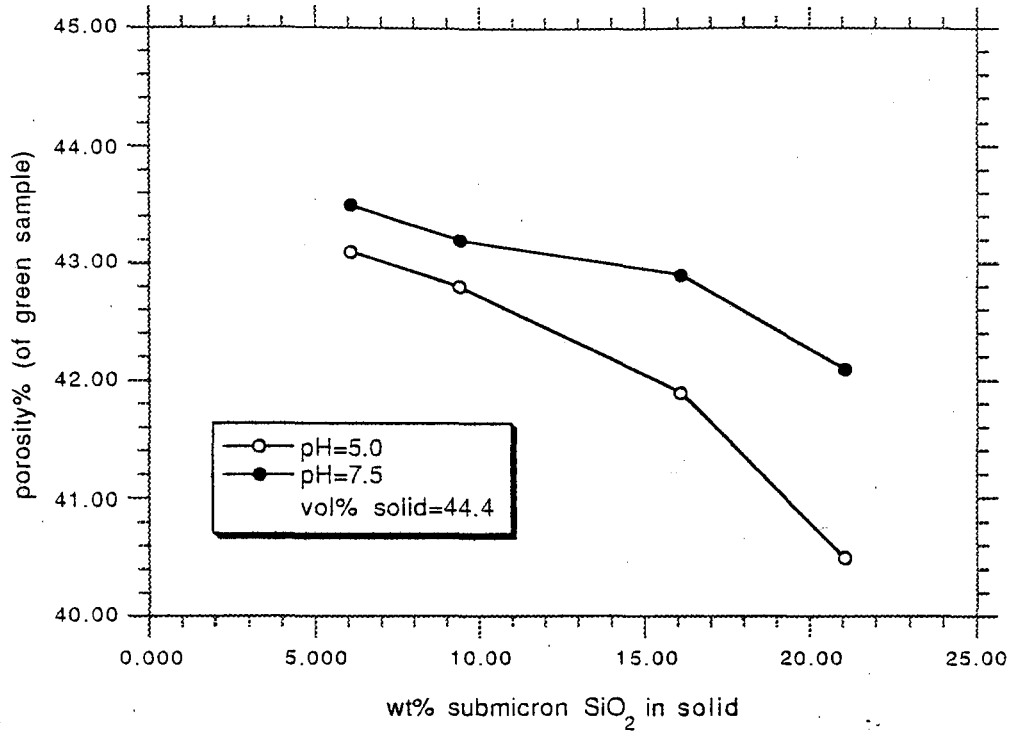

(a)

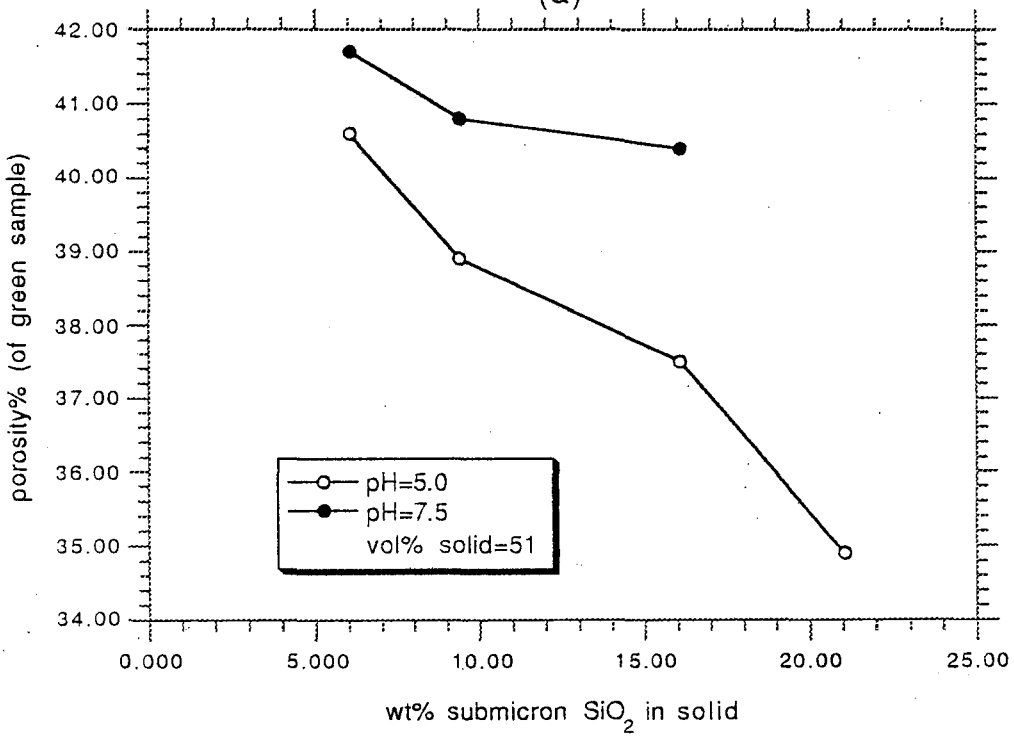

(b)

Figure 7.13. Effect of submicron powder concentration on the porosity level of green compact of cast samples (a) A2j and (b) A3j

7.2.3. Effect of Solid Concentration

The solid concentration of the slips showed a significant effect on the packing density. As the solid concentration increased from 40.4 vol% solid to 60.0 vol% solid, the packing density showed a marked increase. For samples A5j, 55.0 vol% solid, the porosity percentages was around 33%.

The plot of packing density as a function of solid loading, 44.4, 51 and 55 vol% solid, are given in Figures 7.13-14. From 44.4 to 55 vol% solid loading, the packing density increases 10 to 20% as the solid concentration in the suspension increased.

Figure 7.15 shows the processing diagram for reaction 1 from which porosity formation in the green preform can be determined with known processing parameters vol% solid and wt% submicron SiO_2. The bar codes, on the right hand side of the plot, indicate the level of the porosity% on the constrained surface plane of the plot.

In summary, higher the solid loading and submicron concentration, higher the packing densities and/or lower the porosities. One possible explanation for this is that, at low solid concentration, the slip becomes relatively less dispersed and more agglomeration occurs

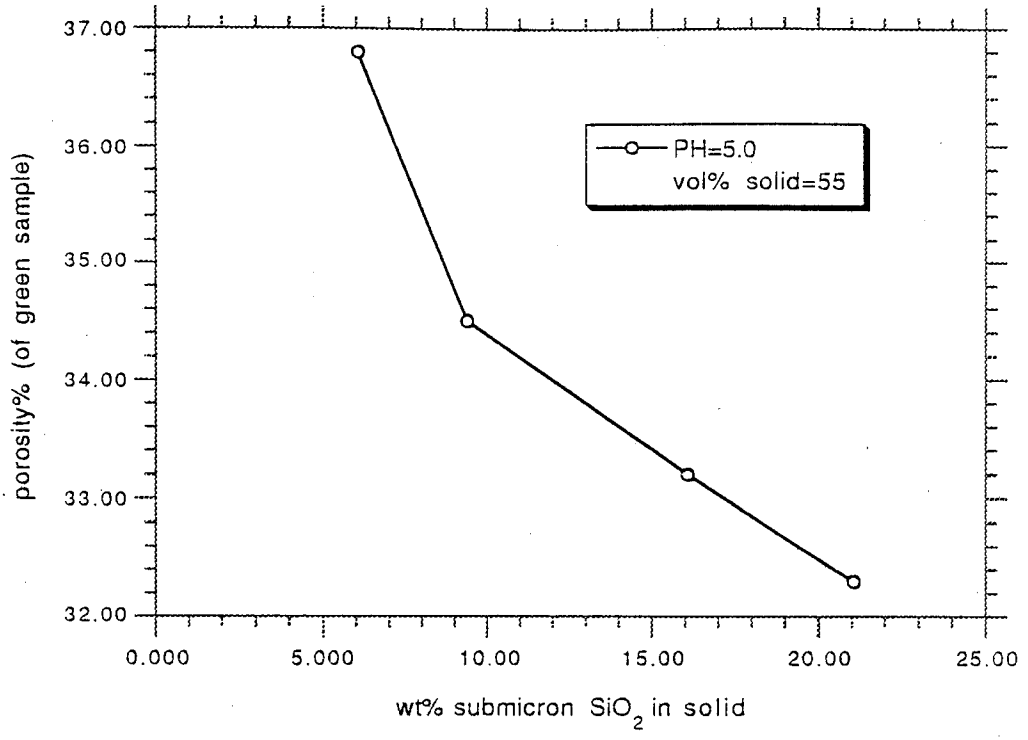

(a)

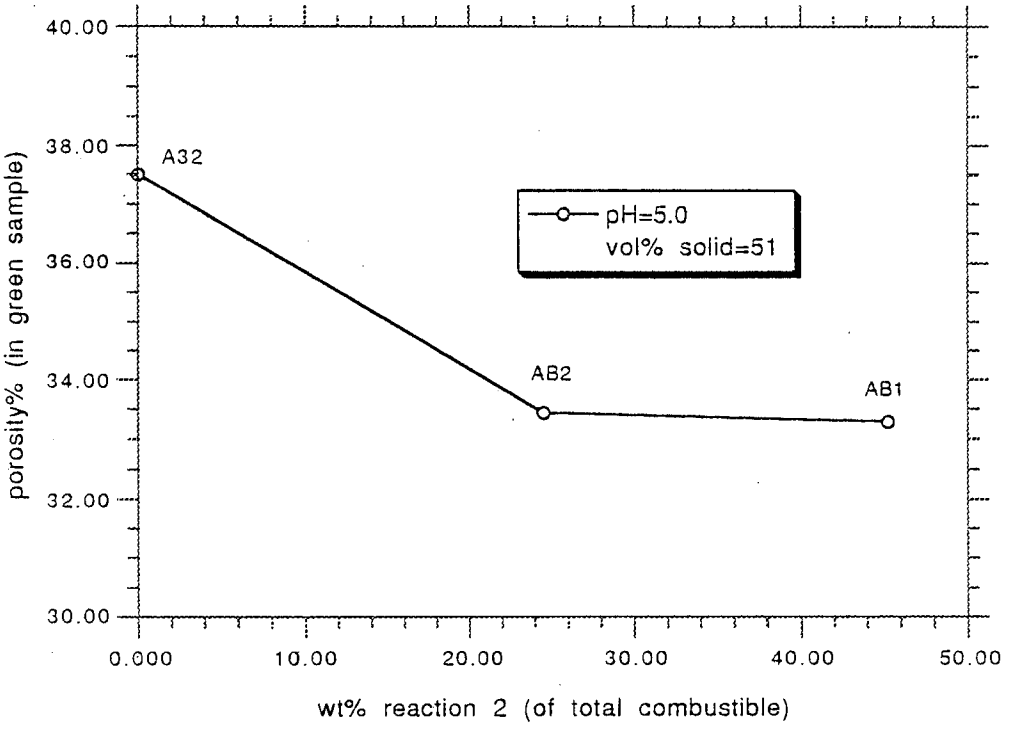

(b)

Figure 7.14. Effect of submicron powder concentration on the porosity level of green compact of cast samples (a) A4j and (b) A32, AB1 and AB2

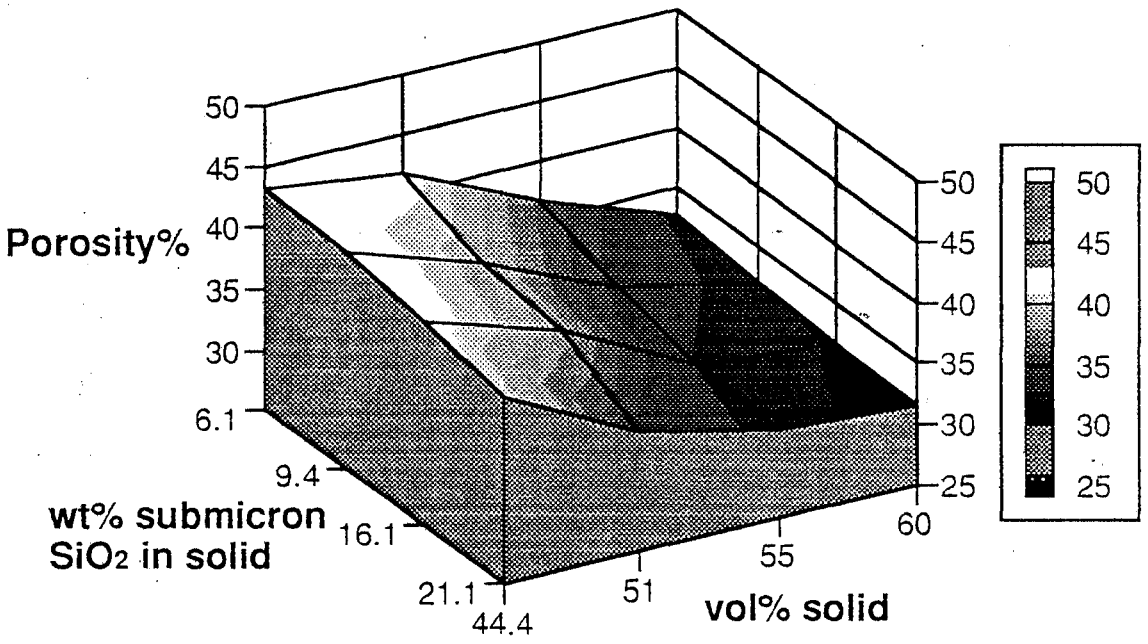

Figure 7.15. A plot of the green porosity as a function of vol% solid and wt% submicron SiO_2 in solid

7.3. Reaction Kinetics

The kinetics of micropyretic reactions are considered to predict the behavior of the reaction during the combustion. For a given system, the combustion mode is influenced by both kinetics and thermodynamic factors leading to either steady or unstable modes for combustion [8, 59-65]. For all compositions studied, the combustion propagation was in the steady-state mode and the possible reaction mechanism was the one that the adiabatic temperature exceeds melting point of Al and the decomposition of SiO_2 precedes interaction between silicon oxide and aluminum film to form Al_2O_3 and Si. The formation of SiC may be due to carburization type process since the melting point of SiC is well above the adiabatic reaction temperature, therefore, the dissolution of C in Si and the precipitation of SiC out of the solution may not be possible. After initial transients, the kinetics become parabolic with time. The reaction rate controlling step is the inward diffusion of Si via grain boundaries of SiC layer, followed by the reaction at the SiC-graphite interface [8,13,131]. The modified analytical model for combustion velocity, presented in Section 5, for slip cast micropyretic system has been developed considering slip parameters and both thermophysical and chemical properties for reactants and products. Application of this model to the micropyretic synthesis of the reaction 1 has been carried out to study the variation of combustion front with the slip casting parameter, vol% solid loading. The comparison with the experimentally determined values for reaction 1 with 21.05 wt%

submicron concentration are noted to be in close agreement for the selected pre-exponential factor, Ko, in the range of 3.5×10^5 to 4.5×10^5.

The results show that as the slip casting parameter, vol% solid loading, is increased, the cast porosity decreases, therefore, the combustion velocity increases giving higher conversion efficiencies for the reaction. As may be noted from equations (5.6), (5.8) and (5.9) vol% solid loading, is directly proportional to the thermal conductivity and density of the reactants and the products. Thus all the thermophysical and chemical properties are required to be considered in the combustion velocity expression [76]. However, the validity of the model is found to be related to how precisely the thermophysical and chemical properties are known or determined. Furthermore, it is concluded that the analytical solution is roughly 80% approximation of the true solution [87]. Both experimental and model results indicate that combustion velocities for reaction 1, 4 to 6.5 mm/sec, are relatively much lower than most micropyretic systems. Preliminary mixing occurs through capillary spreading of the liquid along the surfaces of the non-melting species since melting temperature of some of the reactants is lower than the combustion temperature. At relatively low temperatures, the migration rate of aluminum reaches 1-1.8 cm/sec [132] and its migration rate is faster than the reaction rate, therefore, it allows the migrating component to remove a large amount of heat from the reaction causing further decrease in the reaction rate.

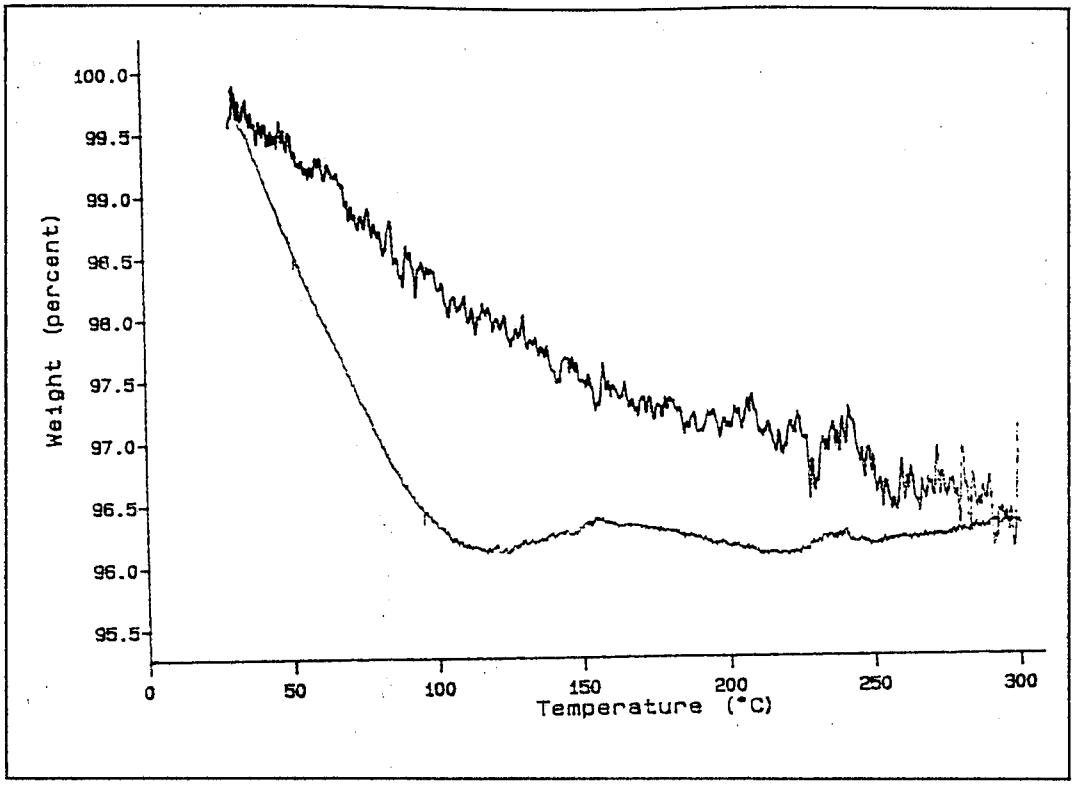

Figure 7.16. Weight losses as a function of time for green sample A10

Combustion velocity and temperature measurements were performed to find out the effect of particle size and packing density (vol% solid loading) for the micropyretic reaction 1. Before micropyretically synthesizing, all samples were dried at 250 °C for 15 minutes. During dehydration, green cast preforms lost weight from 0.75 to 2.5 wt%. An example of TGA curve to dehydration process for sample A1 is shown in Figure 7.16. To measure the combustion velocity, two C type thermocouples at 20 mm apart were placed into the green preform and the sample was micropyretically synthesized with propane torch from one end after preheating the sample to 600 °C since the reaction is weakly exothermic. The wave propagation mode of combustion proceeded from one end to the

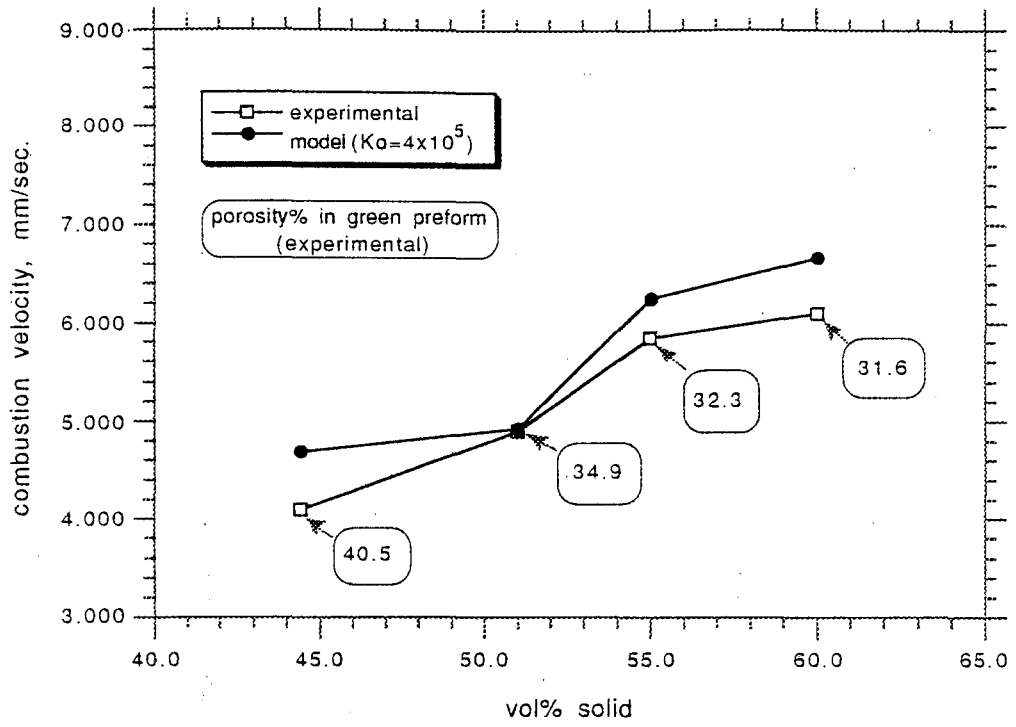

Figure 7.17. A plot of combustion velocity as a function of solid concentration by volume for samples Ai1

other and temperature response recorded with the data acquisition system. Examples for such measurements are given in appendix B. The time taken by the propagation front to travel from one thermocouple to the other were calculated from the temperature against time graph. Since the distance between the two thermocouples are known, the combustion velocity can be calculated from the relation, X = Vt. The combustion velocity measurements were done for samples Ai1, A3j, AB1-2 to which processing variables were vol% solid, wt% submicron concentration and reaction 2 concentration as shown in Figures 7.17, 7.18 and 7.19 respectively. However the maximum temperatures obtained from these measurements was much lower than the adiabatic temperatures for these reactions. The main reasons for this could

be the incompleteness of the reactions and heat losses. It is also possible that the thermocouple response time may not be quick enough to match the very high reaction rates.

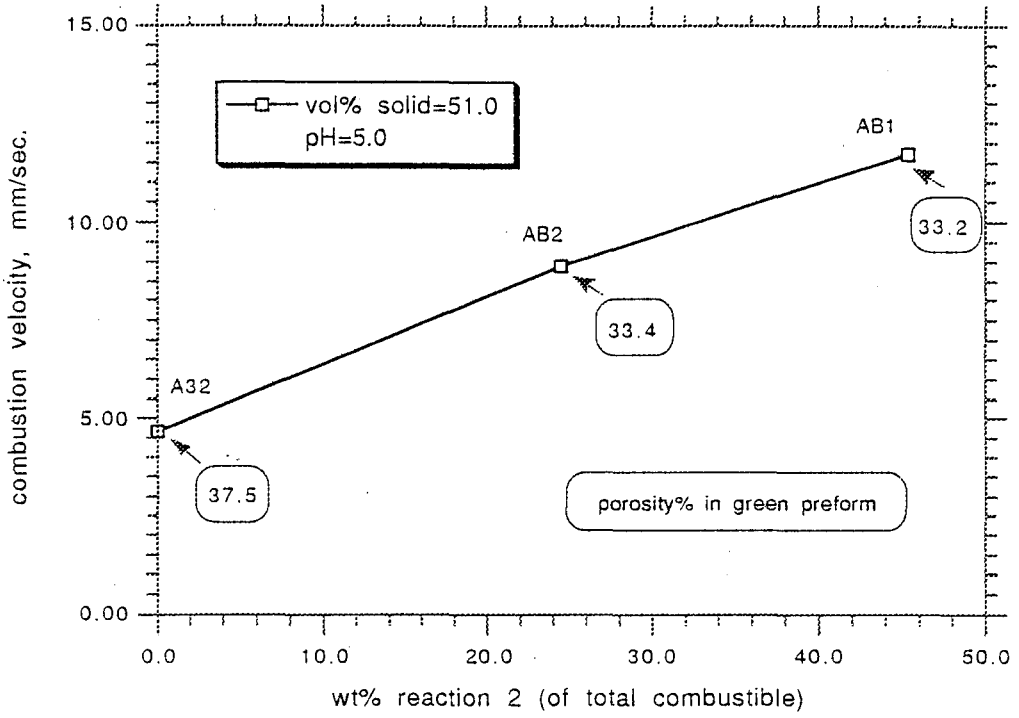

Figure 7.18. A plot of combustion velocity as a function of reaction 2 concentration by weight for samples A32, AB1 and AB2

7.3.1. Effect of Packing Density

The effect of green preform porosity on the combustion velocity has been investigated for compositions Ai1 as shown in Figure 7.17. As the vol% solid loading is increased, the packing density and the combustion velocity increases. Lower densities are indicative of lower particle coordination numbers and hence lower areas of contacts between the reactants. This in turn means lower

reaction temperature and corresponding velocities. The results of Figure 7.17 are consistent with this expectation. Since the samples fabricated by slip casting had lower green porosities than the compacted samples, lower combustion velocities were obtained for compacted samples as shown in Figure 7.20.

7.3.2. Effect of Particle Size and Composition

The effect of particle size on combustion velocity of the compositions A3j (vol% solid = 51) as shown in Figures 7.19 . Figure 7.19 indicates that the fine particles concentration in the preform influences the combustion velocity. The reaction rate may be significantly affected by the addition of catalysts, ignition temperature and maximizing area of contact of the reactant particles. Maximizing the area of contact may be accomplished by using fine particle size and/or high atmospheric pressures [132]. For samples AB1 and AB2, the Cr_2O_3-Al-C and SiO_2-Al-C exothermic reactions were studied together. The wt% of Cr_2O_3-Al-C which is referred to as reaction 2, were 47.7% and 26% respectively. Addition of reaction 2 increases the combustion velocity although its opposite effect on packing density. The packing density was lowered with the addition of reaction 2 due to higher viscosities obtained at the cast condition at which pH was 5. The processing diagram of reaction 1 for the combustion velocity as a function of processing parameters is given in Figure 7.21. The bar codes, on the right hand side of the plot, indicate the level of the combustion velocity.

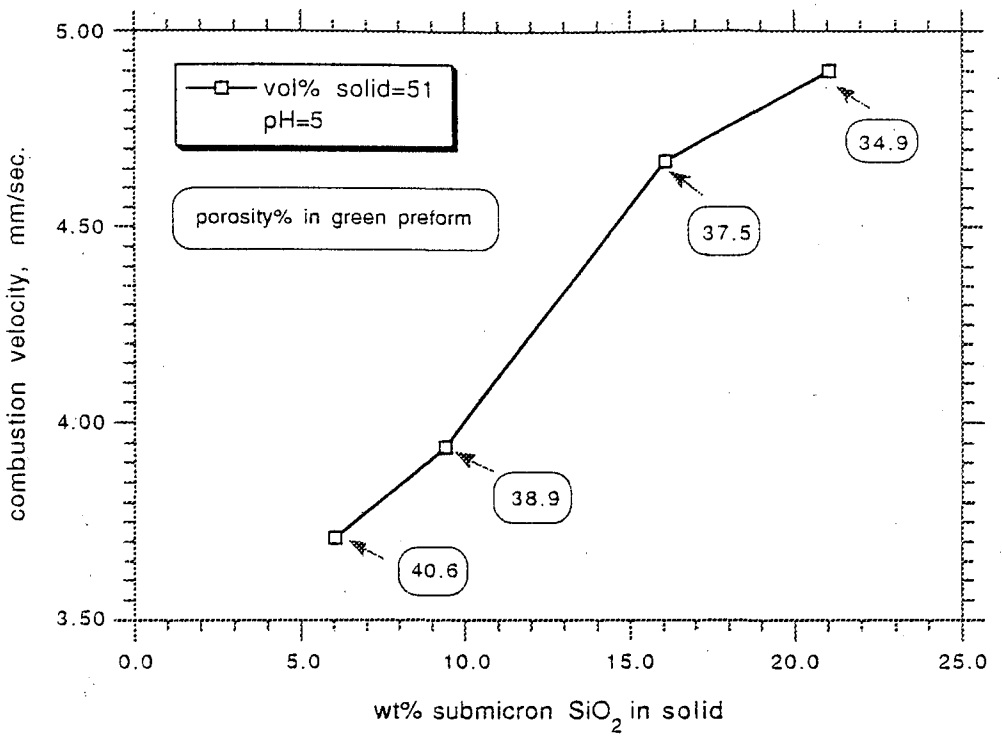

Figure 7.19. A plot of combustion velocity as a function of submicron silica powder concentration by weight for samples A3j

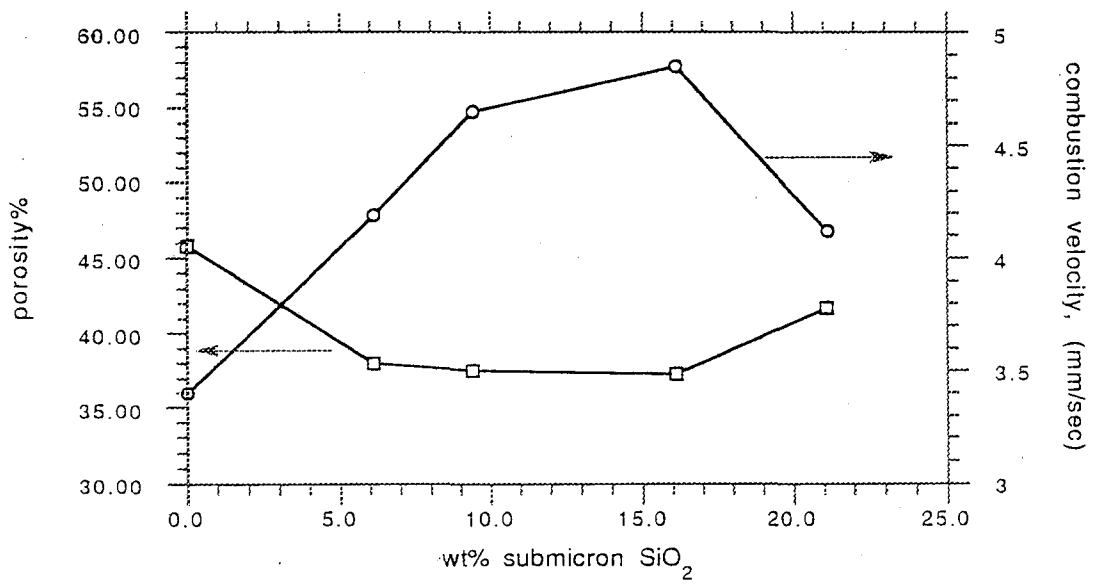

Figure 7.20. A plot of the porosity and combustion velocity as a function of wt% submicron SiO_2 in solid (compaction samples; P1, P3, P4 and P5)

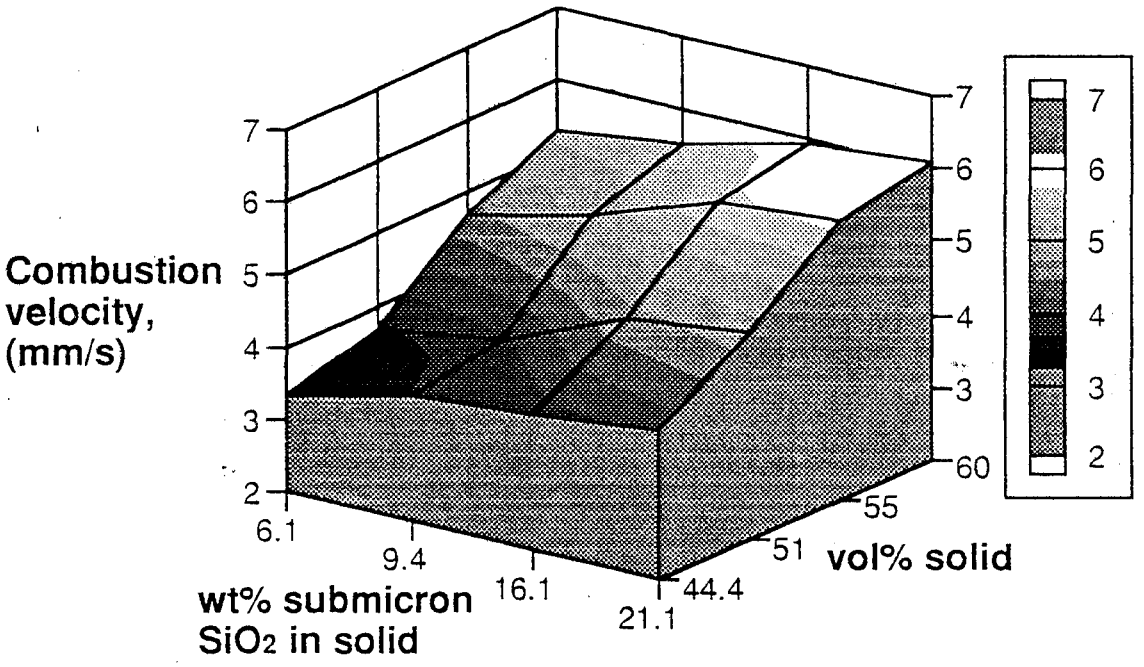

Figure 7.21. A plot of the combustion velocity as a function of vol% solid and wt% submicron SiO_2 in solid

7.4. Microstructure and Property

7.4.1. Porosity Formation

The effect of solid concentration, particle size and composition on pore size and percentages in the synthesized samples were investigated for the samples Ai1, A3j, AB1 and AB2 as shown in Figures 7.22, 7.23 and 7.24 respectively.

Figure 7.22, 7.23 and 7.24 indicate that the porosity level further increases upon synthesizing. The relative change in the final porosity decreases with increase in solid loading and submicron

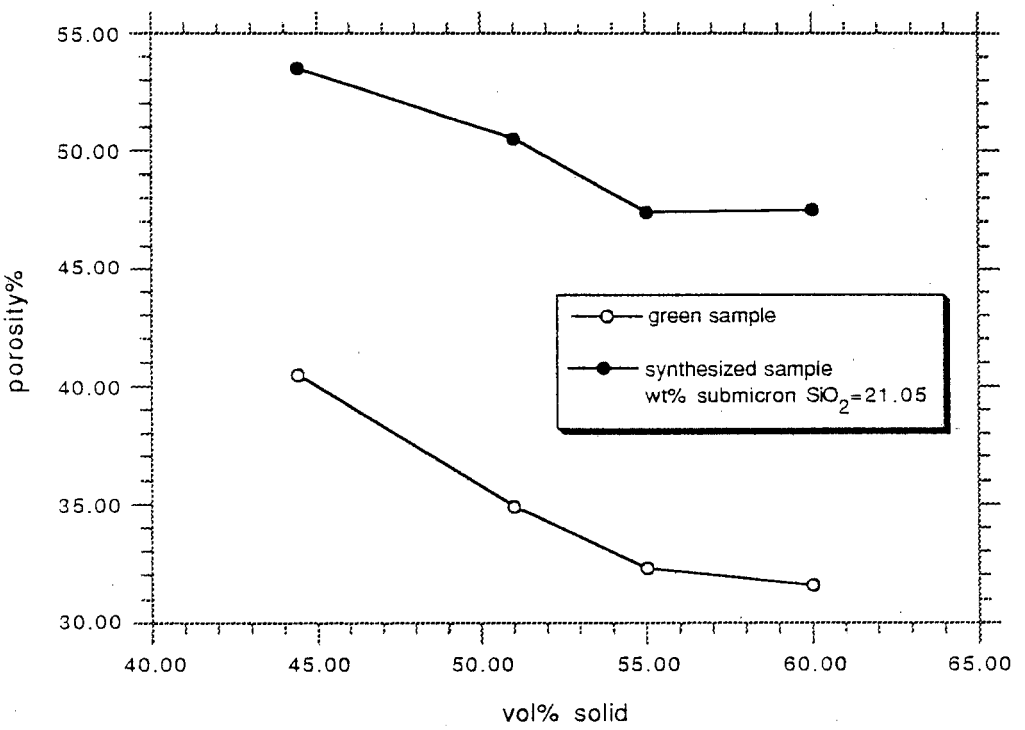

Figure 7.22. A plot of porosity% of green and synthesized samples as a function of solid concentration by volume for samples Ai1

particle concentration, and increases with increase in reaction 2 concentration.

As mentioned earlier, the porosity% of green cast preform is mainly function of solid loading, submicron particle concentration and deflocculation level. However, the final porosity mainly due to the density differences between reactant and product, the conversion efficiency and the initial porosity.

The reaction, $SiO_2 + Al + C \Longrightarrow Al_2O_3 + SiC$, yields around 30% volume change ([volume of products-volume of reactants]/volume of reactants) because of density differences between reactants

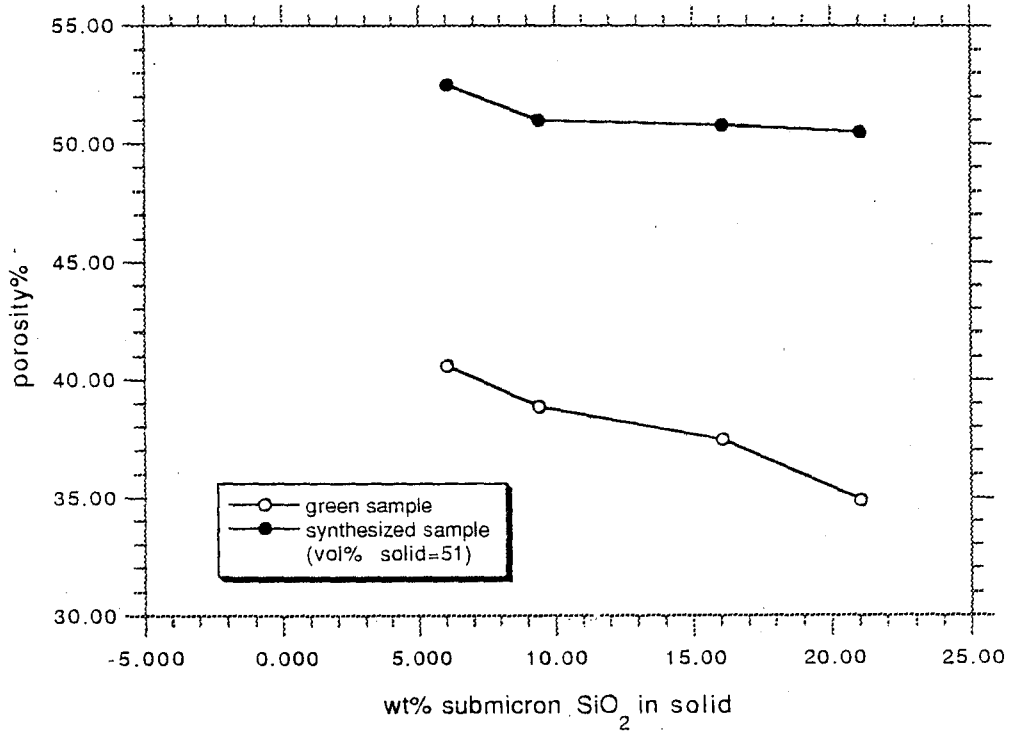

Figure 7.23. A plot of porosity% of green and synthesized samples as a function of submicron silica powder concentration by weight for samples A3j

and products. On the other hand, the experimental values were around 20-25% as shown in Figure 7.25. This indicates that full conversion for the reaction 1 couldn't be achieved. However, the conversion efficiency is improved by increasing solid loading (decreasing initial porosity), submicron particle size and reaction 2 (reaction aid) concentrations. The lowest final porosity, 47.3%, was obtained at 60% solid loading and 21.05 wt% submicron concentration as shown in Figure 7.22. According to the these results, the highest conversion efficiency were at 60 vol% solid loading with 21.05 wt% submicron concentration, sample A41, and 45 wt% reaction 2, sample AB1.

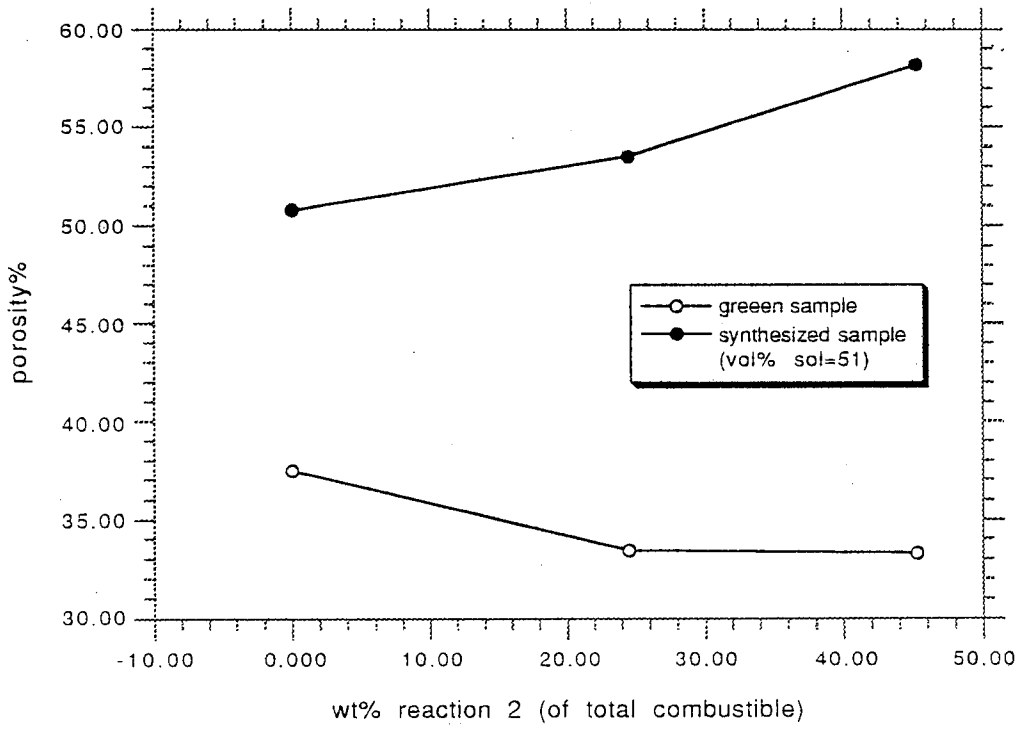

Figure 7.24. A plot of porosity% of green and synthesized samples as a function of reaction 2 concentration by weight for samples A32, AB1 and AB2

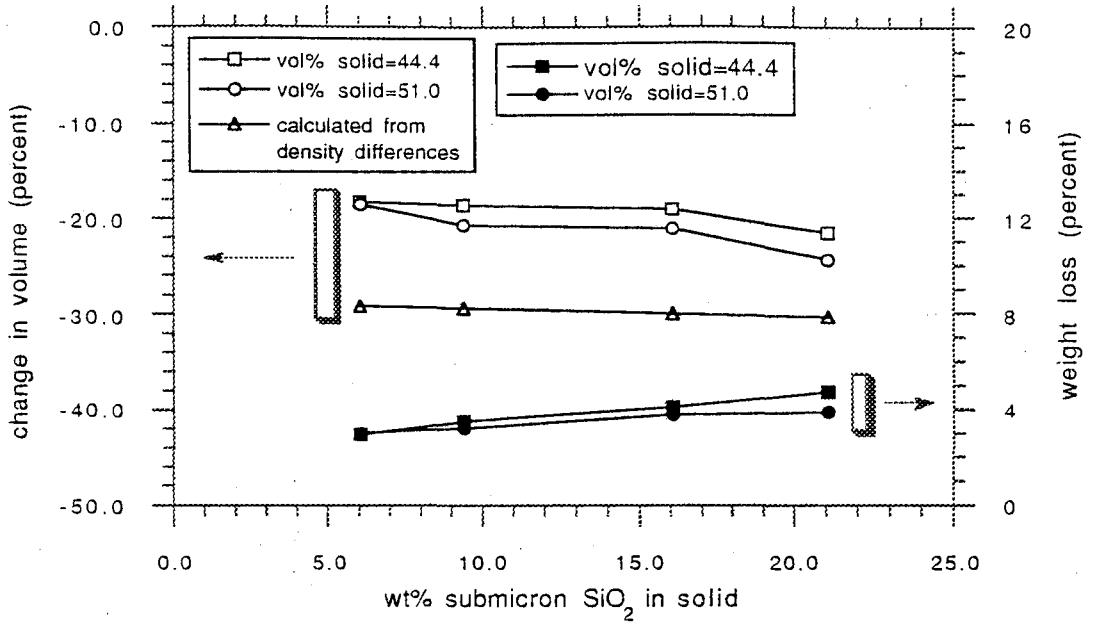

Figure 7.25. A plot of the volume change and weight loss as a function of wt% submicron SiO_2 in solid

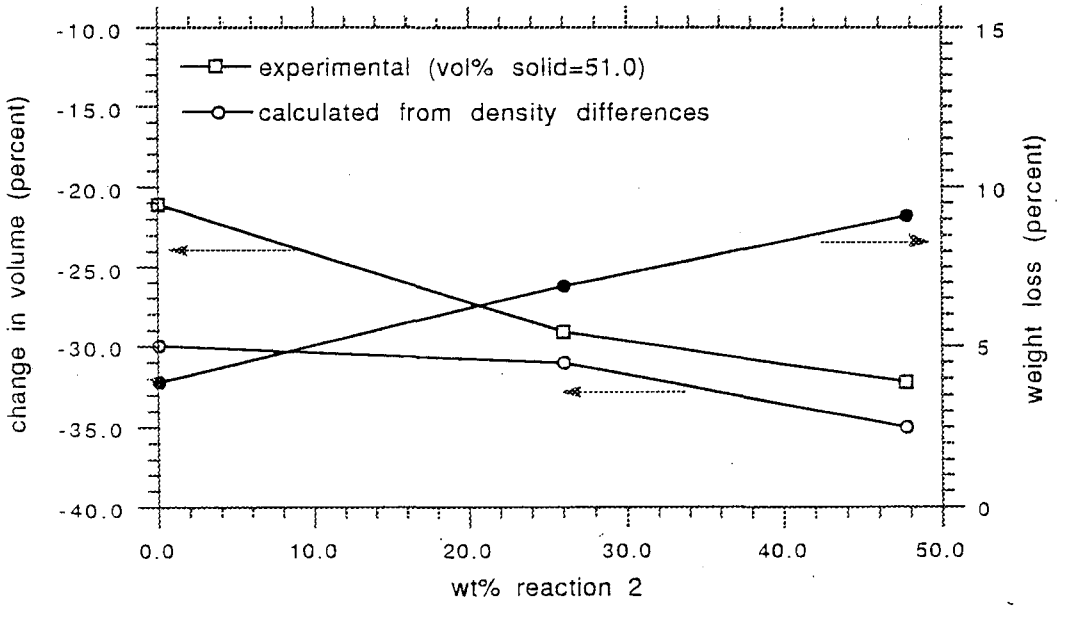

Figure 7.26. A plot of the volume change and weight loss as a function of wt% reaction 2 of total combustible

Figure 7.25 and 7.26 also shows that weight loss% due to combustion increases with increase in vol% solid loading, wt% submicron concentration and wt% reaction 2. This results indicate that some of the porosity formation could be due to the weight losses during the reaction. During synthesis of all the compositions, some gas evolution could be observed because of the impurity content of reactants and possible intermediate steps in the thermite reaction. Cutler and his co-workers [120] have been able to detect the principal gases using in-line mass spectrometer as H_2, CO and SiO ($1.16X10^{-3}$ moles gas/gr reactants) on cold pressed SiO_2-Al-C parts during micropyretic reaction.

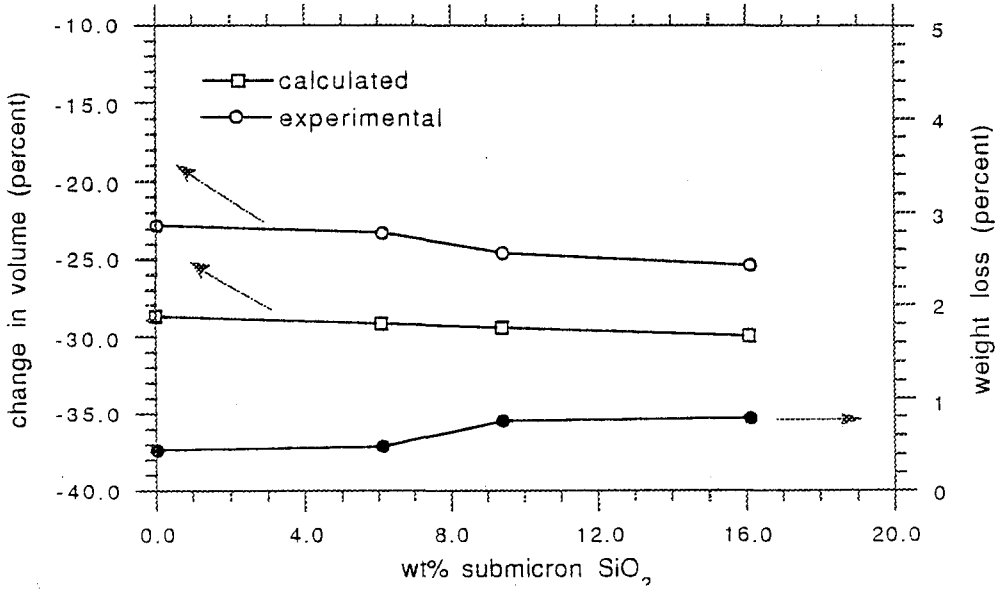

Figure 7.27. A plot of the volume change and weight loss as a function of wt% submicron SiO_2 in solid (compaction samples; P1, P3, P4 and P5)

7.4.2. Product Phases

X-ray diffraction were used to identify phases of synthesized materials. The diffraction patterns as shown in Figures 7.28, 7.29 and 7.30 can be indexed to two main phases: α-Al_2O_3, hexagonal structures and β-SiC, cubic structures. Besides these major phases, Silicon and carbon were also present because of reaction incompleteness. Figure 7.28 shows the diffraction patterns of samples A21, A22 and A23 to which wt% submicron SiO_2 in solid are 21.05, 16.06 and 9.39 respectively. The effect of vol% solid loading is given in Figure 7.29. The samples, A23, A33 and A43 containing 9.39 wt% SiO_2, were cast at 44.4, 51 and 55 vol% solid loading. It is apparent that an increase in wt% submicron SiO_2 and vol% solid loading increase the conversion efficiency (i.e. higher β-SiC intensities). As concluded earlier, increasing the vol% solid and wt% submicron SiO_2 increases packing density and combustion rate, therefore, enhance the conversion efficiency.

The conversion efficiency were further increased with Cr_2O_3-Al-C reaction aid as shown in Figure 7.30. In the Figure 7.30, the reference material which contains 63 wt% α-Al_2O_3 (< 325 mesh, ALFA) and 37 wt% β-SiC (~1μm, Electro Ceram.) is also presented. X-ray patterns show that slip cast micropyretically synthesized material has the peaks with identical values of 2θ and intensities as in commercially available powders.

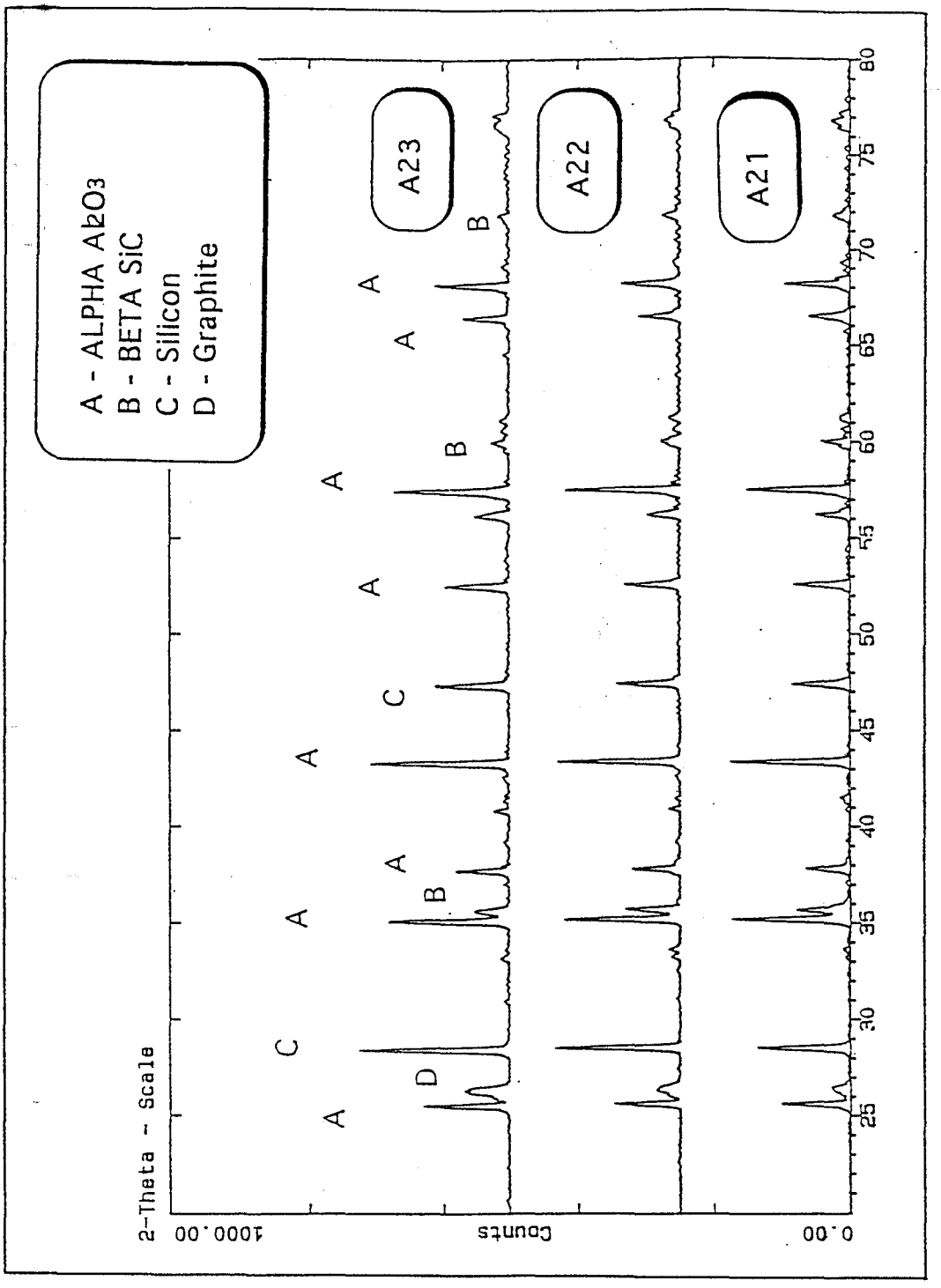

Figure 7.28. X-ray diffraction patterns for micropyretically synthesized samples A21, A22 and A23

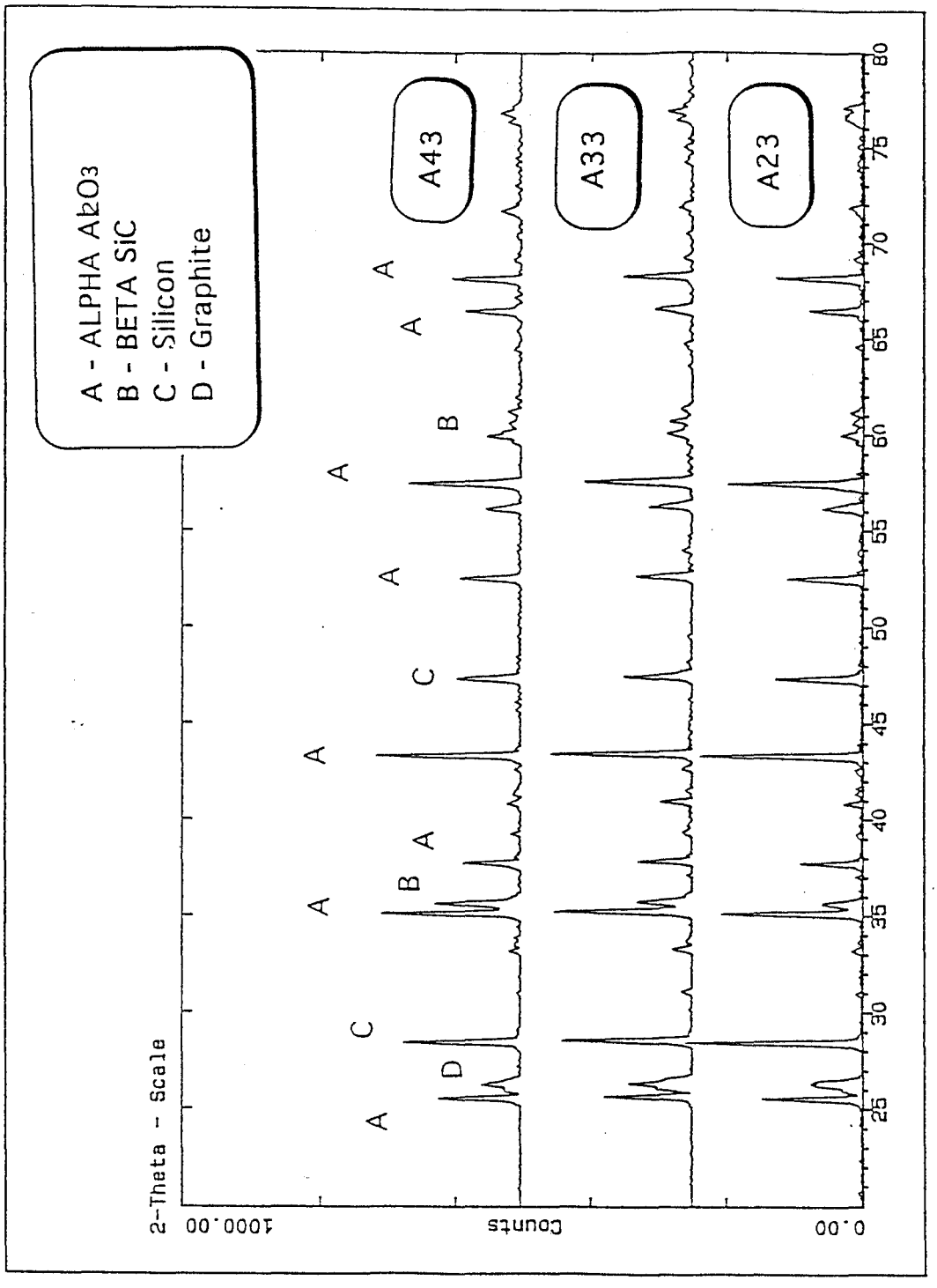

Figure 7.29. X-ray diffraction patterns for micropyretically synthesized samples A23, A33, and A43

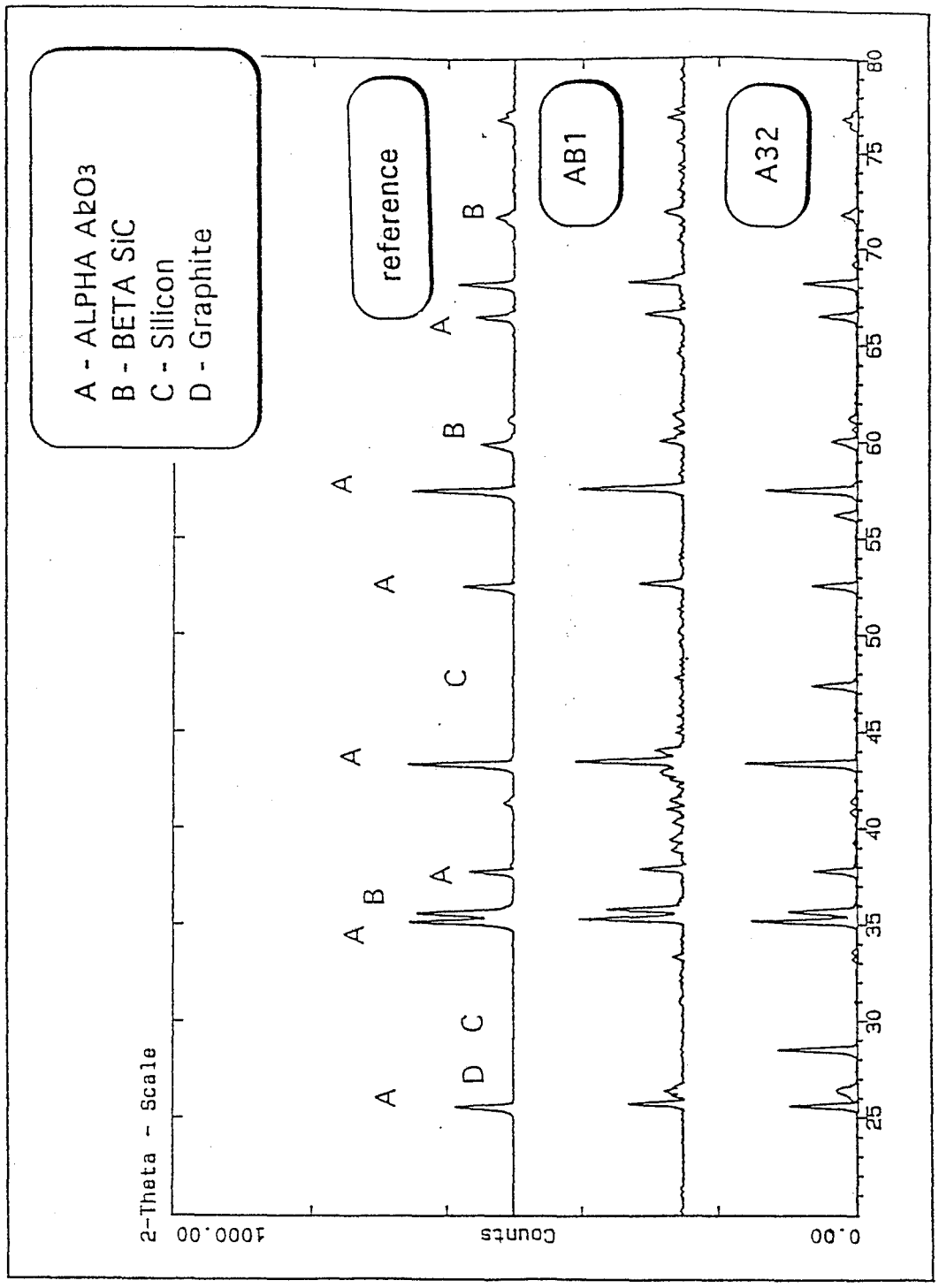

Figure 7.30. X-ray diffraction patterns for micropyretically synthesized samples A32, AB1, and α-Al2O3/β-SiC reference material

The fundamental unit in SiC polytypes is covalently bonded tetrahedron of C atoms with a Si atom at the center. Each C atom is likewise tetrahedrally surrounded by Si atoms. The cubic structure is also referred to as β-SiC and all other remaining types as α-SiC. The conditions of polytype transition in SiC have been affected by both kinetics and thermodynamic factors. The formation of β-SiC has been reported by many researchers for the reaction between silicon and carbon at relatively low temperatures (< 2400 °K) [14,131]. The adiabatic temperature for reaction 1 is well below this temperature range, therefore, β-SiC was obtained for all compositions.

7.4.3. Microstructures

The micrographs of both green and synthesized samples of A21 are shown in Figure 7.31-a. Note that, submicron particles from 1430AT™ totally covers the larger particles to give denser cast. Upon synthesizing, the final microstructure has relatively smaller grain sizes and more porous than the green preform. Note that both product phases and pores are very homogeneously distributed within each other almost in the submicron scale. Figure 7.31-b shows the phases in the sample A21 determined by EDAX analysis: The parent phase is aluminum rich indicating Al_2O_3 (gray); the second phase is silicon rich indicating SiC (dark); the third phase is Si phase (bright).

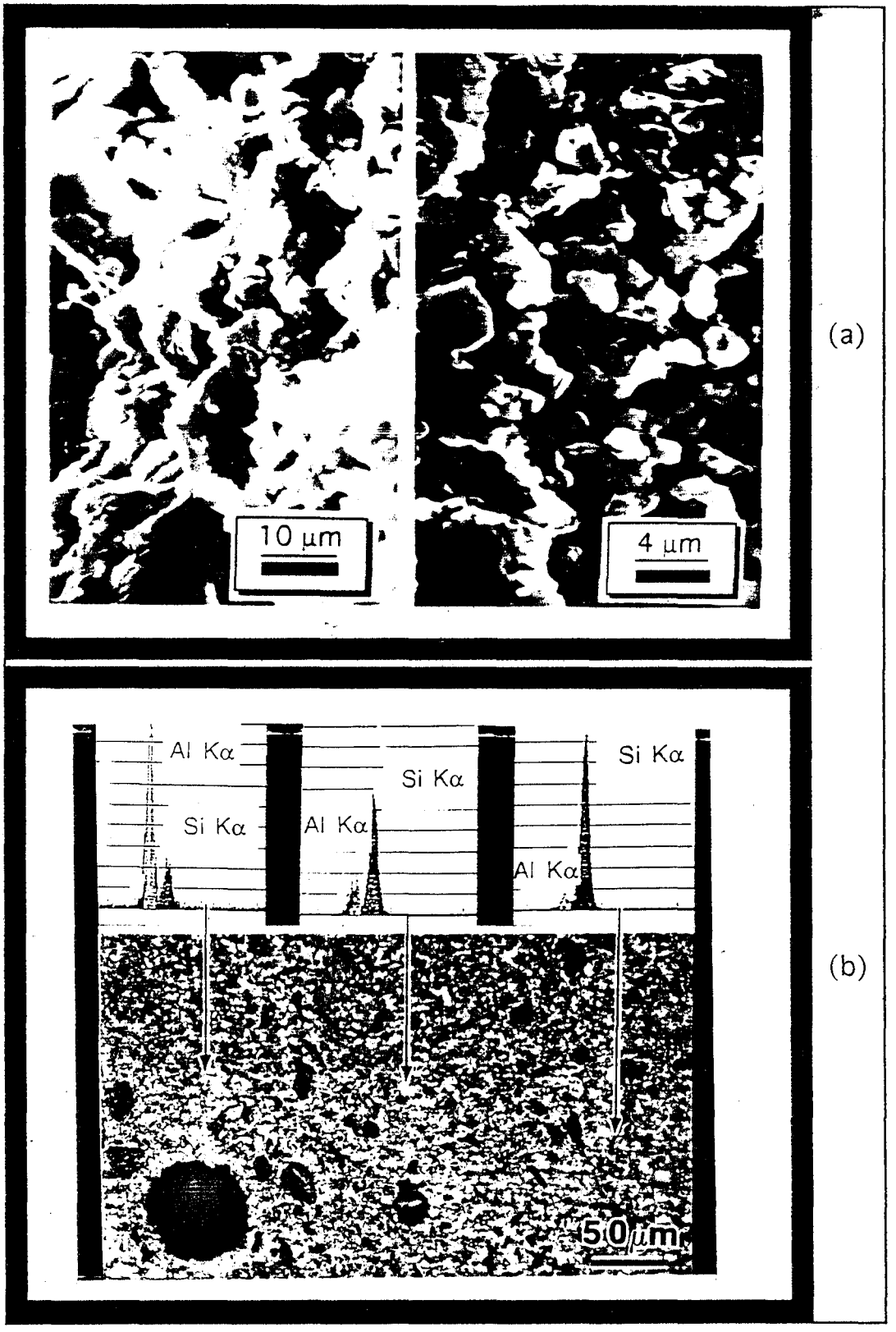

Figure 7.31. Micrographs of sample A21 (a) green and synthesized (b) EDAX patterns

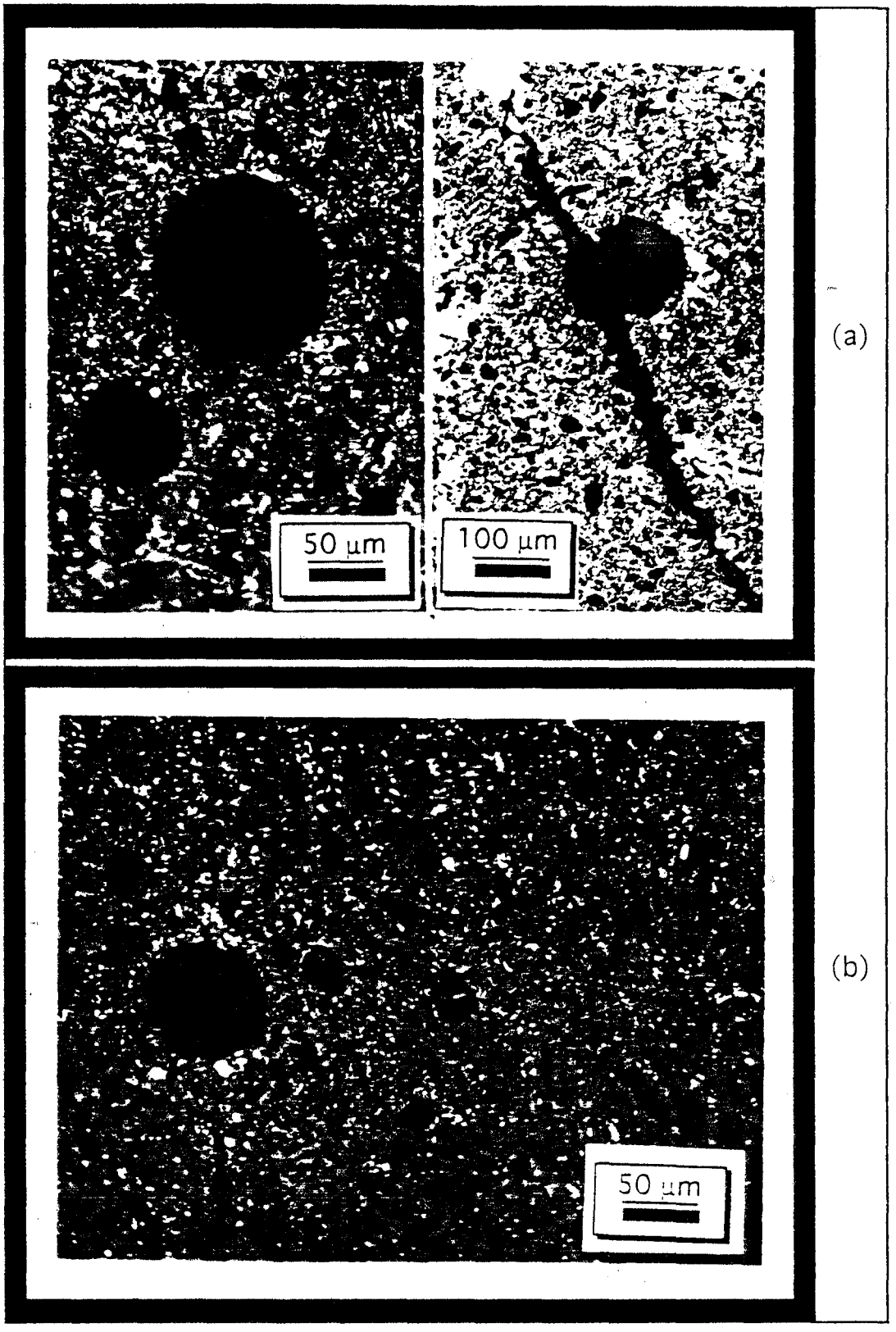

Figure 7.32. Micrographs of samples (a) A23 and (b) 43 (x200)

Figure 7.31 and 7.32 exhibit that Sample A43 has predominantly more SiC grains and less pore sizes than A21 and A23. All these selected samples suggest that higher solid loading and submicron powder content show typical features of higher conversion efficiency and smaller pore sizes. The literature review given by Huang [131], the reactivity was concluded to depend on the microstructure, porosity and specific surface of carbon. It was further concluded that the conversion efficiency into SiC powder increased and its particle size decreased by decreasing the particle size of the starting elements [14,131]. No clear correlation found between the submicron particles concentration and SiC grain sizes in the compositions studied. However, the initial graphite particle size appears to play critical role on final SiC grain size.

Figures 7.33 and 7.34 show the X-ray mapping of Al and Si, the SEM micrograph and selected electron diffraction patterns of β-SiC and α-Al_2O_3 for sample A21. The SEM image, as shown in Figure 7.34-a, exhibits the phases in sample A21 consistent with X-ray mappings for Si and Al. X-ray mapping indicates homogeneous distribution of Al_2O_3 and SiC phases as well as unreacted graphite flakes. It is also noted that graphite particles larger than 5 microns remained unreacted, therefore, decreases overall conversion efficiency for the reaction.

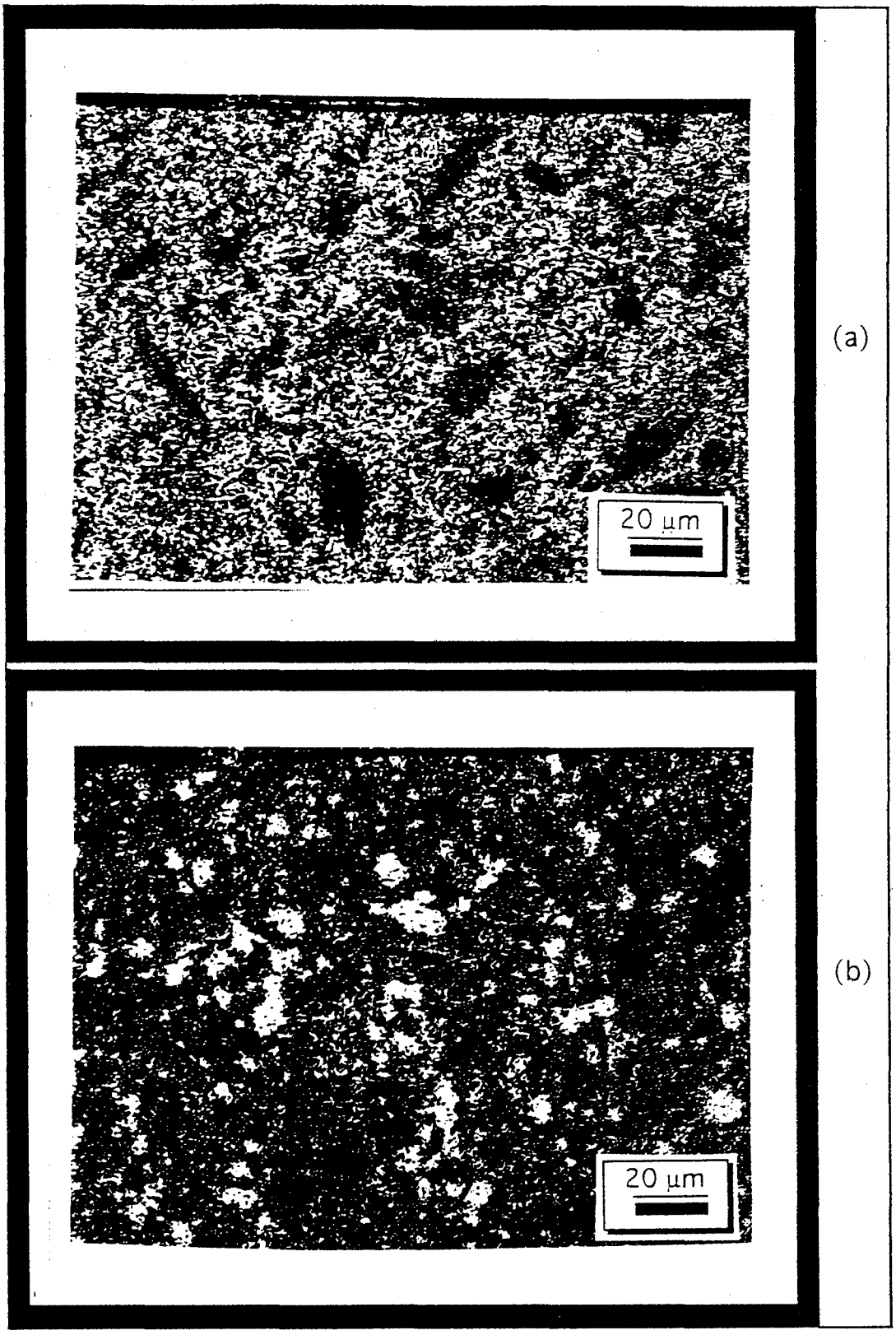

Figure 7.33. X-ray maps of sample A21 for elements (a) Al and (b) Si

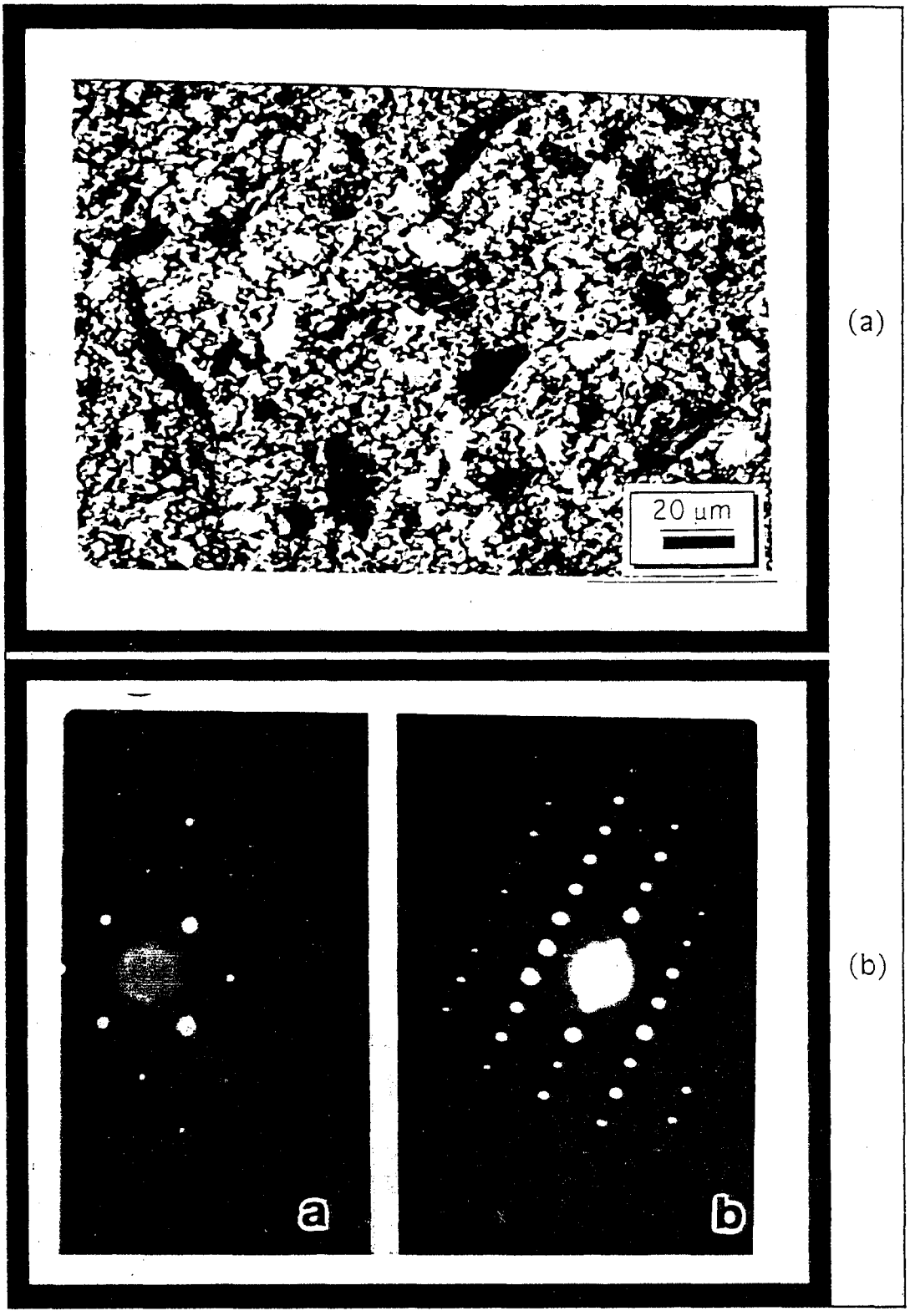

Figure 7.34. Micrograph for sample A21 (a) and selected electron diffraction patterns of β-SiC with the zone axis $[0\,1\,1]$ at left and α-Al_2O_3 with the zone axis $[0\,1\,\bar{1}\,0]$ at right (b).

8. CONCLUSIONS

The thesis has been aimed towards obtaining an optimized processing method to obtain combustible slip cast components. The present study showed that exothermic reactions could be used for producing materials through slip casting process. Based on the above discussions, the following conclusions have been made.

1. In the processing of slip cast micropyretically synthesizable materials suspended with colloidal silica, submicron sized particles can be used not only to obtain suitable rheological behavior of the slip (e.g. castability) but also to control microstructures and property (e.g. porosity and conversion efficiency).

2. Satisfactory suspension and pouring qualities of slurries with colloidal silica, 1430AT™ Nycol, can be achieved by using small additions of HCl at moderate acidity. Satisfactory mold release of castings and sufficient green strength for handling purposes are also possible for slurries suspended with colloidal silica, therefore, no other binder and dispersant required.

3. The wt% submicron SiO_2 in the slurry is critical and conversion efficiency and density of product increases with increasing with submicron SiO_2. However, no clear effect on particle size of carbide formed has been determined.

4. At pH 4 to 5 such a all slurries has its minimum viscosity to which the lowest porosity is obtained for any given vol% solid loading for the compositions studied. All suspensions show thixotropic behavior and thixotropy decreases as vol% solid and wt% submicron powder increases.

5. The compositions higher in vol% solid loading lead to denser cast preforms. However solid loadings higher than 55 vol% solid may yields to unworkable slips of high viscosity which are very sensitive to pH changes.

6. In micropyretic synthesis, the reaction mechanism is greatly influenced with porosity level of cast preform, submicron size particle content and composition. The final synthesized product is highly porous, however, it is comparable with the preforms fabricated by compaction. However, the process is required to be optimized for each particular system through rheological and compositional adjustments.

7. The complex mechanisms of both slip casting and micropyretic synthesis and lack of thermophysical and chemical properties are likely to be a still challenging problem of a complete design modeling for the process. However, comparison of the model results with the experimentally determined values are noted to be in close agreement for the selected pre-exponential factor, Ko, in the range of 3.5×10^5 to 4.5×10^5 for the reaction 1 with 21.05 wt% submicron concentration.

9. ENGINEERING SIGNIFICANCE AND RECOMMENDATIONS

Casting techniques in micropyretic synthesis may have several advantageous over traditional way of fabrication, powder pressing, such as complex shape possibility, comparable particle packing levels, simplicity and cost efficiency.

In the present study, micropyretic synthesis technology was successfully applied to slip cast preforms for the first time. Through the present study, valuable information was obtained regarding this new process and its processing parameters for the Al_2O_3-SiC composite material. The processing diagrams from which feasible processing parameters can be chosen for the objective defined were developed. In relation with the processing diagrams, simplified modeling consideration was also given. Based on the information obtained from the present study, the new processing method can be optimized for variety of application and materials for practical purposes.

The present study could be extented for the following future approaches:

1. Pressure application during casting may be required to get more dense product. The combustion aids such as Y_2O_3, Si_3N_4 could be introduced to the reacting system to improve sinterability and densification.

2. The purity and particle shape of graphite powders used in this particular study could be critical. Other carbon sources to the process are recommended to improve reactivity. Conversion efficiency could also be increased by introducing the trigger reactions which are exothermic enough.

3. The effect of mold material and its porosity level in the process is also important.

4. Casting defects such as shrinkages and drying cracks are required to be studied to obtain sound casts.

5. The potential versatility for synthesizing variety of materials using the thermite reactions such as

$Fe_2O_3 + 2Al \Longrightarrow 2Fe + Al_2O_3$

$MoO_3 + 2Al \Longrightarrow Mo + Al_2O_3$

$Cr_2O_3 + 2Al \Longrightarrow 2Cr + Al_2O_3$

$3NiO + 2Al \Longrightarrow 3Ni + Al_2O_3$

$3TiO_2 + 4Al \Longrightarrow 3Ti + 2Al_2O_3$

and their application as a bulk and film using same technology is possible. Besides Aluminum, several other reducing agents may also be employed to the thermite reactions. The pure metals that have been produced by the thermite reaction can be synthesize to form intermetallic compounds such as silicites, carbides and borides.

10. NOMENCLATURE AND SYMBOLS

Symbol	Meaning	Units
$1/\kappa$	Double layer thickness	m
a	Polarisability of the atom	C m^2/V
α	Stability parameter	
A_i	Interfacial area	m^2
Cp	Heat capacity	J/kg K
Cp(AB)	Heat capacity of the solid product	J/kg K
D	Diffusion coefficient	m^2/sec
d	Separation distance between a pair of atom	m
E	Activation energy	J/mole
Es	Steaming potential	V
e	Permittivity of the medium surrounding both charges	F/m
F	Force between two electric charges	kg/m sec
f	Fraction reacted (0<f<1)	
f(n)	Function of the kinetic order (for n=1)	
Fr	Fractional resistance	kg/m sec^2
G	Free energy	J
γ	Distance between inner and outer Helmholtz planes	m
g	Gravitational constant	m/sec^2
G^{att}	Free energy of attraction between pair of atoms	J
G^{rep}	Free energy of repulsion	J
H	Hamaker's constant	J
h	Planck's constant	J/sec
φ	Permeability	m^2
K	Thermal conductivity	J/m sec K
k	Boltzmann's constant	J/K
K(r)	Thermal conductivity of product	J/m sec k
K(u)	Thermal conductivity of reactant	J/m sec K

Symbol	Meaning	Units
Ko	Pre-exponential factor (for n=1)	1/sec
L	Thickness of cast layer	m
N	Avagadro number	1/mole
n	Reaction order	
η	Viscosity	cps
P	Suction pressure	kg/m sec^2
q	Heat of reaction	J/kg
q1	Electric charges	C
q2	Electric charges	C
R	Gas constant	J/mole
ρ	Density	kg/m^3
r	Particle radius	m
$\rho(r)$	Density of product	kg/m^3
$\rho(\mu)$	Density of reactant	kg/m^3
ρ_l	Density of liquid	kg/m^3
ρ_s	Density of solid	kg/m^3
S	Surface area	m^2
σ	Surface tension	J/m^2
T	Temperature	K
t	Time	sec
Tad	Adiabatic temperature	K
Tc	Combustion temperature	K
Tig	Ignition temperature	K
v	Propagation velocity	m/sec
Vp	Volume of particle or solid (=Vs)	m^3
ω	Void fraction	
X	Particle from its original position along a given axis	m
ψ	Characteristic frequency	1/sec
z	Charge of dissolved ionic species	C
ζ	Zeta potential	V
ΔH^{o}_{To}	Enthalpy of formation of AB(s)	J/kg
F/A	Shear stress	kg/m sec^2
dv/dx	Shear rate	1/sec

11. REFERENCES

1. J.W. McCauley, Ceram. Eng. Sci. Proc., 11 (9-10), 1137 (1990)
2. J. Lis, S. Majarowski, J.A. Puszynski, and V. Hlavacek, Am. Ceram. Soc. Bull., 70 (2), 244 (1991)
3. S.X. Varshney and C.L. Beatty, Ceram. Sci. Eng., 7, 555 (1986)
4. Z.A. Munir and J.B. Holt, J. Mater. Res., 22, 710 (1987)
5. A.G. Merzhanov and I.P. Borovinskaya, Comb. Explos. Shock Waves, 204 (2), 366 (1972)
6. J.A. Puszynski, S. Majorowski and V. Hlavacek, Ceram. Eng. Sci. Proc., 11 (9-10), 1182 (1990)
7. V. Hlavacek, Am. Ceram. Soc. Bull., 70 (2), 240 (1991)
8. Z.A. Munir and U.A. Tamburini, Mat. Sci. Reports, 3, 277 (1989)
9. R.W. Rice, Ceram. Eng. Sci. Proc., 11 (9-10), 1203 (1990)
10. H.C. Yi and J.J. Moore, J. Mat. Sci., 25, 1159 (1990)
11. Z.A. Munir, Am. Ceram. Soc. Bull., 67 (2), 342 (1988)
12. A.G. Merzhanov and I.P. Borovinskaya, Comb. Sci. Tech., 10, 195 (1975)
13. L.L. Wang, E.A. Munir and Y.M. Maximov, J. Mat. Sci., 28, 3693 (1993)
14. O. Yamada, Y. Miyamoto and M. Koizumi, Am. Ceram. Soc. Bull., 64 (2), 319 (1985)
15. Y.M. Chiang, J.S. Haggerty, R.P. Messner and C. Demetry, Am. Ceram. Soc. Bull., 68 (2), 420 (1989)
16. J.A. Sekhar, S.B. Bhaduri, H.P. Li and N.S. Canarslan, US Pat. No., 5,188,678 (1993)
17. J.A. Sekhar, V. Subramanian and N.S. Canarslan, US Pat. App. (1992)
18. Y. Murata and G.W. Weber, UK Patent No. 2078256 A, June (1981)
19. H.C. Yi and J.J. Moore, Am. Ceram. Soc. Bull., 24, 3449 (1989)
20. H.C. Yi and J.J. Moore, Am. Ceram. Soc. Bull., 24, 3456 (1989)
21. L.L. Wang, Z.A. Munir and J.B. Holt, Met. Trans., 21B, 567 (1990)
22. B. Manley, J.B. Holt and Z.A. Munir, Sint. Heter. Catly., 16, 303 (1984)
23. A.G. Merzhanov, Comb. and Flame, 13 (2), 143 (1969)
24. O. Yamada, Y. Miyamoto and M. Koizumi, Am. Ceram. Soc. Bull., 64, (2), 319 (1985)
25. R.A. Cutler, A.V. Virkar and J.B. Holt, Ceram. Eng. Sci. Proc., 6 (7-8), 715 (1985)

26. R.W. Rice, W.J. Mcdonough, G.Y. Richardson, J.M. Kunetz and T. Schroeter, Ceram. Eng. Sci. Proc., 7 (7-8), 751 (1986)
27. J.C. Murray and R.M. German, TMS Conf., New Orleans (1991)
28. R.W. Rice and W.J. McDonough, J. Am. Ceram. Soc., 68 (5), 122 (1985)
29. Y. Miyamoto, M. Koizumi and O. Yamada, Comm. Am. Ceram. Soc. Bull, c-224 (1984)
30. G.Y. Richardson, R.W. Rice, W.J. McDonough, J.M. Kunetz and T. Schroeter, Ceram. Eng. Sci. Proc., 7 (7-8), 751 (1986)
31. M. Ouabdesselam and Z.A. Munir, J. Mat. Sci., 22, 1799 (1987)
32. H.C. Yi, J.J. Moore and A. Petric, (in print)
33. H.C. Yi and J.J. Moore, J. Mat. Sci., 25, 1159 (1990)
34. J.W. McCauley, N.D. Corbin, T. Resetar, and P. Wong,, Ceram. Eng. Sci. Proc., 3 (9-10), 538 (1982)
35. J.B. Holt and Z.A. Munir, J. of Mat. Sci., 21, 251 (1986)
36. W.R. Wrzesinski and J.C. Rowers, J. Mat. Sci. Lett., 9, 432 (1990)
37. S.D. Dunmead, R.W. Readey, C.E. Semier and J.B. Holt, Am. Ceram. Soc. Bull., 72 (12), 2318 (1989)
38. O. Yamada, J. Mat. Res., 1 (1), (1986)
39. A.G. Akopyan, S.K. Dolukhanyan and I.P. Borovinskaya, Comb. Explos. Shock Waves, 14 (3), 70 (1978)
40. H.P. Li, S.B. Bhaduri and J.A. Sekhar, Metall. Trans. A, 23A, 251 (1992)
41. H.P. Li and J.A. Sekhar, Materials Science and Eng., A160, 221 (1993)
42. A.P. Hardt and P.W. Holsinger, Comb. and Flame, 21, 91 (1973)
43. T. Iseki, H. Matsuzaki and J.K. Boadi, Am. Ceram. Soc. Bull., 64 (2), 322 (1985)
44. A.M. Bulaev, Y.A. Gal'chenko, G.A. Vishnyakova, V.I. Yukhvid, I.P. Borovinskaya and A.G. Merzhanov, Comb. Explos. Shock Waves, 5, 178 (1986)
45. O. Odawara, Am. Ceram. Soc. Bull., 73 (3), 629 (1990)
46. O. Odowara and J. Ikenchi, Am Ceram. Soc. Bull., 69 (4), 85 (1986)
47. O. Odowara and J. Ikenchi, Am. Ceram. Soc. Bull., 69 (4), 80 (1986)
48. R.W. Rice R, Ceram. Eng. Sci. Proc., 11 (9-10), 1226 (1990)
49. C.P. Cameron, J.H. Enloe, L.E. Dolhert and R.W. Rice, Ceram. Eng. Sci. Proc., 11 (9-10), 1190 (1990)

50. V.M. Maslov, I.P. Borovinskaya and A.G. Merzhanov, Comb. Explos. Shock Waves, 12 (5), 703 (1976)
51. J.M. Maslov, A.S. Negarov, I.P. Borovinskaya and A.G. Merzhanov, Comb. Explos. Shock Waves, 14 (6), 759 (1978)
52. E.J. Huber, E.L. Head and C.E. Holley, J. Phys. Chem., 68 (10, 3040 (1964)
53. E.J. Huber, J. Chem. Eng., 11 (3), 430 (1966)
54. C.E. Lowell and W.S. Williams, Rev. Scientific Instrum., 32, 1120 (1961)
55. R.W. Rice, G.Y. Richardson, J.M. Kunetz, T. Schroeter and W.J. McDonough, Ceram. Eng. Sci. Proc., 7 (7-8), 736 (1986)
56. Y.S. Naiborodenko and V.I. Itin, Comb. Explos. Shock Waves, 11 (3), 43 (1975)
57. T.S. Azatyan, V.M. Mal'tser, A.G. Merzhanov and V.A. Seleznev, Comb. Explos. Shock Waves, 13 (2), 186 (1977)
58. V.V. Aleksandrov and M.A. Korchagin, Comb. Explos. Shock Waves, 23 (5), 55 (1987)
59. Y.M. Maksimov, A.T. Pak, G.B. Lavrenchuk, Y.S. Naiborodenko and A.G. Merzhanov, Comb. Explos. Shock Waves, 15 (4), 156 (1979)
60. V.M. Shkiro and G.A. Nersisyan, Comb. Explos. Shock Waves, 14 (1), 121 (1978)
61. A.G. Strunina, L.K. Demidova, A.N. Firsov and A.G. Merzhanov, Comb. Explos. Shock Waves, 23 (3), 52 (1987)
62. K.G. Shkadinski, B.I. Khaikin and A.G. Merzhanov, Comb. Explos. Shock Waves, 1, 19 (1971)
63. A.P. Aldushin, T.M. Martem'yanova, A.G. Merzhanov, B.I. Khaikin, Comb. Explos. Shock Waves, 8 (2), 159 (1972)
64. A.A. Zenin, A.G. Merzhanov and G.A. Nersisyan, Comb. Explos. Shock Waves, 17 (1), 79 (1981)
65. A.G. Merzhanov and B.I. Khaikin, Prog. Energy Comb. Sci., 14, 1 (1988)
66. A.P. Aldushin and B.I. Khaikin, Comb. Explos. Shock Waves, 10 (3), 313 (1974)
67. E.V. Okolovich, A.G. Merzhanov, B.I. Khaikin and K.G. Shkadinski, Comb. Explos. Shock Waves, 13 (3), 326 (1977)
68. E.A. Nekrasov, Y.M. Maksimov, M.K. Ziatdinov and A.S. Shteinberg, Comb. Explos. Shock Waves, 5, 26 (1978)
69. S.B. Margolis, Prog. in Energy and Comb. Science, 17 (2), 135 (1991)

70. A.P. Hardt and P.V. Phung, Comb. and Flame, 21, 77 (1973)
71. A.G. Strunina, T.M. Martem'yanova, V.V. Barzykin and V.I. Ermakov, Comb. Explos. Shock Waves, 10 (4), 518 (1974)
72. E.I. Maksimov, A.G. Merzhanov and V.M. Shkiro, Comb. Explos. Shock Waves, 1 (4), 24 (1965)
73. E.I. Maksimov and K.G. Shkadinski, Comb. Explos. Shock Waves,7 (3), 454 (1971)
74. B.I. Khaikin and A.G. Merzhanov, Comb. Explos. Shock Waves, 2 (3), 22 (1966)
75. J.B. Holt, D.D. Kingman and G.M. Bianchini, J. Mat. Sci. Eng., 71, 321 (1985)
76. M.G. Lakshmikantha and J.A. Sekhar, J. Am. Ceram. Soc. (1994) (in print)
77. A.V. Dvoryankin, A.G. Strunina and A.G. Merzhanov, Comb. Explos. Shock Waves, 21 (4), 44 (1985)
78. V.M. Shkiro and I.P. Borovinskaya, Comb. Explos. Shock Waves, 12 (6), 945 (1976)
79. S.A. Karataskov, V.I. Yukhvid and A.G. Merzhanov, Comb. Explos. Shock Waves, 21 (6), 41 (1985)
80. A.I. Kirdyashkin, Y.M. Maksimov and A.G. Merzhanov, Comb. Explos. Shock Waves, 22 (6), 65 (1986)
81. Y.S. Naiborodenko, V.I. Itin, B.P. Belozerov and V.P. Ushakov, Comb. Explos. Shock Waves, 11, 34 (1973)
82. S.G. Vadchenko, Y.M. Grigor'ev and A.G. Merzhanov, Comb. Explos. Shock Waves, 12 (5), 676 (1976)
83. M.A. Korchagin and Podergin, Comb. Explos. Shock Waves, 15 (3), 48 (1979)
84. M.A. Korchagin and V.V. Aleksandrov, Comb. Explos. Shock Waves, 17 (1), 72 (1981)
85. V.V. Aleksandrov, M.A. Korchagin, B.P. Tolochko and M.A. Sheromov, Comb. Explos. Shock Waves, 19 (4), 65 (1983)
86. J. Puszyunski, J. Degreve and V. Hlavacek, J. Eng. Chem. Res., 26, 135 (1987)
87. M.G. Lakshimikanta, A. Bhattacharya and J.A. Sekhar, Metall. Trans. A, 23A, 23 (1992)
88. M.G. Lakshimikanta and J.A. Sekhar, Metall. Trans. A, 24A, 617 (1992)

89. A.P. Aldushin, B.I. Khaikin and K.G. Shkadinskii, Comb. Explos. Shock Waves, 12 (6), 819 (1976)
90. I.P. Borovinskaya, A.G. Merzhanov, N.P. Novikov and A.K. Filonenko, Comb. Explos. Shock Waves, 10 (1), 4 (1974)
91. A.I. Kirdyashkin, Y.M. Maksimov and E.A. Nekrasov, Comb. Explos. Shock Waves, 17 (4), 33 (1981)
92. V.A. Knyazik, A.G. Merzhanov, V.B. Solomonov and A.S. Shteinberg, Comb. Explos. Shock Waves, 21 (3), 69 (1985)
93. J.S. Reed, Int. to Prin. of Ceram. Proc., John Wiley and Sons (1989)
94. G.W. Phelps, S.G. Maguire, W.J. Kelly and R.K. Wood, Rheology and Rheometry of Clay-Water Systems (1982)
95. D.W. Richerson, Modern Ceram Eng., Marcel Dekker Inc. (1982)
96. J.G.P. Binner, Adv. Ceram. Proc. and Tech., Noyels Pub. (1990)
97. F.F. Wang, Treatise on Mat. Sci. and Tech, Ceram Fab. Proc., Academic Pres. (1976)
98. J.W. Goodwin, Ceram. Bull., 69 (10), 1694 (1990)
99. J.A. Mangels and G.L. Messing, Adv. Ceram. (V-9 Form. of Cram.), Am. Ceram. Soc., 76 (1984)
100. R.R. Rowlands, Ceram. Bull., 45 (1), 16 (1966)
101. J.J. Callahan, W.L. Garforth, W.J. Polestak and E.J. Sare, Ceram. Eng. S 12 (1-2), 80 (1991)
102. P.A. Smith and R.A.Haber, Ceram. Eng. Sci. Proc., 12 (1-2), 93 (1991)
103. P.A. Smith and R.A. Haber, Ceram. Eng. Sci. Proc., 10 (1-2), 1 (1989)
104. C. Parkinson, S. Matsumoto and P. Sherman, J. Coll and Int. Sci., 33 (1), 150 (1970)
105. T. Dabak and O Yucel, Powder Tech., 52, 193 (1987)
106. P.E. Remoes, B.C. Weber and M.A. Schwartz, Ceram. Bull., 37 (7), 334 (1958)
107. R.D. Nelson, Handbook of Pow. Tech., Dis. Pow. in Liq., V7 (1988)
108. D.H. Everett, Basic Prin. of Coll. Sci., Royal Soc. of Chem. (1988)
109. J.A. Mangels and G.L. Messing, Adv. Ceram. (V-9 Form. of Cram.), Am. Ceram. Soc., 85 (1984)
110. J.A. Mangels and G.L. Messing, Adv. Ceram. (V-9 Form. of Cram.), Am. Ceram. Soc., 95 (1984)
111. J.A. Mangels and G.L. Messing, Adv. Ceram. (V-9 Form. of Cram.), Am. Ceram. Soc., 105 (1984)
112. P.J. Anderson and P. Murray, J. Am. Ceram. Soc., 42 (2), 70 (1959)

113. A.K. Nikumbh, H. Schmith, K. Martin, F. Porz and F. Thummler, J. Mat Sci., 25, 15 (1990)
114. R. Moreno, J.S. Moya and J. Requena, Ceram. Int., 17, 37 (1991)
115. S. Inada, T. Kimura and T. Yamaguchi, Ceram. Int., 16, 369 (1990)
116. Users Manual, Brookfield Co. (1993)
117. G.H. Geiger and D.R. Poirier, Trans. Phe. in Met., Addison-Wesley Pub. Co. (1973)
118. G. Crume and D.R. Dinger, Ceram. Eng. Sci. Proc., 12 (1-2), 68 (1991)
119. B. Kostic, D. Kicevic and M. Gasic, Ceramics International, 16, 281 (1990)
120. F.M. Tiller and C. Tsai, J. Am. Ceram. Soc., 69 (12), 882 (1986)
121. C. Chanyanavich, Rheology of Spherical Sil. Part., PhD Thesis, Rutgers Unv. (1983)
122. R.D. Sudduth, J. App. Poly. Sci., 48, 25 (1993)
123. M. Mooney, J. Colloid. Sci., 6, 162 (1951)
124. D. Quemada, Rheologica Acta, 16, 82 (1977)
125. D. Quemada, Rheologica Acta, 17, 632 (1978)
126. T.B. Massalski, H. Okamoto, P.R. Subramanian and L. Kacprzak, Binary Alloy Phase Diag., ASM International (1990)
127. I. Barin and O. Knacke, Thermochemical Prop. of Inorg. Subst., Springer-Verlag (1973)
128. A. Goldsmith, T.E. Waterman and H.J.Hirschhorn, Handbook of Thermophysical Prop. of Solid Mater., MacMillan, Vol 1-3 (1961)
129. J. Askill, Tracer Diff. Data for Metals, Alloys and Simple Oxides, IFI/Plenum, New York (1970)
130. H.K. Liu and A.P. Majidi, Ceram. Inter., V15 (1), 14 (1991)
131. C.T. Huang, Reaction Between Carbon and Silicon Alloys, PhD Thesis, Unv. Cincinnati (1991)
132. W.L. Frankhouser, F.W. Brendley, M.C. Kieszek and S.T. Sullivan, Gasless Comb. Syn. of Refrac. Comp., Noyes Pub., New Jersey (1985)

12. APPENDICES

12.1. Appendix A

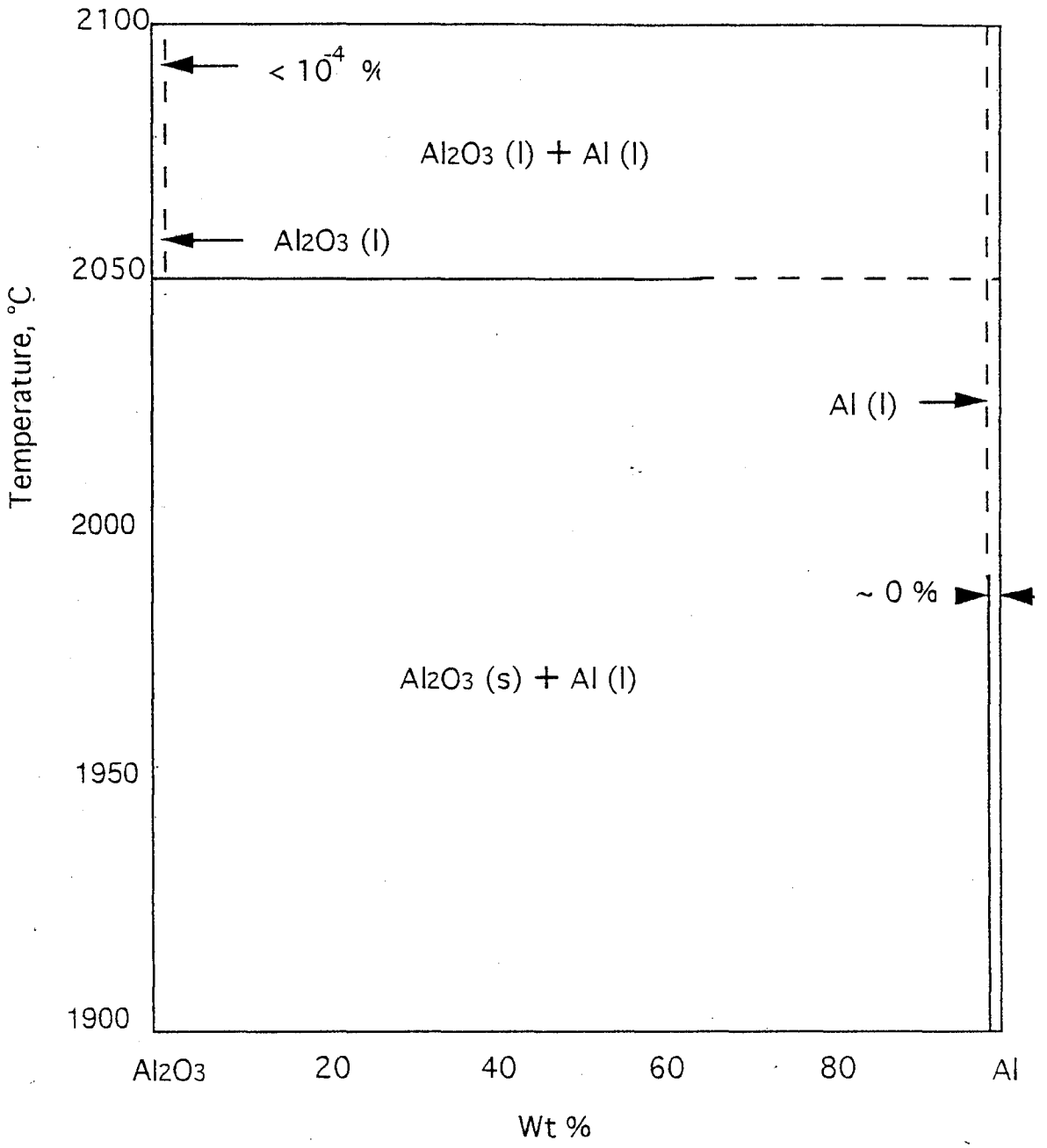

Figure 12.1. Phase diagram for system Al2O3-Al [126]

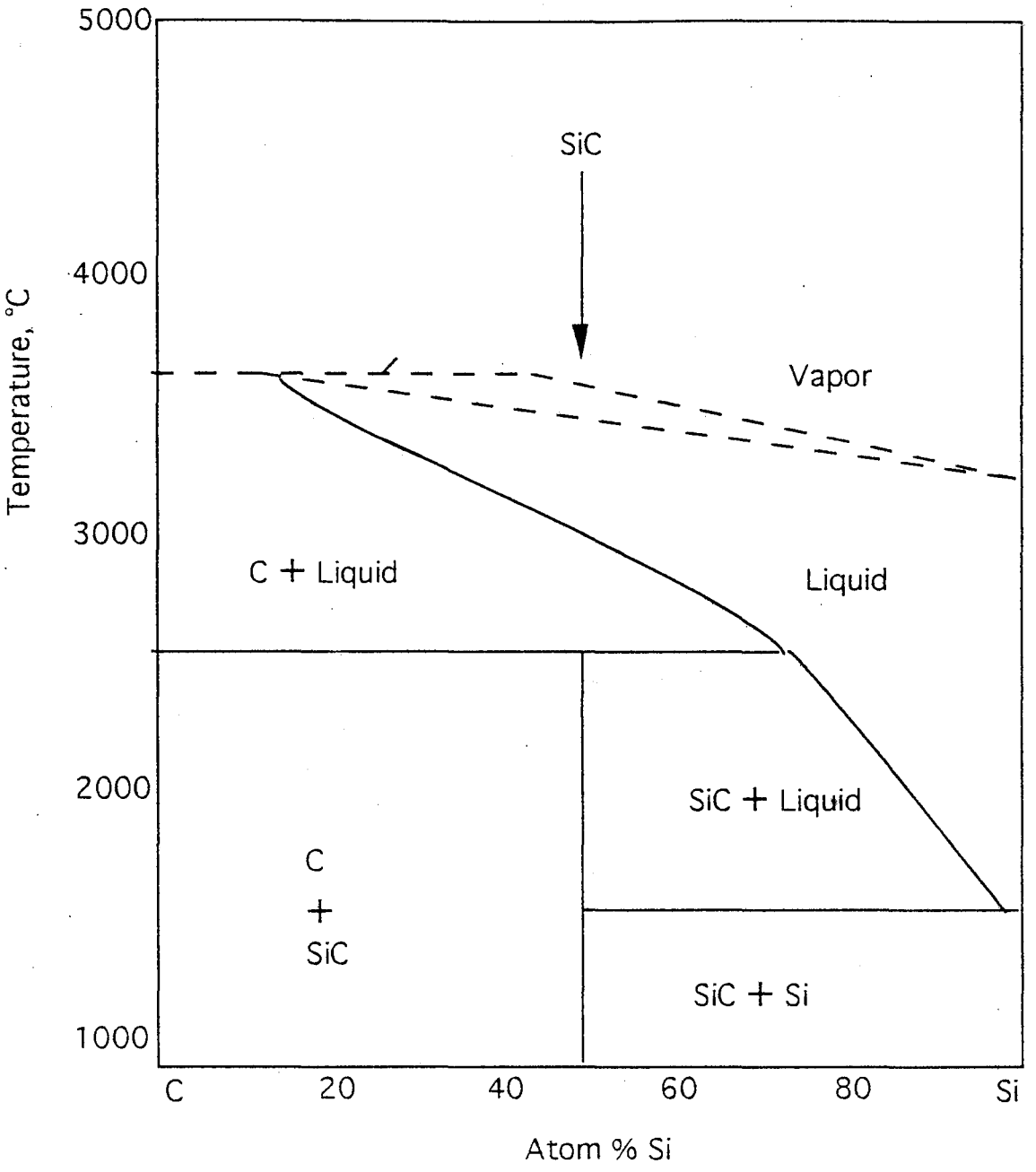

Figure 12.2. Phase diagram for system Si-C [126]

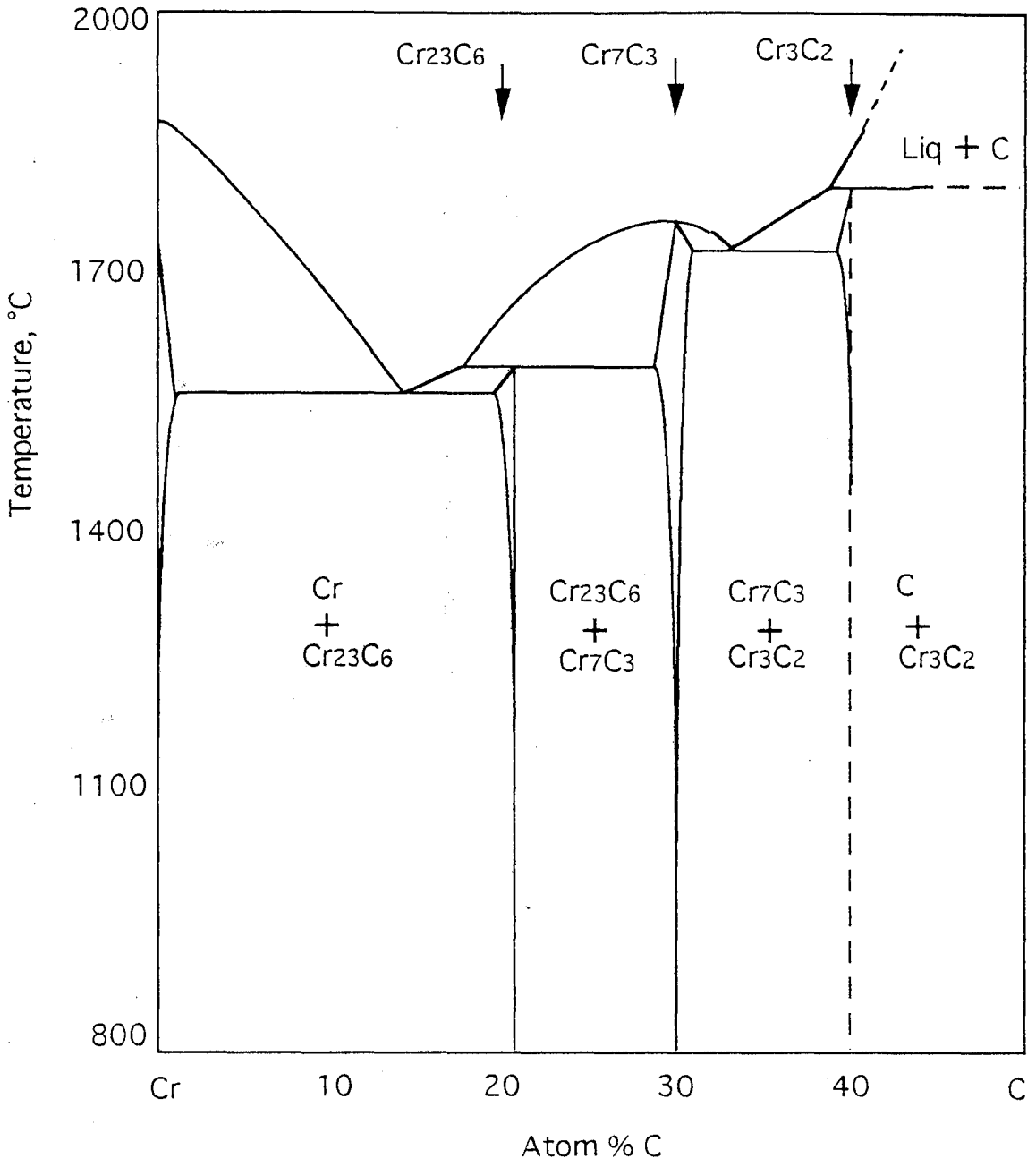

Figure 12.3. Phase diagram for system Cr-C [126]

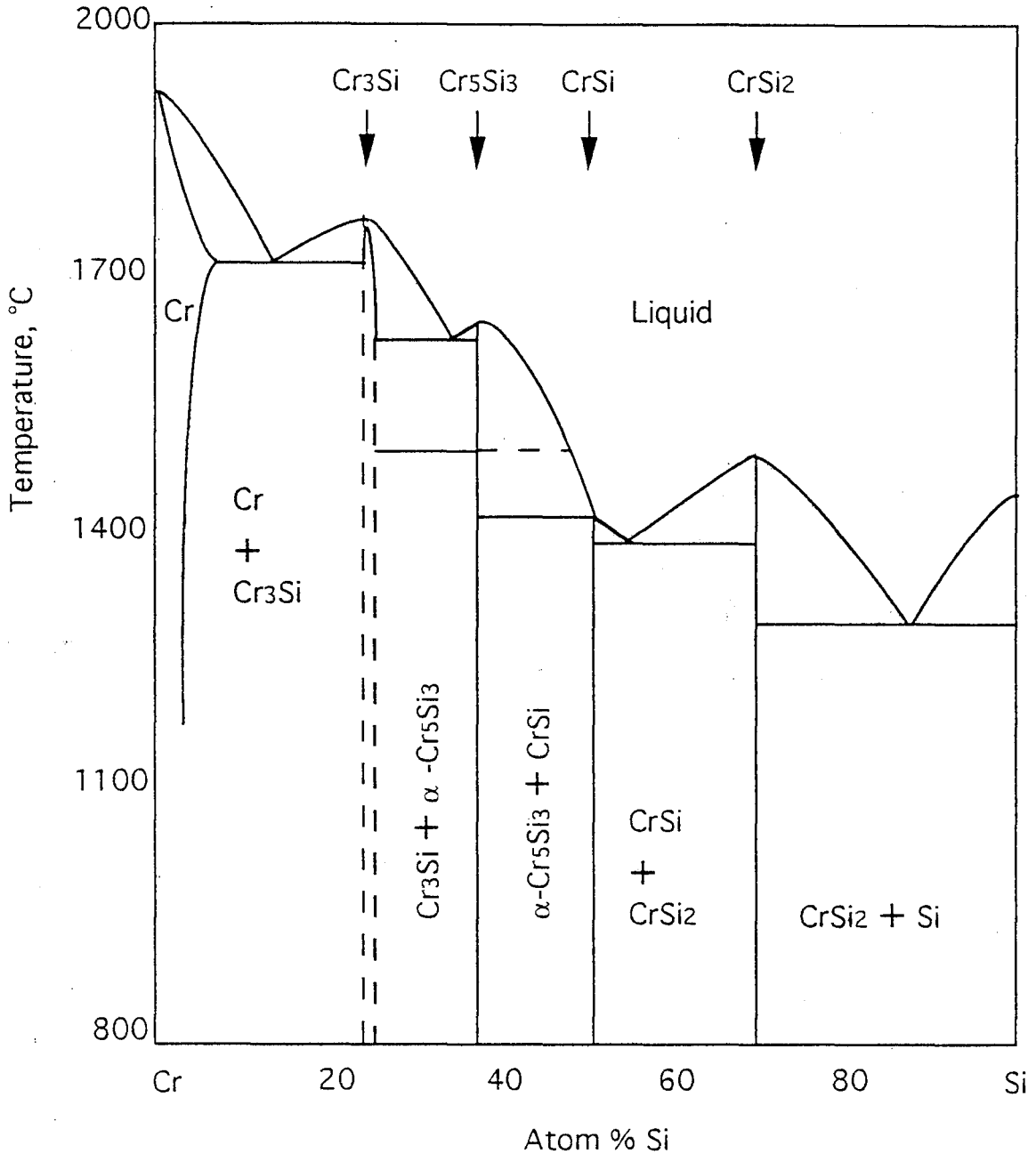

Figure 12.4. Phase diagram for system Cr-Si [126]

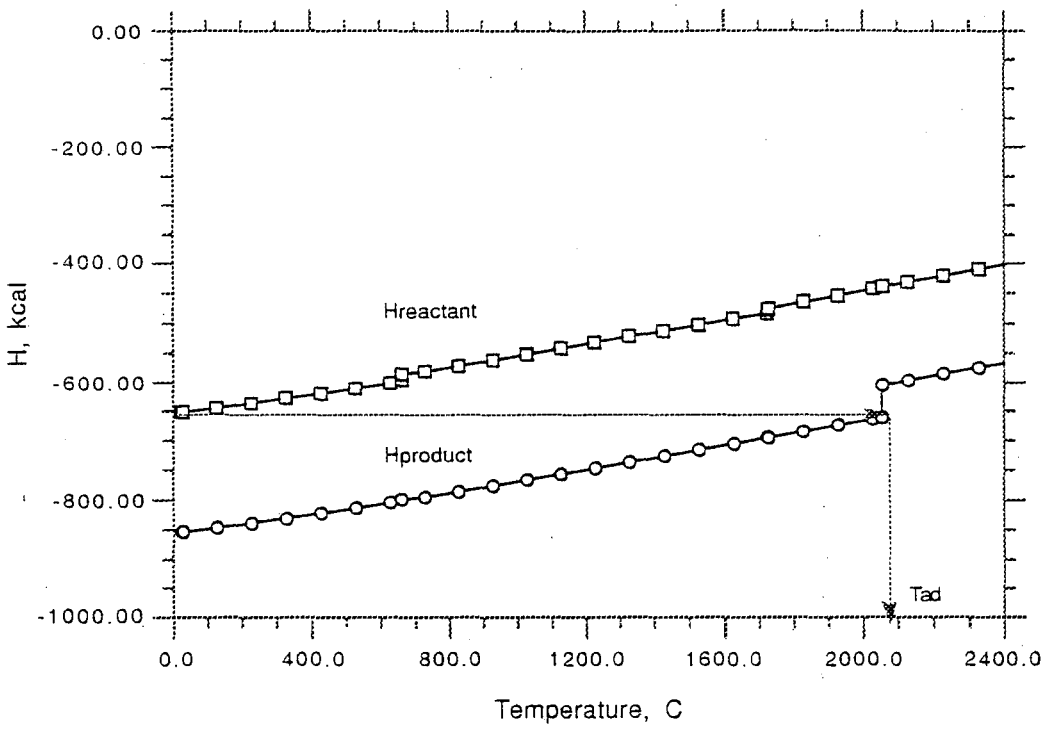

Figure 12.5. Enthalpy as a function of Temperature for reaction 1 [127]

12.2. Appendix B

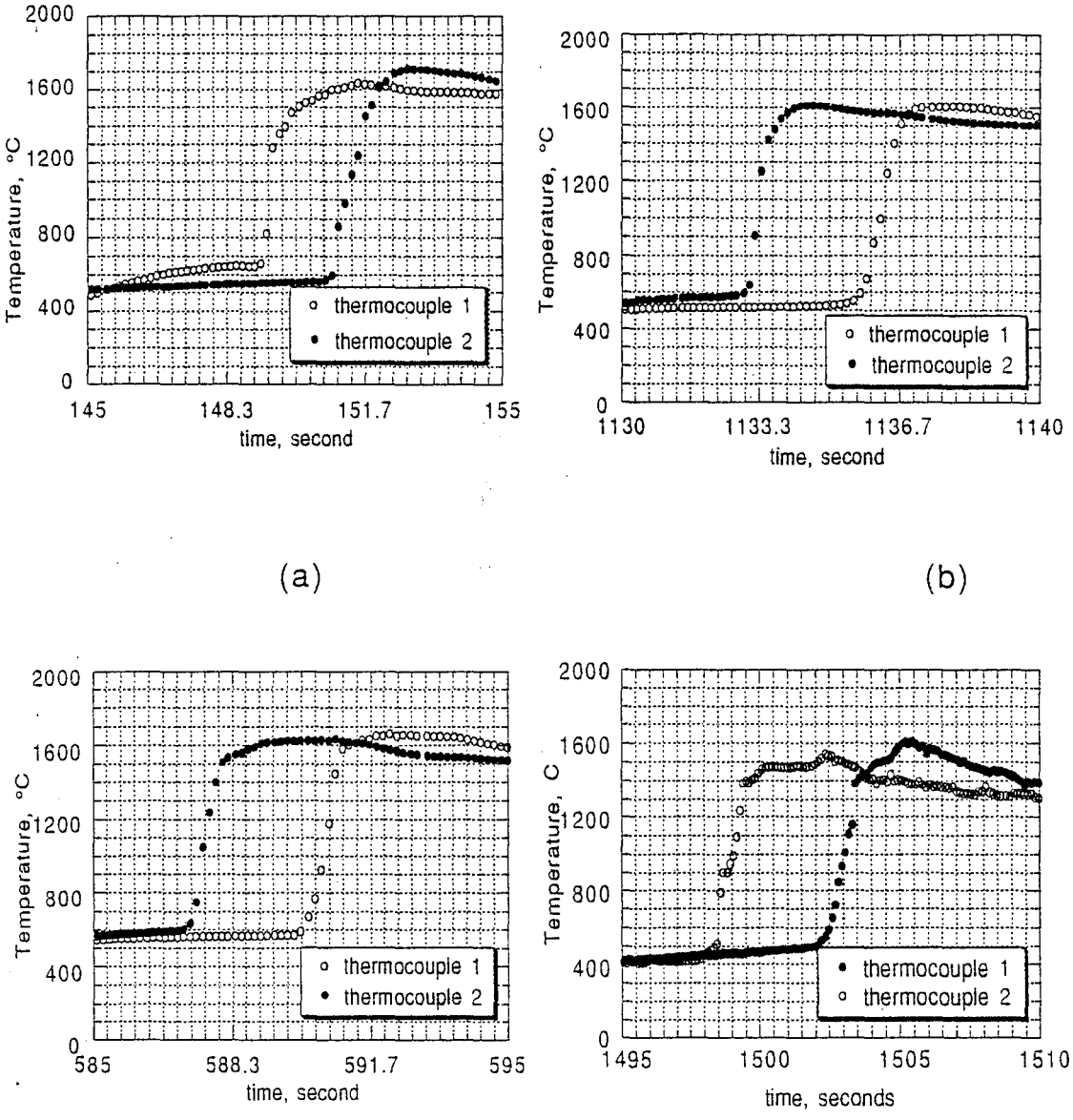

Figure 12.6. Combustion temperatures as a function of time for samples (a) A10, (b) A21, (c) A32 and (d) A43

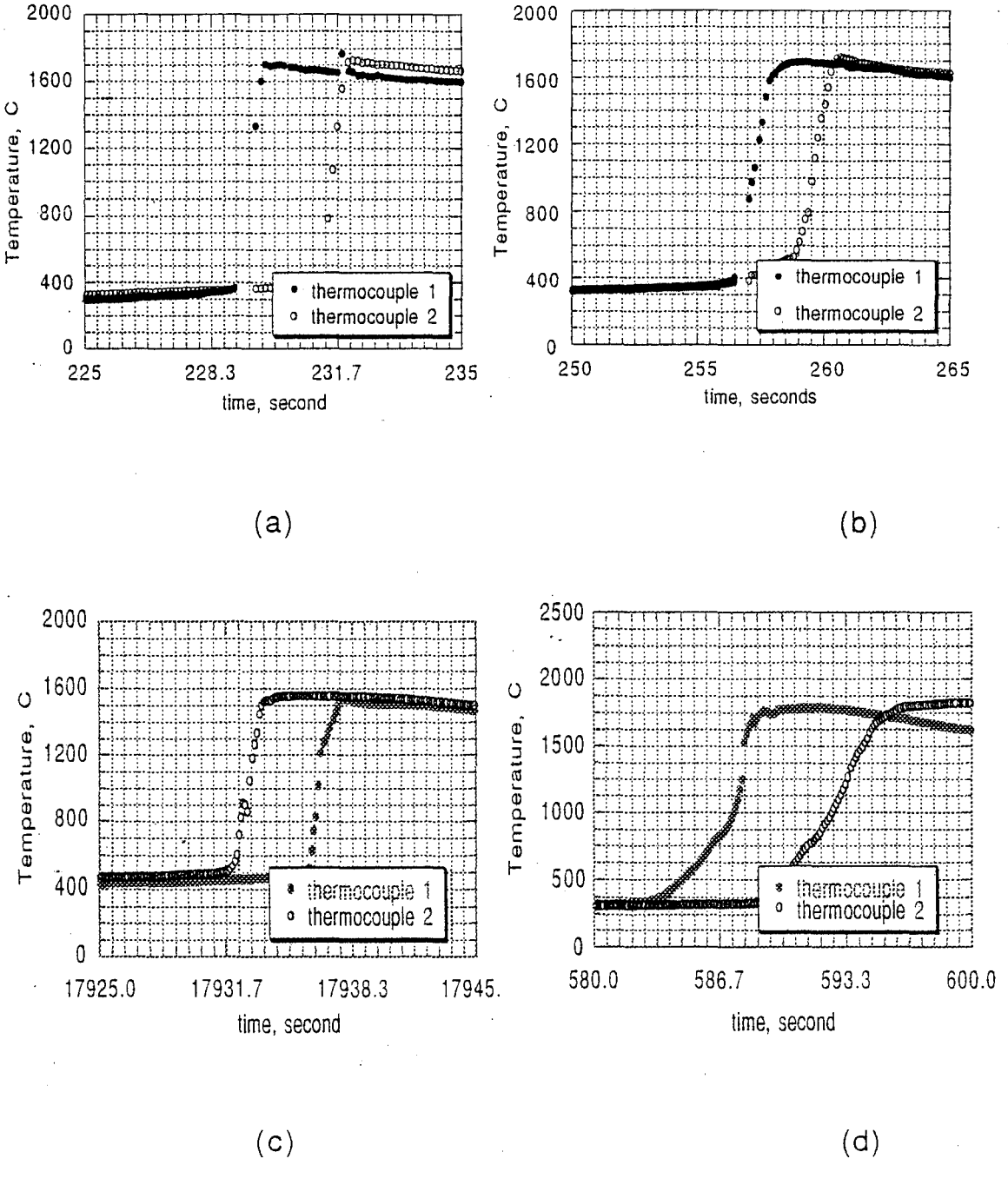

Figure 12.7. Combustion temperatures as a function of time for samples (a) AB1, (b) AB2, (c) A33 and (d) A36

12.3. Appendix C

- J.A. Sekhar, S. Bhaduri, H.P. Li and N.S. Canarslan, U.S. Patent, 5,188,678, Feb. 23, 1993

- J.A. Sekhar, V. Subramanian and N.S. Canarslan, U.S. Patent, App. Serial No. 07/753,216 Filed Aug. 30, 1991

- N.S. Canarslan and J.A. Sekhar, J. Materials Research (1994) (to be submitted)